
# Studies of multiheme proteins from the disimilatory metal reducing bacteria *Shewanella oneidensis* MR-1 *and Geobacter sulfurreducens*

**Sally Atkinson**

**Thesis presented for the degree of Doctor of Philosophy**

**University of Edinburgh**

**2009**

## DECLARATION

The work presented in this thesis is the original work of the author, except where specific reference is made to other sources. It has not been submitted in part, or in whole, for any other degree. Some of the results have already been published.

Sally J. Atkinson

April 2009

**ABSTRACT**

Genomic analysis of the dissimilatory metal-reducing bacteria *Shewanella oneidensis* MR-1 and *Geobacter sulfurreducens* PCA has shown that both are capable of expressing an unprecedented number of multiheme cytochromes. The isolation and characterisation of two of the multiheme cytochromes from these bacteria is the subject of this thesis.

-

Octaheme tetrathionate reductase (OTR) from *Shewanella oneidensis* has been previously shown to catalyse the reduction of tetrathionate to thiosulfate (Rothery, 2003). Despite having an amino-acid sequence suggesting the presence of eight standard CXXCH heme-attachment motifs, the crystal structure of OTR has shown the enzyme to contain seven normally-coordinated bis-histidine-ligated hemes, with one unusual lysine-coordinated heme at the active site. Analysis of the structure of this enzyme has shown its heme architecture to have a significant similarity to those of hydroxylamine oxidoreductase and the pentaheme cytochrome *c* nitrite reductases.

An improved protocol for the purification of OTR has been developed, and work has been carried out in order to identify further possible substrates for the enzyme. Results show that OTR is capable of reducing nitrite, hydroxylamine, nitrous oxide and nitric oxide, suggesting that OTR may have a role as a nitrogen cycle enzyme. In particular, the reactions of OTR with hydroxylamine and nitrite have been shown to be more efficient than that with tetrathionate ($k_{cat}$ / $K_M$ = 5.3 x $10^5$ $M^{-1}$ $s^{-1}$ and 3.9 x $10^5$ $M^{-1}$ $s^{-1}$ respectively). The product of the reactions of nitrite and hydroxylamine with OTR has been directly

detected in solution and shown to be the ammonium ion. This activity is consistent with a nitrogen cycle enzyme, with the conversion of nitrite to ammonium representing a "short cut" in the cycle, as performed by the cytochrome *c* nitrite reductases. In addition to this, site-directed mutagenesis has been used to investigate the catalytic properties of key active site residues, including the unusual heme-ligating lysine.

The complete genome sequence of *Geobacter sulfurreducens* PCA was determined in 2003 and genomic analysis predicted the presence of a putative octaheme protein, GSU0357. This protein was predicted to contain an unusual CXXCK heme-binding amino acid motif and showed a high sequence similarity to the pentaheme cytochrome *c* nitrite reductase from *Desulfovibrio desulfuricans* ATCC 27774. The purification of GSU0357 has been non-trivial and a range of approaches have been used. The ability of GSU0357 to act as a nitrite reductase has been confirmed.

## ACKNOWLEDGEMENTS

I would like to thank my supervisors Prof. Steve Chapman and Prof. Graeme Reid for their guidance, support and understanding over the course of this Ph.D. Many thanks also to Dr. Caroline Miles for all her hard work with the molecular biology and Dr. Chris Mowat for crystallography and helpful discussions. I am also particularly grateful to Dr. Emma Rothery and Dr. Dominic Hunter for guidance and encouragement at the start of this project and to Vivek Jassal for being a dedicated project student. Thanks are also extended to all members of the Chapman, Daff and Reid groups I have worked with over the past 4 years.

Many thanks, of course, to the Biotechnology and Biological Sciences Research Council for funding. I would also like to thank Dr. Tanya Peshkur of the Contaminated Land Assessment and Remediation Research Centre for her invaluable assistance in the ammonium detection assays.

I would like to thank my family for their support and patience. Finally, many thanks go to Dr. Kelly, Dr. Sal and Tim for encouragement when all seemed lost, endless support and more tea and cake than is proper for any person to eat.

# ABBREVIATIONS

**Amino acids:**

| | |
|---|---|
| C | cysteine |
| H | histidine |
| K | lysine |
| X | any amino acid residue |

**Buffers:**

| | |
|---|---|
| CHES | 2-[N-cyclohexylamino]ethanesulfonic acid |
| $KP_i$ | potassium phosphate: $K_2HPO_4/KH_2PO_4$ |
| MES | 2-[N-morpholino]ethanesulfonic acid |
| Tris | tris(hydroxymethyl)aminomethane |

**Kinetic parameters:**

| | |
|---|---|
| $k_{cat}$ | rate constant at substrate saturation |
| $k_1$ | rate constant for the fast phase of a biphasic reaction |
| $k_2$ | rate constant for the slow phase of a biphasic reaction |
| $K_M$ | Michaelis constant |
| $K_D$ | dissociation constant |

**Chemical abbreviations:**

| | |
|---|---|
| ADP | adenosine diphosphate |
| ATP | adenosine triphosphate |
| DEAE | dithylaminoethyl |
| $dH_2O$ | distilled water |
| $D_2O$ | deuterated water |
| DMSO | dimethyl sulfoxide |
| DTT | dithiothreitol |
| EDTA | ethylene diamine tetra-acetic acid |
| EtOH | ethanol |
| FAD | flavin adenine dinucleotide |
| FMN | flavin mononuclotide |
| IPTG | isopropyl-β-D-thiogalactopyranoside |
| MGD | *bis*(molybdopterin guanine dinucleotide) |
| PMSF | phenylmethylsulfonyl fluoride |
| SDS | sodium dodecylsulfate |
| TMBZ | 3,3',5,5'-tetramethyl benzidine |

**Protein abbreviations:**

| | |
|---|---|
| CCHL | cytochrome *c* heme lyase |
| HAO | hydroxylamine oxidoreductase |
| NAP | periplasmic nitrate reductase |
| NAR | membrane-bound nitrate reductase |
| c*c*NIR | cytochrome *c* nitrite reductase |
| *cd*$_1$NIR | cytochrome *cd*$_1$-containing nitrite reductase |
| CuNIR | copper-containing nitrite reductase |
| NOR | nitric oxide reductase |
| NOS | nitrous oxide reductase |
| Nrf | cytochrome *c* nitrite reductase |
| OTR | octaheme tetrathionate reductase |

**Standard Units**:

| | |
|---|---|
| Å | Angstrom |
| ° C | degrees Celcius |
| g | gram |
| l | litre |
| m | metre |
| M | molar |
| s | second |
| V | volt |

**Textual abbreviations:**

| | |
|---|---|
| Abs | absorbance |
| ANAMOX | anaerobic ammonium oxidation |
| Da | Daltons |
| EPR | electron paramagnetic resonance |
| $E_x$ | extinction coefficient at wavelength *x* |
| FPLC | fast protein liquid chromatography |
| GPES | General Purpose Electrochemistry Software |
| ΔG° | Gibbs Standard Free Energy Change |
| ΔG* | Activation energy |
| LB | Luria Bertani |
| ox | oxidised |
| PAGE | polyacrylamide gel electrophoresis |
| PDB | Protein Data Bank |
| red | reduced |
| TIGR | The Institute for Genomic Research |
| UV | ultraviolet |
| Vis | visible |

# TABLE OF CONTENTS

## LIST OF FIGURES

LIST OF TABLES

# *CHAPTER 1*

# *INTRODUCTION*

# 1 INTRODUCTION

## 1.1 METALS IN BIOLOGY

Metal ions play an essential role in biology. They are utilised in a wide variety of processes in living organisms, including catalysis, signalling, energy storage, electron transfer and the maintenance of structures in biological materials.

Many of the biomolecules that use metal ions are proteins and, more specifically, enzymes (Figure 1.1). Metal ions are often employed at the active sites of enzymes, where they are involved in important processes, including redox reactions. These metalloenzymes facilitate an extensive variety of reactions, such as hydrolysis (catalysed by hydrolases), redox reactions (oxidases, oxygenases and reductases) and the rearrangement of carbon-carbon bonds (synthases and isomerases).

The application of metal ions in such an array of processes is a consequence of their varied chemistry. Metal ions, positioned at an active site, can act as redox centres, promoting reactions involving atom or electron transfer. The specific characteristics of the metal ion involved confer reaction selectivity; for example, the metal ion employed in a reactive site must be of the correct size, hard-soft character, stereochemical preference or reduction potential in order to function correctly.

**Figure 1.1: Classification of some metal-containing biomolecules.**

*Figure adapted from Ibers et al (1980).*

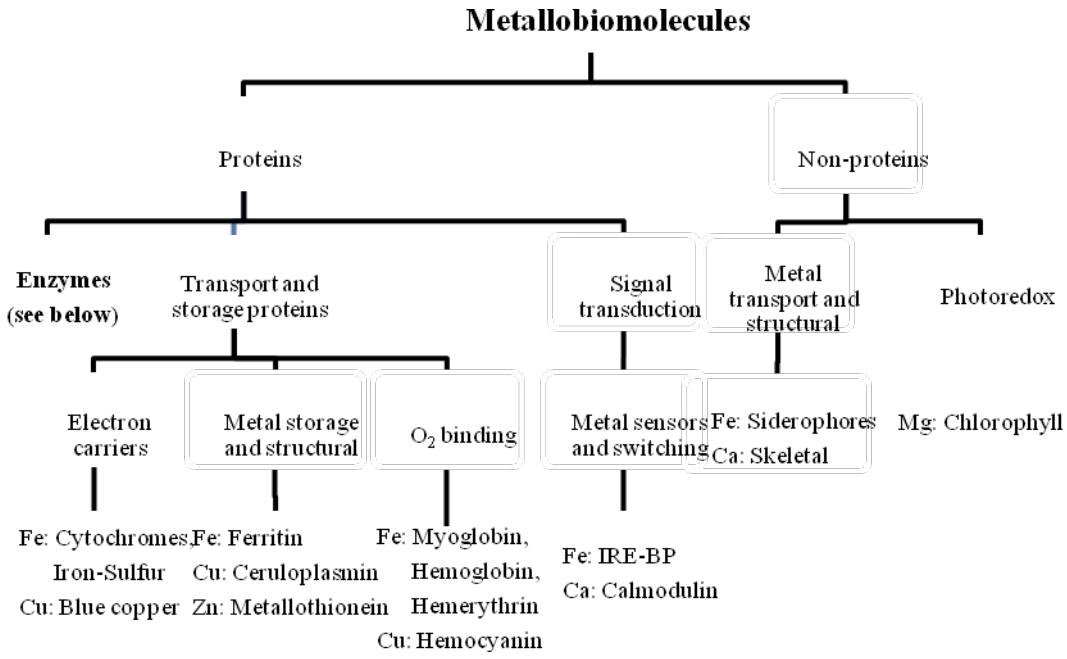

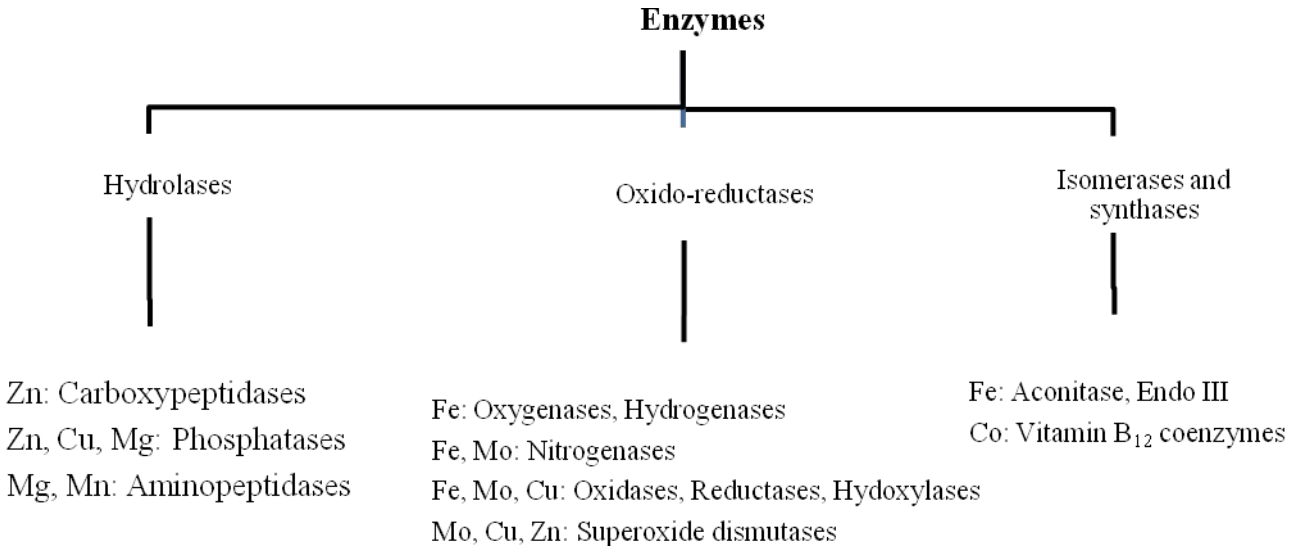


## 1.2 BIOLOGICAL ELECTRON TRANSFER

The most fundamental of chemical processes is the simple, one-electron transfer. Outer-sphere electron-transfer reactions do not involve the making and breaking of bonds and are often simply referred to as redox reactions. One-electron transfers are of great importance in biology, where they are utilised extensively in photosynthesis and respiration via electron-transport chains.

There are three types of electron transfer reactions (Moser *et al*, 1995):

**Non-adiabatic Electron Transfer:** Single electrons are transferred between two weakly coupled inter- or intra-molecular redox centres. For example, an electron exchange reaction, in which one electron moves between two redox centres.

**Electron Pair Exchange:** A pair of electrons is cooperatively inserted or removed from a system. For example, the transfer of a pair of electrons as a hydride from NAD(P)H.

**Transduction:** A redox centre collects a number of single electrons a multiple of times and then transfers them in single steps, or *vice versa*. For example, the flavin group of membrane-bound succinate dehydrogenase collects two electrons from succinate oxidation and the electrons are then transferred sequentially to an iron-sulfur cluster.

### 1.2.1 Redox Catalysis

A redox reaction is one in which electrons are transferred from one species to another. This process results in a change in the oxidation state of an element and may be accompanied by additional changes, such as ion or atom transfer. Enzymes catalysing oxidation and reduction reactions play a major metabolic role. For example, such redox reactions are the basis of two important energy conversion processes, respiration and photosynthesis. In these processes, electrons are passed from one protein to another, and this occurs *via* their redox centres. These centres commonly contain metal ions, although organic species such as flavins and quinones are also capable of mediating electron transfer. Chains of redox centres are found within cell and mitochondrial membranes, providing the means for electrons to be transferred to the necessary location within the cell from both intra- and extra-cellular redox cofactors.

The construction of these "chains" of electron-carrying proteins is of great significance; the width of the cell membrane is approximately 60 Å (Birch-Andersen *et al*, 1953) and electron transfer cannot occur between two redox centres separated by such a large distance. The rate of electron transfer decreases exponentially as the distance between the redox centres increases and at distances greater than 14 Å electron transfer has been found to be too slow to support catalysis. Therefore, in order to transfer electrons over the long distances required in the cell, a chain of redox centres permits the electrons to travel in a series of discrete steps, each no longer than 14 Å (this concept is further examined in Section 1.2.4).

### 1.2.2 Electron Transfer in Inorganic Systems

There are two classes of electron transfer in simple inorganic systems:

**Outer-Sphere Redox Reactions:** In an outer-sphere redox reaction, the reacting ions diffuse together through the solvent. When the ions are in contact an electron migrates from one ion to the other and they subsequently diffuse apart. The contact of the coordination spheres provides a route for the transfer of the electron. In this process, only a minimal change occurs in the positioning of the elements of the redox centres; the original coordination spheres are intact and a small adjustment in the metal-ligand bond lengths may occur as a result of the change in radius of the central metal ion as a consequence of its change in oxidation state. Electron transfer by this method can be fast.

**Inner-Sphere Redox Reactions:** In an inner-sphere redox reaction, the reacting ions diffuse together through the solvent and a ligand substitution reaction occurs once they are in contact, creating a transitory ligand-bridged species. The bridging ligand transfers from one ion to the other, leading to a change in the oxidation state of the redox centres and a change in the composition of the coordination spheres.

If electron transfer is faster than ligand substitution, the reaction must have an outer-sphere mechanism. Similarly, a substitution in the coordination sphere of a reactant indicates an inner-sphere mechanism.

**Figure 1.2: Outer- and inner-sphere electron transfer.**

*Figure A shows a schematic of outer-sphere electron transfer: the reacting ions diffuse together until their coordination spheres come into contact. An electron migrates from one ion to the other and the ions diffuse apart.*
*Figure B shows a schematic of inner-sphere electron transfer: the reacting ions diffuse together until their coordination spheres come into contact at which point a ligand substitution reaction occurs, forming a transitory ligand-bridged species. The bridging ligand transfers from one ion to the other, leading to changes in both the oxidation states of the redox centres and the composition of the coordination spheres.*

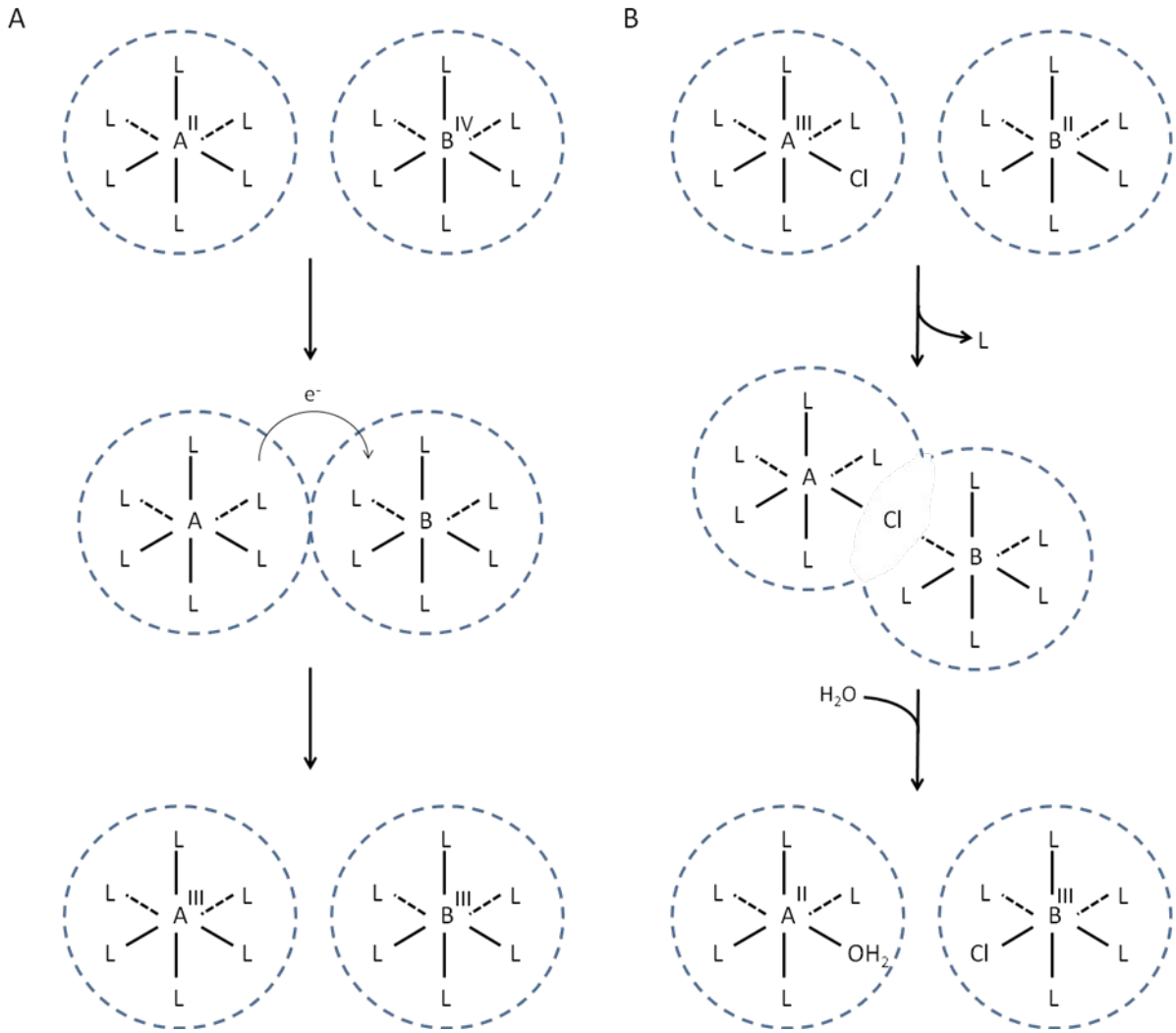


### 1.2.3 Electron Transfer in Biological Systems

Inner- and outer-sphere electron transfer reactions occur in biological processes. The respiratory electron-transport chain is an example of a system in which both types of reaction are observed. It is of further relevance to examine adiabatic and non-adiabatic electron transfer in biological systems:

#### 1.2.3.1 Adiabatic Electron Transfer

As previously defined, inner-sphere redox reactions involve the formation of ligand-bridged intermediates before electron transfer can occur. Therefore, in comparison to the outer-sphere reaction, the energetic barrier to the formation of the transition state is large. This is in accordance with the Franck-Condon Principle, which states that as nuclei are significantly more massive than electrons, an electronic transition (or electron rearrangement) occurs so fast that the relative positions of the nuclei remain unchanged. Outer-sphere electron transfer reactions are mechanistically facile and follow transition state theory.

#### 1.2.3.2 Non-Adiabatic Electron Transfer

Electron-transfer reactions between metal centres in proteins are considered to be non-adiabatic in nature. This is a consequence of the large inter-metal centre distances and the insulating character of their protein surroundings. These factors combine to result in very weak coupling between the donor and acceptor potential energy surfaces, leading to a low probability of a successful reaction. An elementary description of non-adiabatic electron transfer is given by Marcus Theory (Marcus, 1956).

#### 1.2.3.3 Marcus Theory

In the non-adiabatic electron transfer described by Marcus Theory, the reactant and product may be defined as harmonic oscillators, each contained in a separate, parabolic, potential

energy well. The point of minimum potential energy in each well represents the normal equilibrium positions of all nuclei involved in the reaction. The electronic transitions taking place during electron transfer occur sufficiently rapidly that the nuclei do not change their positions during the timescale of the transition, and so are considered to be stationary according to the Franck-Condon Principle.

In order for the reaction to occur, the positions of the nuclei of the reactants and products must be the same. This position corresponds to the point at which the product and reactant potential energy parabolas intersect (Figure 1.3). The activation energy of the reaction, $\Delta G^*$, is defined by Equation 1.1 and represents the energy required for the reaction to overcome the barrier to product formation.

$$\Delta G^* = \frac{(\Delta G^\circ + \lambda)^2}{4\lambda} \qquad \textbf{Equation 1.1}$$

The reorganisation energy ($\lambda$) of the system is the energy required to rearrange the atomic nuclei of the reactants into those of the products and is comprised of two separate components; the inner-sphere rearrangement energy, $\Delta G^*_{IS}$, arising from changes within the inner spheres of the reacting centres (such as adjustments in bond lengths), and the outer-

**Figure 1.3: The reaction profile of an electron transfer reaction.**

*The diagram shows the two potential energy parabolas of the reactants (or reduced species, left) and the products (or oxidised species, right.) The activation energy of the reaction is shown by $\Delta G^*$, while the thermodynamic driving force is given by $\Delta G^\circ$, the standard free energy change of the reaction. The electronic interaction (or matrix coupling element) is defined by V and the reorganisation energy (the energy required to displace the configuration of the reactant nuclei to that of the products) is shown as $\lambda$.*

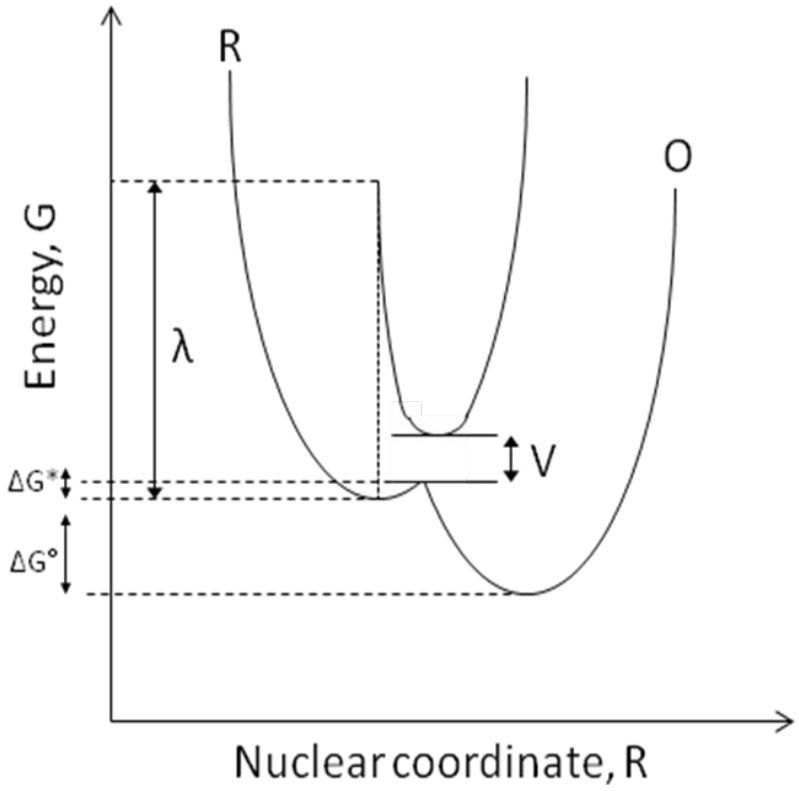


sphere rearrangement energy, $\Delta G^*_{OS}$, which is due to changes in the surrounding medium (such as solvent reorientation or movements within the protein matrix). Determining the value of λ for reactions in proteins is consequently a complicated process, although methods have been developed to assist in its calculation (Moser *et al*, 1992).

In addition to the reorganisation energy of the system, the rate of electron transfer is also dependent on the extent of the electronic coupling between the reactant and the product and the Franck-Condon factor. These factors are contained in Fermi's Golden Rule (Equation 1.2):

$$k_{ET} = \left(\frac{2\pi}{\hbar}\right) H^2 F_C \qquad \textbf{Equation 1.2}$$

where $k_{ET}$ is the rate of electron transfer, H is the matrix coupling element and $F_C$ is the Franck-Condon term (Equation 1.4).

The matrix coupling element, H, is dependent on the distance between the donor and acceptor orbitals and the nature of the intervening medium, and may be determined according to Equation 1.3:

$$H^2 = H_0^2 \exp(-\beta R) \qquad \textbf{Equation 1.3}$$

where $H_0$ is the value of the matrix coupling element to give maximum electronic coupling, β is a measure of the efficiency of the intervening medium to mediate electron transfer and R is the distance between the donor and acceptor orbitals.

The Franck-Condon term ($F_C$) is dependent on the reorganisation energy of the system (λ) and the driving force for the reaction (ΔG°), as defined in Marcus' classical expression (Equation 1.4; Marcus *et al*, 1985):

$$F_C = \frac{1}{\sqrt{(4\pi\lambda k_B T)}} \exp\left(\frac{-(\Delta G^\circ + \lambda)^2}{4\lambda k_B T}\right) \qquad \textbf{Equation 1.4}$$

The rate of electron transfer, $k_{ET}$, is therefore:

$$k_{ET} = \left(\frac{\pi V^2}{\hbar\sqrt{(\pi\lambda k_B T)}}\right) \exp\left(\frac{-(\Delta G^\circ + \lambda)^2}{4\lambda k_B T}\right) \qquad \textbf{Equation 1.5}$$

In the non-adiabatic case, when the electronic coupling, H, is very small, the harmonic oscillator functions of the reactant and product remain on separate surfaces and no reaction occurs. However, if the activation energy barrier is sufficiently small, a fast reaction can take place.

According to Equation 1.5, the thermodynamic driving force for a reaction is limited in three ways relating to the rate of electron transfer. Marcus Theory predicts an approximately parabolic dependence of the logarithm of the electron transfer rate with – $\Delta G°$, varying such that the rate increases with the driving force of the reaction to the maximum point of the parabola, when $\Delta G° = - \lambda$. Once the driving force of the reaction becomes greater than $\lambda$, the rate of electron transfer decreases.

Marcus Theory predicts three regions for electron transfer, each requiring different conditions, as described in Figure 1.4 A. Figure 1.4 B shows the potential energy diagrams relating to each case.

**The normal region:** when $\lambda > - \Delta G°$, the rate increases as the driving force increases.

**The activationless region:** when $\lambda = - \Delta G°$, there is no activation barrier to the reaction, therefore $k_{ET} = k_{max}$.

**The Marcus inverted region:** when $\lambda < - \Delta G°$, the rate of electron transfer decreases as the driving force increases.

In most redox reactions, where the reaction Gibbs energy is non-zero, the potential energy parabolas of the reactant and product are at different heights. If the product curve is above the reactant curve then the crossing point is raised, resulting in a higher activation barrier. However, if the product curve is lower than the reactant curve then two things may happen; the crossing point is lowered, reducing the activation barrier, until the point at which the position of the crossing moves across to the opposite side of the reactant curve occurs, causing the activation barrier to rise again.

If the potential energy well is steep so that there is a rapid increase in energy with bond extension, then the crossing point and therefore the activation energy of the reaction will be high. The more negative the standard Gibbs free energy of the reaction the lower the activation energy of the reaction.

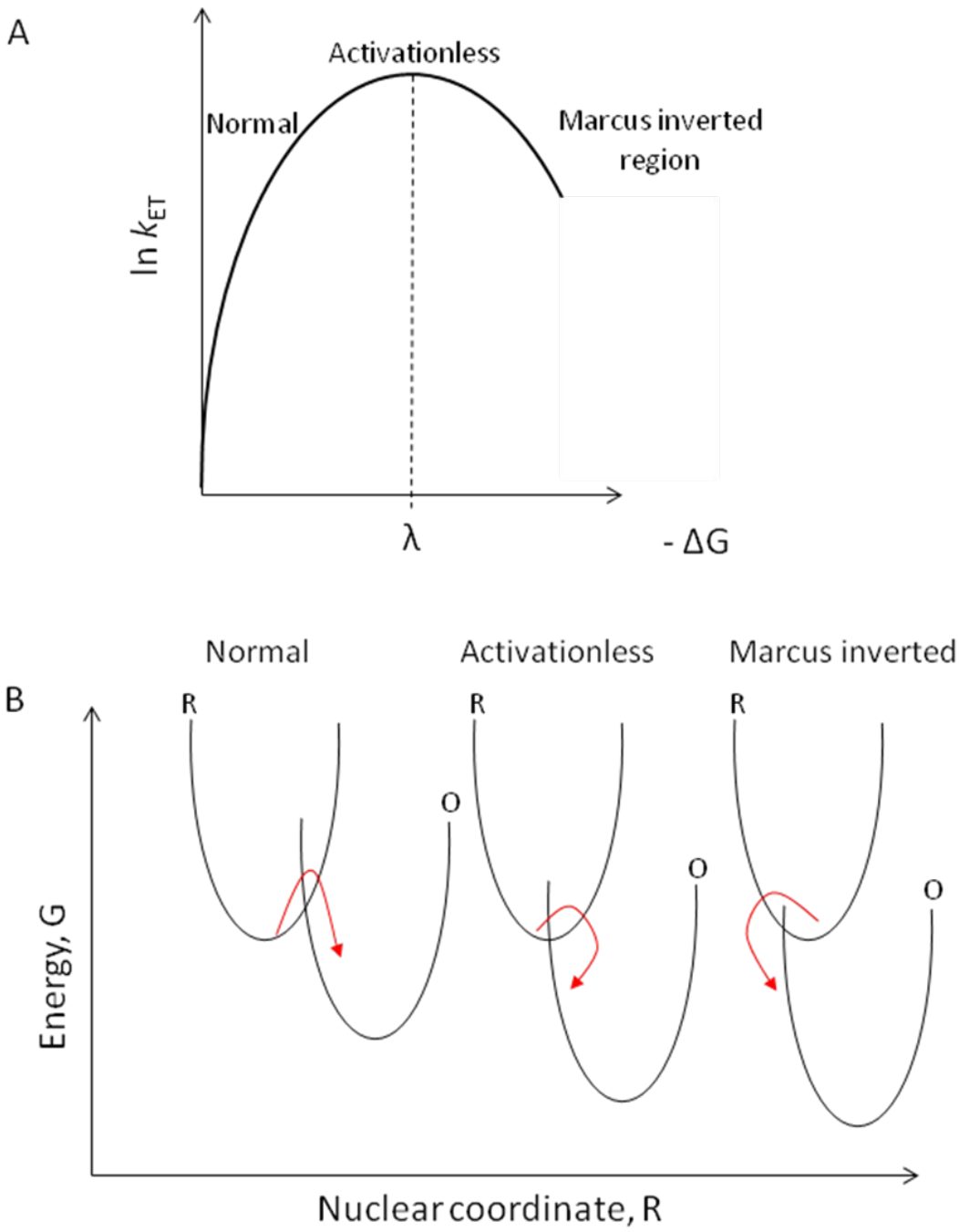


**Figure 1.4: The three regions of electron transfer according to Marcus Theory.**

*Panel A shows the three regions of electron transfer, normal, activationless and Marcus inverted, with the log of the electron transfer rate constant ($k_{ET}$) plotted as a function of the free energy of the reaction ($\Delta G°$). The reorganisation energy of the reaction, λ, occurs at the apex of the curve. Panel B shows each of the three regions of electron transfer in terms of the nuclear coordinates of their reactants and products. The activated complex is located at the intersection of the two potential energy curves.*

A reaction that does not appear to fit the Marcus equation is likely to be atypical and the discrepancy may be the result of a change in spin or symmetry during the electron transfer.

As previously described, the magnitude of the matrix coupling element (Equation 1.3) is dependent on the distance between the two redox centres, R, and the nature of the intervening medium, β. These two factors are significant to the rate of the electron transfer reaction in the following way: the rate is proportional to the overlap between the donor and acceptor wavefunctions, and this overlap is dependent on both the distance between the two centres and the composition of the medium between them.

The extent of overlap between the orbitals decreases exponentially with distance, so that the rate of electron transfer increases as overlap increases. The rate of electron transfer can thus be expressed as a function of orbital overlap and the nature of the intervening medium (Equation 1.6):

$$k_{max} = 10^{13} \exp ( -\beta ( R - R_0 )) \qquad \textbf{Equation 1.6}$$

It can therefore be determined that the maximum rate of electron transfer for a given reaction occurs at the maximum orbital overlap (the van der Waals contact of the two centres) at $10^{13}$ $s^{-1}$. The rate decreases as the distance between the centres increases. Dutton has shown that at distances greater than 14 Å electron transfer is slowed to such an extent that it is unlikely to result in a productive reaction (Page *et al*, 2003).

### 1.2.4 Electron Transfer in Systems with Multiple Redox Centres

As described in Section 1.2.1, electron transfer in biological systems commonly occurs over distances significantly greater than 14 Å. In cases such as these, electron transfer is achieved across chains of redox centres, strategically positioned in the protein matrix at distances of less than 14 Å apart.

The significance of the nature of the intervening medium, β, has resulted in a number of studies to empirically determine its value in a number of specific media. Two extreme cases have been considered; for an absolute vacuum between the redox centres $\beta = 2.8 – 3.5$ $Å^{-1}$ (Moser *et al*, 1992; Beratan *et al*, 1991), while in a through-bond singly-bridged covalent system $\beta = 0.9$ $Å^{-1}$ (Smalley *et al*, 1995). However, as neither case alone accurately describes the nature of the non-uniform medium of the protein matrix, the use of a weighted average of the two extremes has been proposed (Moser *et al*, 1992) and β is taken as $1.4 \pm 0.2$ $Å^{-1}$.

The precise nature of electron transfer through chains of redox centres in enzymes remains elusive and is currently defined by two key disparate hypotheses; electron transfer is considered as occurring either *through bond* or *through space*. In *through bond* electron transfer, electrons travel along specific pathways within the protein matrix, and so are sensitive to variations in the value of β. Conversely, *through space* electron transfer only requires a single value of β and this is taken as an average across the total pathway.

Electron-transfer pathways have been studied in a number of oxidoreductase systems with available crystal structures. These studies have indicated that electron transfer through a protein is not significantly perturbed by changes in ΔG, λ or the nature of the intervening medium, β

(Page *et al*, 1999). Rather, the electron transfer pathway of a protein is arranged so that discrete electron transfer steps do not need to be "maximised" in order for efficient electron flow. This is achieved as a result of the redox centres being sufficiently close together to permit high rates of electron transfer. The forward reaction has a small favourable ΔG, causing the forward reaction to occur at a significantly faster rate than the reverse, resulting in a defined directionality to the electron flow. This concept is illustrated in the light-energy harvesting photosynthetic reaction centre, in which closely located chlorin groups allow rapid electron transfers with favourable ΔG values to occur at a rate sufficiently fast to prevent competing decay processes, such as fluorescence, from occurring. The cofactors in this system are arranged in the manner described above so that the overlap of donor and acceptor orbitals is as great as possible. Therefore, it can be said that in this instance the *through space* model of electron transfer is most appropriate.

In other cases, such as when the redox centres are not as suitably arranged, the *through bond* model may be more suitable. Here, electron transfer occurs along a well-defined pathway, both as a series of steps through covalent and hydrogen bonds and as a series of short hops across the intervening space. Studies of ruthenated cytochrome *c* derivatives (Karpishin, *et al*, 1994) have indicated that as the distance between the donor (ruthenium) and acceptor (heme) moieties varies, correlation with the *through bond* distance is closer than the *through space* distance.

Despite the differences in these two electron transfer models, in both cases it is the distance between cofactors, reorganisation energy and driving force for the reaction that are responsible for the rate of electron transfer. It appears that both models are equally valuable in describing electron transfer in different situations; if cofactors are closely situated then electron transfer is

appropriately described as a *through space* hop, while widely spaced cofactors adhere more closely to the *through bond* mechanism.

## 1.3 REDOX COFACTORS

Many enzymes require additional small molecules in order to act as efficient catalysts. These molecules are known as cofactors and may be organic (such as coenzymes), or inorganic (such as metallic cations). The cofactor usually binds tightly to a specific site on the enzyme in order to confer activity. An enzyme lacking its essential cofactor is described as an *apoenzyme*, while the intact enzyme with the cofactor bound is described as a *holoenzyme*.

Many redox cofactors in enzymes that contain metal ions have been extensively characterised. Common iron-containing cofactors include hemes (Section 1.3.1) and the various forms of iron-sulfur clusters, and many other cofactors based around metals such as copper, molybdenum and nickel have also been studied.

The organic cofactors found in enzymes include the flavins and the quinones (Figure 1.5). The flavin cofactors are based around the isoalloxazine ring. These molecules have three redox states available to them (the oxidised form, the single-electron-reduced semiquinone form and the two-electron-reduced form) and may behave as cations, anions or neutral moieties, depending on their protonation state. These characteristics give flavins great versatility in their reactions. The flavin cofactor occurs in biological systems as either FAD (Flavin Adenine Dinucleotide) or FMN (Flavin Mononucleotide). Quinones are based around

**Figure 1.5: The structures of some flavin cofactors.**

*The structures of flavin mononucleotide (A) and flavin adenine dinucleotide (B). Figure C shows the oxidised and reduced states of the flavin ring.*

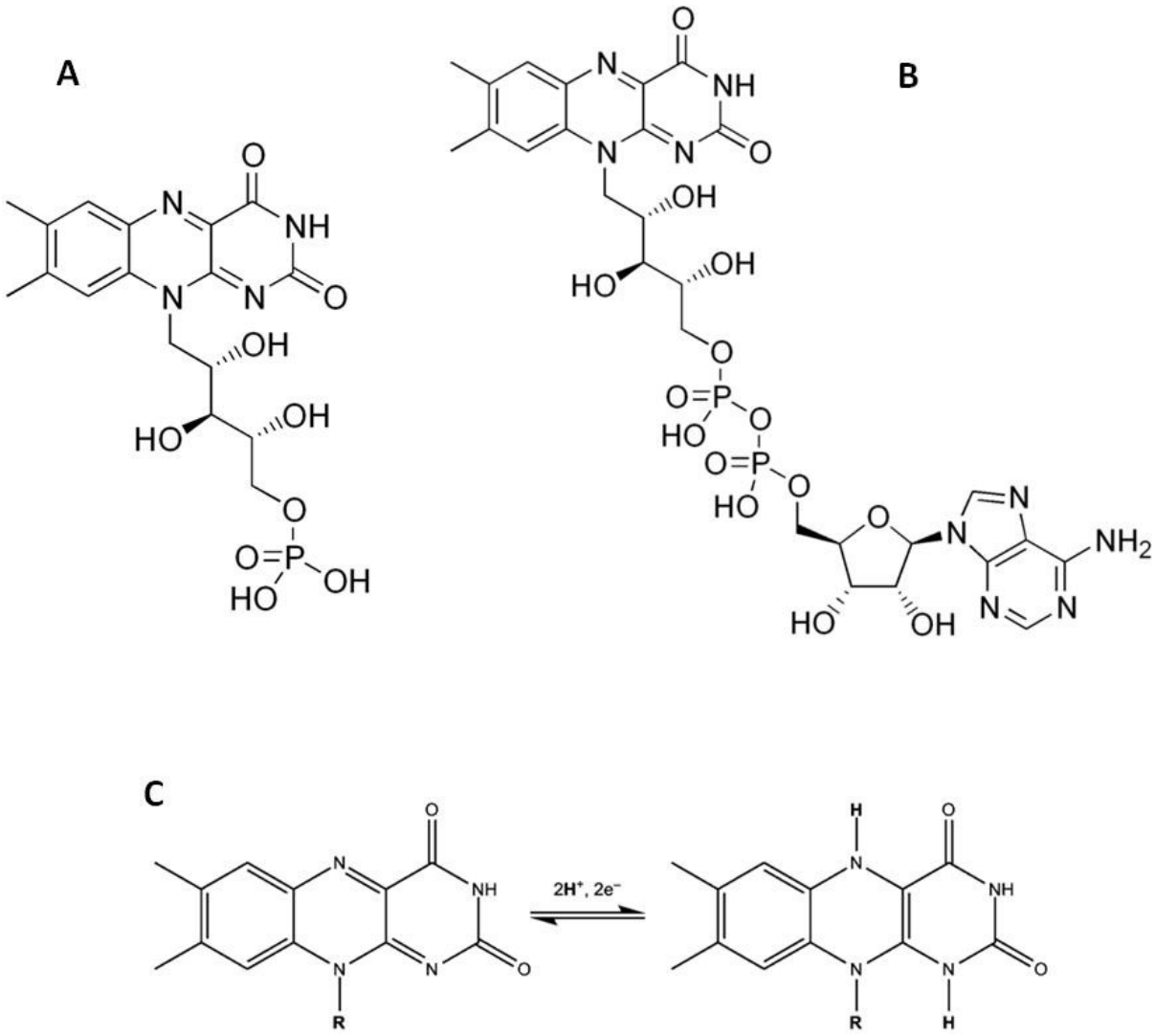

the quinone ring and are similarly able to access three oxidation states. They are hydrophobic molecules and so are found as electron carriers in membrane and lipid systems.

Yet other cofactors are found as mobile species within the cell. Examples of this class of cofactor include quinols (related to the quinones), $NAD^+$ and $NAD(P)^+$ (Figure 1.6). These last two cofactors are readily reduced to NADH (Nicotinamide Adenosine Dinucleotide) and NAD(P)H (Nicotinamide Adenosine Dinucleotide Phosphate) by the transfer of a proton and a pair of electrons, in what is formally a hydride transfer. These species are used as reducing agents within the cell, with NADH commonly acting as a cofactor to enzymes involved in catabolic pathways and NAD(P)H used in anabolism.

**Figure 1.6: The structures of $NAD^+$ and $NADP^+$.**

*The structural difference between $NAD^+$ and $NADP^+$ is the addition of a phosphate at the adenosyl C-2' position.*

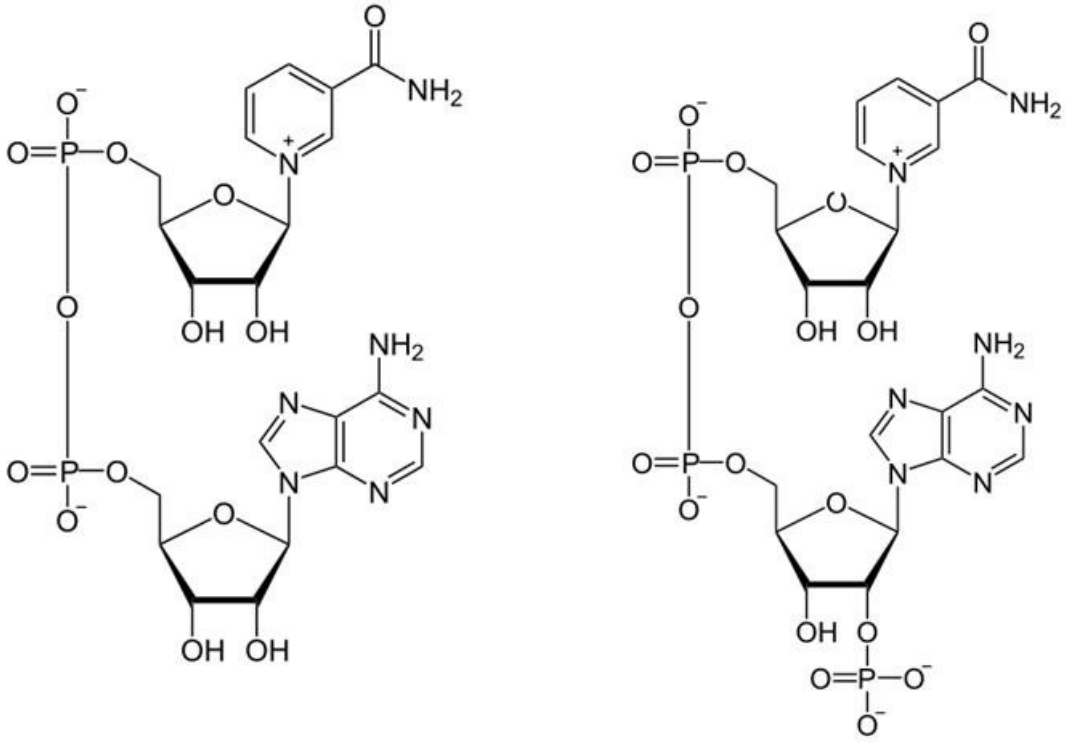

### 1.3.1 Heme

The cofactor of primary interest in this thesis is heme and it shall therefore be examined in closer detail. The heme cofactor is the most common form in which iron is bound in biological systems and is involved in a number of different enzymes concerned with the reactions of oxidation and reduction.

The heme moiety consists of a central iron atom that is coordinated by four nitrogen atoms in a square planar arrangement, leaving two vacant coordination sites for further ligation (Figure 1.7). These nitrogen atoms are derived from four pyrrole groups that are connected by methylene bridges to form the protoporphyrin IX macrocycle. The two vacant coordination sites of the iron are filled by either amino-acid side chains from the protein backbone or exogenous ligands. The coordination of the iron atom may, therefore, be any of square planar (with no ligation of the fifth and sixth positions), square-based pyramidal (with ligation at the fifth position) or octahedral (fully ligated with no vacant coordination sites).

The heme cofactor commonly occurs as a one-electron cofactor, with the central iron atom found in either of its most stable oxidation states as the ferrous ($Fe^{II}$) or ferric ($Fe^{III}$) form. In addition to this, the ferryl ($Fe^{IV}$) form has also been found to occur in some cases, such as the cytochromes P450 and the heme-copper oxidases.

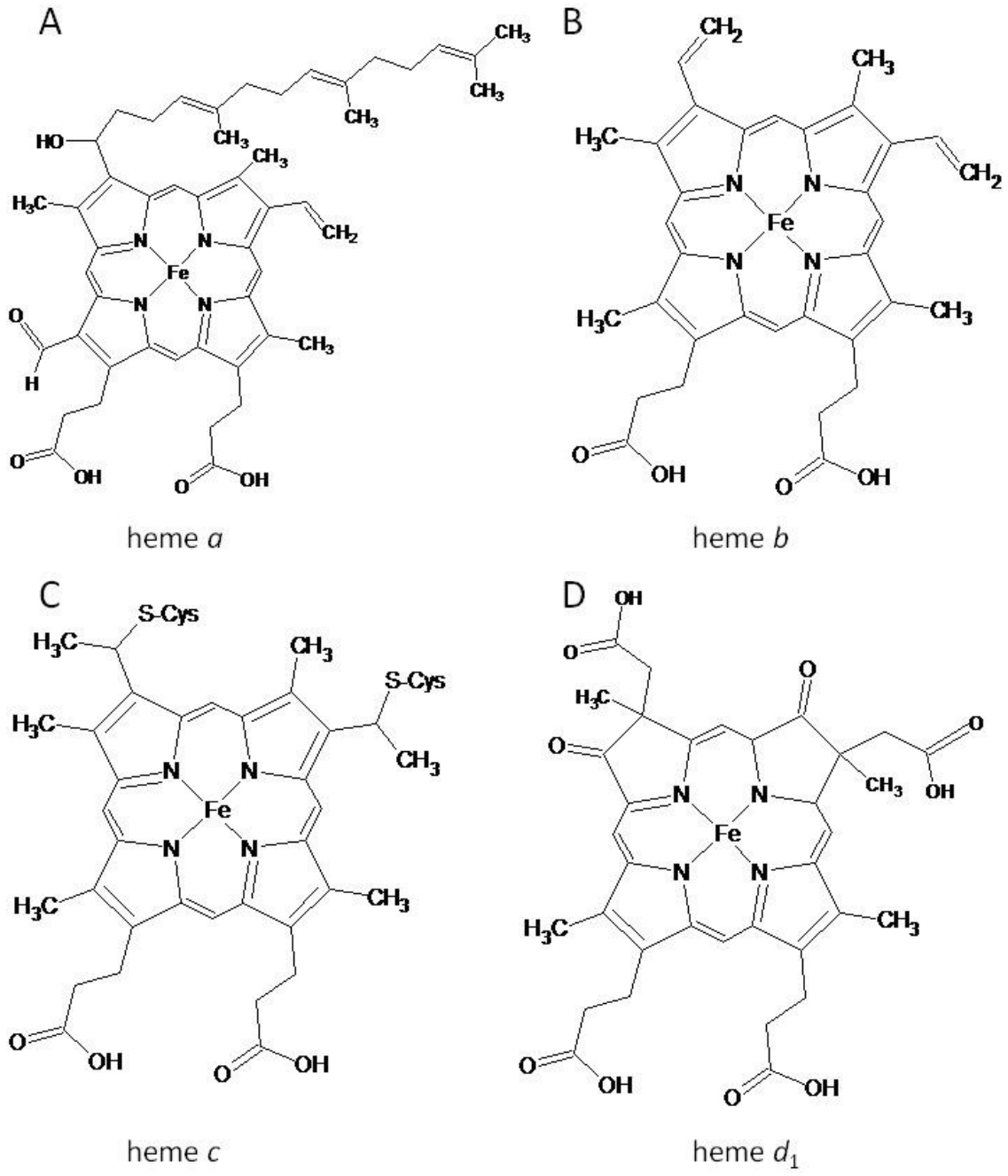


**Figure 1.7: The structures of four different types of heme; *a*, *b*, *c* and $d_1$.**

*Structures A-D show the arrangements of the four different types of heme group; a, b, c and $d_1$ respectively. Structure B shows the configuration of the protoporphyrin IX system, heme b, and the remaining structures are modifications of this system. Heme a has an additional hydroxyethylfarnesyl side chain and formyl group. Heme c has two thioether linkages to cysteine residues, through which the heme is covalently attached to the protein backbone. Heme d contains two additional carboxylic acid groups and the porphyrin ring has fewer double bonds.*

There are four main classes of heme (*a, b, c* and $d_1$), which are characterised by the different substituents on the periphery of their porphyrin ring (Figure 1.7). The iron-protoporphyrin IX system, as described above, is known as the *b*-type heme. The *a*-type heme is characterised by the presence of an additional formyl group and a seventeen-carbon hydroxyethylfarnesyl side chain. Heme *c* is distinguished from the other classes of heme by its covalent attachment to the protein backbone. This attachment is formed by the reaction of two vinyl groups of the porphyrin ring with two cysteine residues from the protein, producing two thioether linkages. The $d_1$ type heme contains fewer double bonds than heme *b* within the porphyrin ring and also features additional carboxylic acid groups. Two additional classes of heme are encountered within bacterial respiratory chains and these are known as heme *d* and heme *o*. Heme *d* is similar in structure to heme $d_1$, while heme *o* appears to be intermediate between types *a*- and *b*-, with the addition of the farnesyl moiety but no formyl group.

Heme complexes exhibit characteristic visible absorption spectra dominated by $\pi \rightarrow \pi^*$ electronic transitions in the porphyrin ring. These spectra differ depending on the oxidation state of the iron atom and the nature of its ligands and this allows the different classes of heme to be readily distinguished.

## 1.4 CYTOCHROMES

Cytochromes are versatile heme-containing proteins that are involved in a number of processes, including electron transport, signalling, catalysis and some regulation of protein expression. They are found throughout Nature in all forms of aerobic life and display a diverse range of biological functions, including a central role in photosynthesis and respiration. Cytochromes

are classified according to the structure of their heme group. Many cytochromes have been intensively studied and characterised, leading to a wealth of high resolution three-dimensional structures.

### 1.4.1 *C*-type cytochromes

The major feature distinguishing *c*-type cytochromes from *b*-type cytochromes is the presence of a covalently attached heme moiety that is linked via thioether bonds between the two vinyl groups of the heme and two cysteinyl residues which form part of a characteristic C-X-X-C-H motif. The histidinyl residue of this motif acts as the axial ligand to the heme iron. The sixth ligand to the iron is also generally a strong field ligand, such as histidine or methionine, and so the resulting complexes are octahedral and low-spin. This octahedral structure leaves no vacant sites for further coordination and these types of *c*-type cytochromes are usually involved in simple electron transfer reactions.

Cytochromes *c* generally function by a reversible change in the redox state of the central iron. The reduced, ferrous ($Fe^{II}$) form of cytochrome *c* is pink in solution, with absorption bands at 551, 522 and 415 nm (Figure 1.8). These bands are known as the α, β and γ (or Soret) band respectively. It is readily oxidised to give an orange solution with absorption bands at 530 and 400 nm.

The *c*-type cytochromes are one of the largest families of heme-containing proteins and recent advances in the genomic analysis of bacteria have indicated a wealth of genes encoding novel *c*-type cytochromes that contain multiple numbers of heme cofactors.

**Figure 1.8: The Typical UV/visible absorption spectrum of a *c*-type cytochrome.**

*The reduced, ferrous ($Fe^{II}$), spectrum is shown in black, while the oxidised, ferric ($Fe^{III}$), spectrum is given in black. The α, β and γ bands are indicated on the reduced spectrum.*

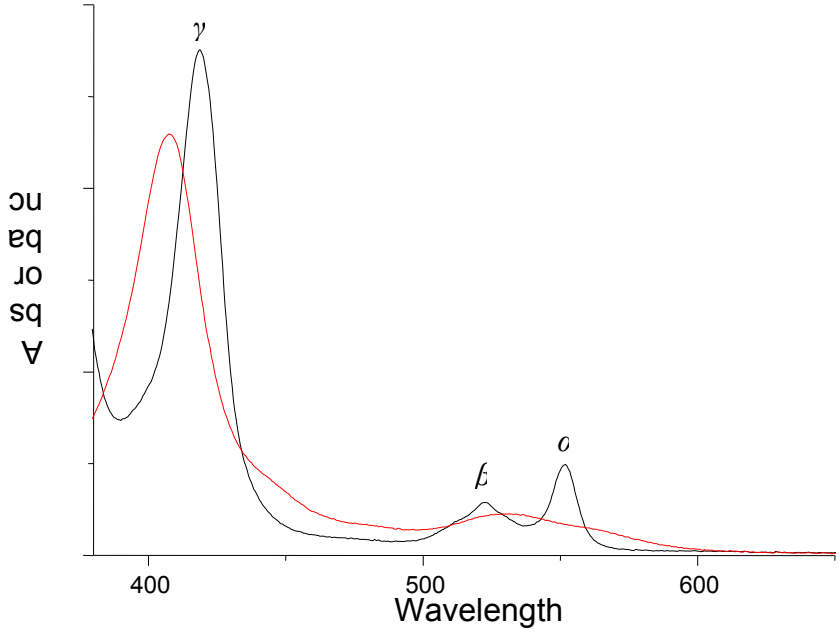


These multiheme cytochromes are commonly found in sulfur- and sulfate-reducing bacteria including the *Desulfovibrio*, *Geobacter* and *Shewanella* genera, where they are involved in electron transfer pathways. There is also a well-characterised group of multiheme cytochromes which have the ability to bind substrates at one of their heme groups, leading to enzymatic activity. There is increasing evidence that homology between the arrangement of the heme groups in these proteins is significant to their functions (Mowat & Chapman, 2005). Multiheme structures are therefore of significant interest for study and will be further examined in this thesis (Section 1.7.2.3).

In addition to the well-characterised electron-transport roles of *c*–type cytochromes in respiration and photosynthesis, additional functions within the cell have been described. The release of cytochrome *c* from the mitochondria of eukaryotes has been found to be a requirement for programmed cell death, or apoptosis (Kluck *et al*, 1997; Adrain *et al*, 2001). There is evidence that, in certain prokaryotes, defects in the biogenesis of cytochrome *c* leads to a dramatic 100-fold increase in the production and excretion of heme biosynthetic intermediates (Biel *et al*, 1990). Further to this, in *Pseudomonas fluorescens* faults in some of the cytochrome *c* biogenesis genes can result in the loss of copper resistance (Yang *et al*, 1996) and the production of pyoverdine (Gaballa *et al*, 1996), while similar genetic faults in *Rhizobium leguminosarum* lead to iron acquisition (Yeoman *et al*, 1997). It therefore seems to be the case that *c*-type cytochromes have applications within the cells in the area of signalling.

The advancement of techniques used to produce recombinant cytochromes *c* has motivated the emergence of new research into aspects beyond their physiological roles; medical, experimental and technical applications of *c*-type cytochromes are now being investigated. Knowledge of the ability of cytochrome *c* released from the mitochondria to trigger apoptosis may have applications in tumour treatment. Studies have found that exogenous cytochromes can have a similar effect and have been shown to induce apoptosis in macrophages and melanoma cells when used in combination with azurin (Yamada *et al*, 2002). The characteristic red colour of the heme absorbance of cytochromes is leading to its applications in fusion proteins to track the expression of other periplasmic proteins, and the *Geobacter* cytochrome PpcA is being investigated as a biosensor (Londer *et al*, 2004). Another possibility for the use of cytochromes lies in bioelectronics, where their high electron transfer efficiency is exploited in chains of polymeric cytochrome $c_7$-like molecules that are assembled into "nanowires" to

transfer electrons between the periplasm or outer membrane to environmental substrates, providing a model for the design of superconductors (Gilardi *et al*, 2001).

### 1.4.2 Cytochrome *c* Biogenesis

The biogenesis of *c*-type cytochromes is carried out by the cytochrome *c* maturation (C*c*m) system. It is a complex process, involving the separate transport of component parts of the cytochrome across membranes to specific subcellular locations, followed by their subsequent post-translational assembly into native heme-containing conformations. The characteristic reaction of cytochrome *c* biogenesis occurs at the Cys-Xxx-Yyy-Cys-His amino acid motif and involves the covalent ligation of the heme vinyl groups to the two cysteinyl residues of the apocytochrome.

The formation of the thioether bonds which covalently attach the heme to the apocytochrome is not a simple process and there has been some discussion as to why this covalent attachment is advantageous in *c*-type hemes when it is not required in any other form of heme (Barker *et al*, 1999; Allen *et al*, 2003b; Stevens *et al*, 2004). Studies on cytochrome $c_{552}$ from the thermophilic bacterium *Hydrogenobacter thermophilus*, in which the mutation CXXCH to AXXAH results in the loss of both thioether bonds, produces a non-covalently bound heme with a tertiary structure close to that of wild type (Tomlinson *et al*, 2000a; Wain *et al*, 2004). This conversion of *c*-type to *b*-type heme in the protein led to decreased thermal and chemical stability of both the oxidised and reduced forms, while the reduction potential was only shifted by a comparatively small -70 mV. Mutation to AXXCH or CXXAH, resulting in the loss of only one thioether bond, has a much smaller influence on stability and potential (Tomlinson *et*

*al*, 2000b). The reason for the large effect of just one thioether bond is unclear, although it is thought that the smaller entropy gain on the unfolding of a *c*-type compared to a *b*-type cytochrome (in which the heme dissociates from the apocytochrome) may be significant. The covalent attachment of *c*-type hemes may also be advantageous in allowing greater heme incorporation for a given number of amino acids by fixing the hemes spatially *via* their thioether bonds (Allen *et al*, 2003b). This increased heme packing, observed in some of the multiheme cytochromes, allows the rapid electron transfer commonly observed in such proteins.

Analyses of genomic sequences combined with studies of a number of organisms, including *Saccharomyces, Neurospora*, model bacteria and *Chlamydomonas*, have led to the belief that three distinct systems exist in nature for the biogenesis of *c*-type cytochromes (Kranz *et al*, 1998). These have been designated as systems I, II and III in order of their supposed evolutionary progression and decreasing complexity from system I to III. Recent speculation has also suggested the possibility of two additional systems, proposed to be systems IV and V (Allen *et al*, 2005).

Systems I and II are used by prokaryotes, plant mitochondria and chloroplasts, and are characterised by the use of dedicated mechanisms for heme delivery, apocytochrome transport and thioreduction. System III has evolved in fungal mitochondria, vertebrates and invertebrates and is distinguished by the use of the enzyme cytochrome *c* heme lyase (CCHL) in the mitochondrial intermembrane space. The unusual mitochondrial cytochromes *c* from the trypanosomatids and euglenids do not appear to be matured by any of Systems I-III, leading to the proposal that they require the putative Systems IV and V.

It is believed that the three main systems follow a number of common general principles and requirements (Allen *et al*, 2005). All *c*-type cytochromes contain one or more heme binding amino acid motifs (CXXCH), in which the cysteine residues are the points of covalent attachment for the heme. They all contain an N-terminal signal sequence which directs their movement from the location of apocytochrome synthesis to their place of function. This may be from the cytoplasm to the mitochondria or chloroplasts, or in bacteria *via* the type II secretion pathway to the periplasm. The apocytochrome *c* is transported to its site of function prior to heme attachment. The apocytochrome cysteines must then locate the heme (which has also been transported to this location from its site of synthesis) and stereospecifically attack the carbons of the heme vinyl side chains. In order for this to occur the cysteines must be reduced. Finally, heme ligation is thought to precede the folding of the protein into its native conformation.

As a consequence of this there are several key characteristics required for a cytochrome *c* maturation system; the apocytochrome *c* must be recognised, the heme cofactor transported to the site of maturation, the proper stereospecific alignment of the heme vinyl groups achieved and the apocytochrome cysteine residues orientated for their subsequent reaction to form thioether bonds.

However, a number of questions concerning these processes arise (Allen *et al*, 2003b). If the assembly of the holocytochrome *c* is carried out at the site of function, how are the heme and apocytochrome transported to their final destinations in the cell? How are the heme and the apocytochrome cysteinyl side chains kept reduced (in order for ligation to occur) in the presence of oxygen and other reactants? By what mechanism does covalent heme attachment occur?

Although some commonalities in these processes exist between systems, there are also a number of dissimilarities. It should also be noted that the cytochrome *c* maturation genes from different organisms are frequently described using a variety of alternative names (for example, the *Escherichia coli* gene *ccmA* is known in *Bradyrhizobium japonicum* as *cycV* and in *Rhizobium etli* as *helA* (Thöny-Meyer, 1997). For the sake of clarity, the following description will use the nomenclature assigned in *Escherichia coli* as described by Page *et al* (1998) as far as possible.

#### 1.4.2.1 System I

Cytochrome *c* maturation system I is observed most commonly in Gram-negative bacteria, such as *Escherichia coli*, and plant mitochondria. The most complex and most characterised cytochrome *c* maturation system to date is that of *E. coli* (Thöny-Meyer, 1997 and 2002), which is comprised of the maturation proteins CcmABCDEFGH, located in the periplasm and/ or the cytoplasmic membrane (Figure 1.9). The delivery and attachment of heme to the apoprotein is thought to be carried out by these proteins, which may be assembled into a membrane protein complex. The Ccm system is periplasmically-located, with all bacterial cytochromes *c* being either periplasmic or anchored to the periplasmic face of the cytoplasmic membrane. The precise roles of many of the Ccm proteins are unknown and research into this area is ongoing.

Apocytochrome *c* is transported from the bacterial cytoplasm to the periplasm by the Sec system and the peptide leader sequence cleaved by the Lep peptidase (Thöny-Meyer *et al*,

**Figure 1.9: Pathway of System I cytochrome *c* maturation.**

*(Adapted from Thöny-Meyer, 2002). The pre-apocytochrome c is transported to the periplasm by the Sec pathway and its leader sequence cleaved by the Lep peptidase. CcmG reduces the cysteines of the heme-binding site and CcmH guides the apocytochrome to the CcmEF complex to facilitate heme attachment. The heme is exported to the periplasm by CcmCD prior to ligation to His130 of CcmE. CcmA and –B are potential heme transporters, whose precise role is unclear. CcmE binds transiently to the heme, which is then transferred by CcmF to the apocytochrome c.*

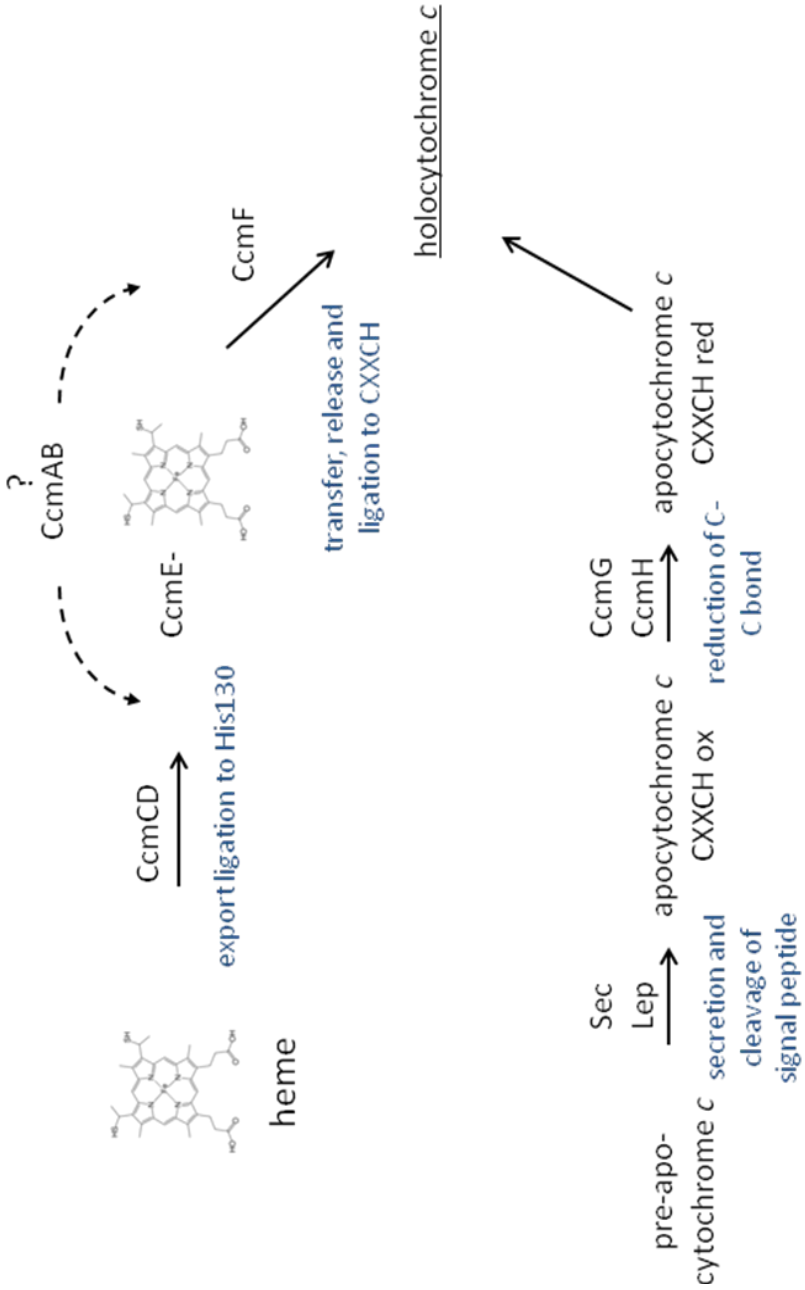

1997). The method by which heme is transported to the periplasm is unclear, however CcmA and CcmB are thought to be potential heme transporters, possibly acting in conjunction with CcmC and CcmD, as a result of sequence analysis which suggests that they may form a putative ATP-dependent transporter. While the precise functions of CcmABC and -D are unclear, it is known that the next stage of maturation, the attachment of heme to CcmE, is CcmC-dependent (Schulz *et al*, 1999). CcmE is a key component of the Ccm maturation apparatus and is a periplasmic-facing heme chaperone, anchored to the membrane, which transiently binds the heme (Schulz *et al*, 1998).

CcmE forms a covalent bond between its completely conserved histidine residue and one of the heme vinyl groups (Daltrop *et al*, 1992), assumed to be a C-N bond. On the subsequent transfer of the heme to the apocytochrome *c*, the breaking of this covalent bond is dependent on CcmFG and -H. It is unknown whether CcmE acts as part of a CcmCEF complex or simply functions as a heme-shuttle between CcmC and CcmF (Thöny-Meyer, 2003). However, some interesting points about the mechanism of heme attachment are known;

1. The precise stereochemistry of heme attachment is conserved in every *c*-type cytochrome structurally characterised to date (although spontaneous thioether bond formation is possible, the reaction results in heterogeneous products, suggesting that CcmE may select one of the heme vinyls specifically (Allen *et al*, 2003a)).

2. Heme transfer can only occur in cytochromes with two cysteine residues in their heme attachment motif (suggesting that the Ccm system may recognise the two thiols of the CXXCH motif and that the two thioether bonds compensate for the breaking of the single histidine-heme bond of the CcmE-heme complex (Allen *et al*, 2002)).

3. System I cannot function without the presence of a reductant (the DsbD protein acts as the physiological reductant). The requirement for a reductant may be a consequence of a need to reduce a disulfide in the CXXCH motif or to maintain iron in the 2+ oxidation state. CcmG is a thioredoxin-like protein (Edeling *et al*, 2002) and CcmH has some similarity to a disulfide reductase (Thöny-Meyer, 2000), indicating that they are probably involved in the transfer of reductant from DsbD to the heme or CXXCH disulfide.

Following transient attachment to CcmE, it is proposed that CcmF catalyses the transfer of the bound heme to the apocytochrome (Thöny-Meyer, 2002). CcmF has been found to interact directly with both CcmE and CcmH (Ren *et al*, 2002) and has been described as the bacterial heme lyase.

CcmG is a periplasmic thioredoxin that interacts with DsbD to transfer electrons to the apocytochrome, reducing the cysteines of the heme binding site (Katzen *et al*, 2000). CcmG is thought to act in conjunction with CcmH, a protein which is proposed to recognise the heme binding sites of the apocytochrome and guide them to the CcmEF complex to facilitate heme attachment (Thöny-Meyer, 2000).

Despite the ambiguity in the functions of many areas of the Ccm apparatus, it appears that the Ccm system first recognises the CXXCH amino acid motifs in the unfolded apocytochrome and then attaches the hemes. The folding of the protein to its native state is the final stage of the process.

Interestingly, *E. coli* also contains two orthologues of the cytochrome *c* maturation proteins CcmF and CcmH, known as NrfE and NrfF respectively. NrfE has been shown to have a role in the assembly of unconventionally lysine-ligated binding site of the pentaheme cytochrome *c* nitrite reductase, NrfA. Attachment of the heme to this unusual binding site in NrfA requires NrfEF and –G, while the attachment of the remaining four conventionally-ligated hemes is carried out by the Ccm proteins (Eaves *et al*, 1998).

#### 1.4.2.2 System II

System II is found in some Gram-negative bacteria (the α-, some β- and most γ-proteobacteria), most Gram-positive bacteria, cyanobacteria and plant and algal chloroplasts. It is thought that System II biogenesis requires three or four proteins (ResA, -B and -C and CcdA), but the precise functioning of this system is, again, unclear.

The precise method of translocation of the heme across the cytoplasmic membrane is unknown, as for System I. The disulfide bond between the thiol groups of the apocytochrome cysteine residues is reduced by electrons transferred by CcdA. In addition to this, disulfide bond formation, in at least some organisms with System II, is catalysed by the Bbd proteins, which show some similarity to the Dsb proteins of System I.

The structure of the soluble domain of ResA reveals a cleft thought to be tuned for binding the apocytochrome CXXCH motif (Crow *et al*, 2004). No CcmE analogue to transiently bind the heme has yet been identified in System II, although stereospecificity in heme attachment is retained.

#### 1.4.2.3 System III

System III is found in the mitochondria of fungi, vertebrates and invertebrates and is also present in the genomes of the bacteria *Chlamydomonas reinhardtii* and the malaria parasite *Plasmodium falciparum.*

System III is the simplest of the cytochrome *c* maturation systems and investigations into cytochrome *c* maturation in the mitochondria of yeast and *Neurospora crassa* have revealed the existence of just a single enzyme, cytochrome *c* heme lyase (CCHL), which is required for thioether bond formation between the heme and the apoprotein (Nicholson *et al*, 1987 and 1988).

In fungal mitochondria, different CCHLs are used to produce the different *c*- and $c_1$-type cytochromes (for example, yeast uses two different heme lyases (Bernard *et al*, 2003)).

#### 1.4.2.4 Systems IV and V

Systems IV and V seem to be present in the euglenids and trypanosomatids, where the mitochondrial *c*- and $c_1$- type cytochromes unusually contain only a single cysteine residue in their heme-binding motif (e.g. XXXCH). In these cytochromes there is, therefore, only one thioether bond joining the heme to the apocytochrome. It has been shown that none of systems I-III are present in the genome of any trypsanosomatid (Allen *et al*, 2004), giving rise to the proposal of the existence of these additional systems.

#### 1.4.2.5 Evidence for the use of multiple biogenesis systems in some organisms

It must also be noted that, contrary to previous belief, recent studies have indicated that some organisms contain more than one biogenesis system functioning simultaneously. Genomic analysis has shown the malarial mosquito *Anopheles gambiae* to contain components of all of Systems I-III (Thöny-Meyer, 2003) and other analyses have indicated that the β-proteobacteria *Bordetella bronchiseptica* and *Bordetella parapertussis* contain all parts of Systems I and II. Any functional degeneracy in these organisms is yet to be determined.

## 1.5 RESPIRATION

Respiration is the sequence of reactions by which adenosine triphosphate (ATP) is regenerated, a process that is fundamental to all life. It involves redox reactions which occur in a series of steps, or chains, allowing oxidation and reduction to be carried out in stages. Respiration requires an ultimate electron acceptor, which may be inorganic or, in the case of some organisms, a simple organic compound (such as fumarate). There are two types of respiration; aerobic and anaerobic.

Aerobic respiration occurs in the presence of oxygen and is the only type of respiration available to mammalian systems. Bacteria, however, are commonly able to respire anaerobically, in the absence of oxygen, on a wide variety of other substrates.

The process of respiration involves the use of respiratory chains, or assemblies of discrete electron carriers that are grouped together into larger respiratory complexes which are commonly associated with either the mitochondrial inner-membrane or the bacterial cytoplasmic membrane. Electrons are transferred through these complexes across the membranes, resulting in a flow of electrons from a low potential donor (the quinol pool) to a higher potential acceptor (such as oxygen). The respiratory complexes simultaneously pump protons back in the reverse direction across the cell membrane to create a proton gradient ($\Delta\mu H^+$), leading to an increased acidity in the periplasm or mitochondrial inner-membrane space which drives ATP synthesis by a "proton motive force".

Aerobic respiration, also known as oxidative phosphorylation, is the more efficient of the two processes as it produces the largest proton gradient across the membrane. However, in anaerobic environments, bacteria are able to express a range of different respiratory enzymes, allowing them to use a wide range of terminal electron acceptors for respiration.

### 1.5.1 Aerobic Respiration

The respiratory pathways of plants and mammals show very little variation and are, in general, composed of five multi-component respiratory complexes. A brief description of this respiratory chain follows (Figure 1.10):

Complexes I-IV move electrons through the membrane and generate a proton gradient across the inner membrane. Complex V then uses this proton gradient to drive the catalytic production of ATP from ADP and inorganic phosphate.

Complex I, the NADH:quinone oxidoreductase (or NADH dehydrogenase), is the largest of the respiratory complexes and catalyses the transfer of two electrons from NADH to the quinol pool and the movement of two protons in the reverse direction across the membrane. This is a highly complex enzyme, for which a crystal structure has not yet been obtained, but is thought to contain a number of iron-sulfur clusters and an FMN molecule.

Complex II is the succinate:quinone oxidoreductase enzyme and catalyses the two-electron oxidation of succinate to fumarate, which is coupled to a two-electron reduction of the quinol pool.

Complex III, the ubiquinone: cytochrome *c* oxidoreductase (cytochrome $bc_1$), is a globular protein containing a Rieske iron-sulfur cluster, two *b*-type hemes and a cytochrome $c_1$ and acts as a functional dimer. Electrons are passed to Complex III in a complicated process involving the two turns of the Q cycle, from the quinol pool, first to the Rieske centre, then along the redox chain to cytochrome $c_1$ and finally to the small mobile electron shuttle protein, cytochrome *c*. This process releases two electrons to Complex IV and oxidises one ubiquinol ($UQH_2$) molecule to ubiquinone (UQ).

**Figure 1.10: The arrangement of the aerobic respiratory pathway (p. 39).**

*The schematic in Panel A shows the electron transport complexes I-IV with their cofactors and the flow of electrons. Complexes I, III and IV pump protons across the membrane, producing an electrochemical gradient that is used by Complex V to drive ATP synthesis. Panel B shows the crystal structures (where available) of the respiratory complexes. The structure shown for succinate dehydrogenase is that of the closely related fumarate reductase from Wolinella succinogenes.*

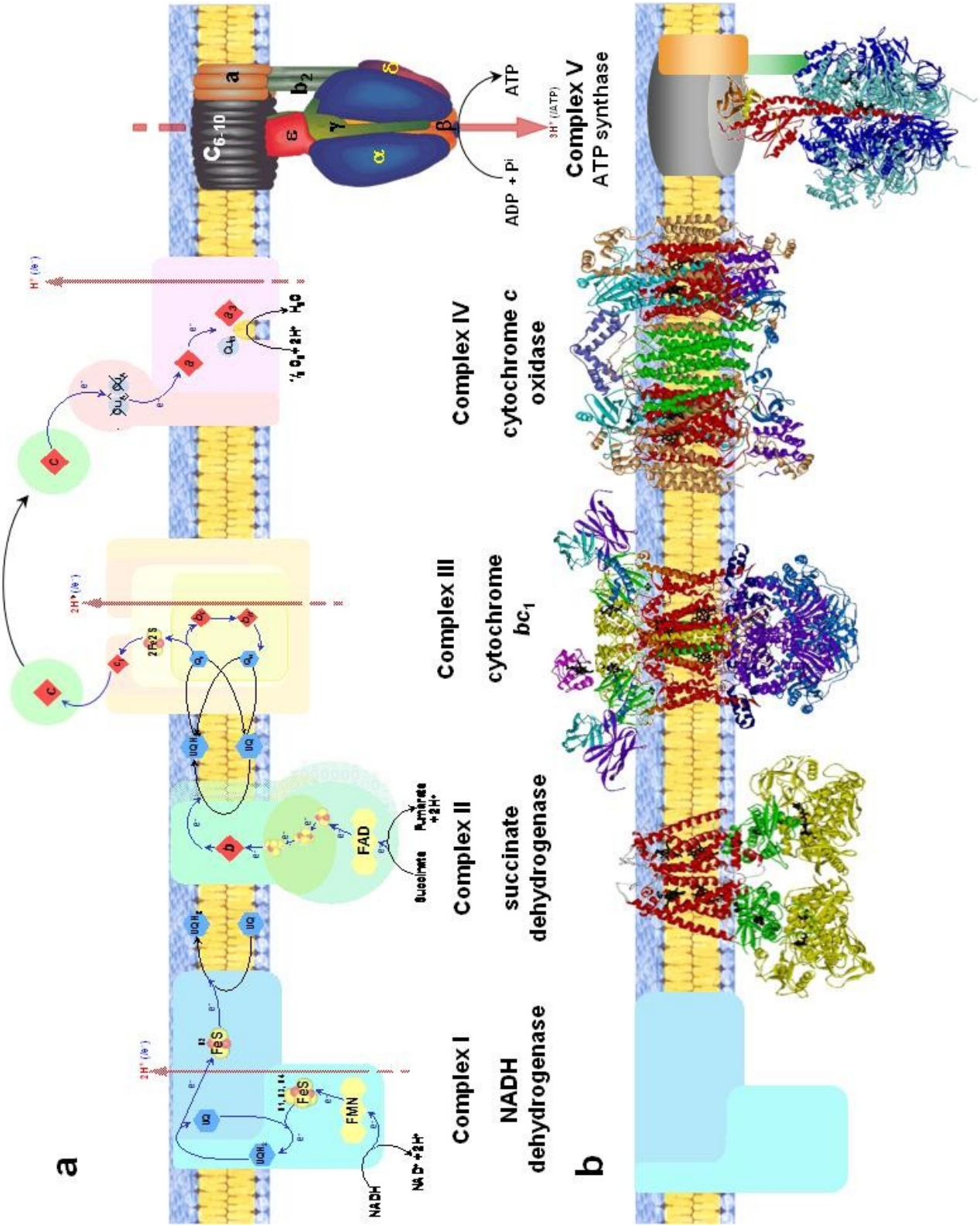
a
b
Complex I
NADH
dehydrogenase
Complex II
succinate
dehydrogenase
Complex III
cytochrome
$bc_1$
Complex IV
cytochrome *c*
oxidase
Complex V
ATP synthase
ATP
ADP + $P^i$
FAD
FMN
FeS
NADH
UQ
UQH$_2$
Cyt *c*

Complex IV, the ferricytochrome:$O_2$ oxidoreductase (cytochrome *c* oxidase) enzyme, is the terminal complex in the aerobic respiratory pathway and reduces molecular oxygen to water in the inter-membrane space whilst pumping protons across the membrane. Complex IV has two subunits; subunit I contains one *a*-type and one $a_3$-type heme and a $Cu_B$ centre, while subunit II contains a $Cu_A$ centre which is the location of docking of the cyctochrome *c* electron shuttle. The shuttle passes one electron to the $Cu_A$ centre, which is rapidly transferred to the *a*- and then the $a_3$-type heme. The $a_3$-type heme forms a dinuclear oxygen binding site with the $Cu_B$ centre. Dioxygen reduction to water occurs *via* a number of intermediates at the cytoplasmic face of the enzyme and four protons are taken up from the cytoplasm. This reduces the acidity in the cytoplasm and increases the proton gradient across the membrane.

Complex V, the $F_1$-$F_0$-ATP synthase, consists of two regions; the $F_1$ region of the enzyme is soluble and is located in the periplasm, while the $F_0$ region is membrane bound and contains a transmembrane channel. They are joined by a "stalk" which allows the $F_1$ region to rotate in a process driven by the flow of protons through the channel from the acidic periplasm back to the less acidic cytoplasm. The driving force for ATP synthesis is this rotation of the Complex V system (Leslie & Walker, 2000; Rubinstein *et al*, 2003).

### 1.5.2 Anaerobic Respiration

The composition of the electron transport chains of anaerobic respiratory apparatus can vary widely, as a result of the different electron sources and acceptors that can be used by prokaryotic organisms. These chains can even vary within a particular organism as a response to specific growth conditions which may be encountered.

In anaerobic conditions, many bacteria express alternatives to the oxygen-reducing Complex IV. They are capable of using a wide range of terminal electron acceptors and may produce a number of different terminal complexes in order to respond to varying environmental conditions. For example, the common terminal electron acceptor fumarate is reduced to succinate by the quinol:fumarate reductase.

Anaerobic respiration is similar to aerobic respiration in that it is concerned with the production of a $\mu\Delta H^+$ gradient to drive ATP synthesis. Anaerobic respiratory chains are generally shorter than their aerobic counterparts and contain fewer components, although these components are distinctly more variable. For example, a hydrogenase and/or formate dehydrogenase may provide the means to reduce the membrane-bound quinones, and fumarate reductase in turn takes electrons from the quinol pool to reduce the terminal electron acceptor, fumarate.

The bacterial genus *Shewanella* is known to respire on a particularly wide range of terminal electron acceptors (Section 1.7).

## 1.6 THE BIOLOGICAL NITROGEN CYCLE

The biological nitrogen cycle (Figure 1.11) describes the diverse number of redox reactions, primarily occurring in bacteria, that interconvert nitrogen species across the range of their oxidation states, from nitrate (+5) to ammonia (-3). These reactions occur via a series of intermediates including dinitrogen, nitrite, nitric oxide, nitrous oxide and hydroxylamine, and are catalysed by a number of metalloenzymes. The structures and mechanisms of some of

**Figure 1.11: The biological nitrogen cycle.**

*This figure shows the reactions of the biological nitrogen cycle, in which a number of redox reactions are involved in the interconversion of nitrogen-containing species. The processes by which nitrite is reduced to dinitrogen are described as respiratory denitrification, while the conversion of ammonium to nitrate via hydroxylamine and nitrite is termed respiratory nitrification. The direct reduction of nitrite to ammonium is called respiratory nitrite ammonification. The enzymes that carry out each reaction are shown in blue and the section of this thesis in which each process is described is indicated in parentheses.*

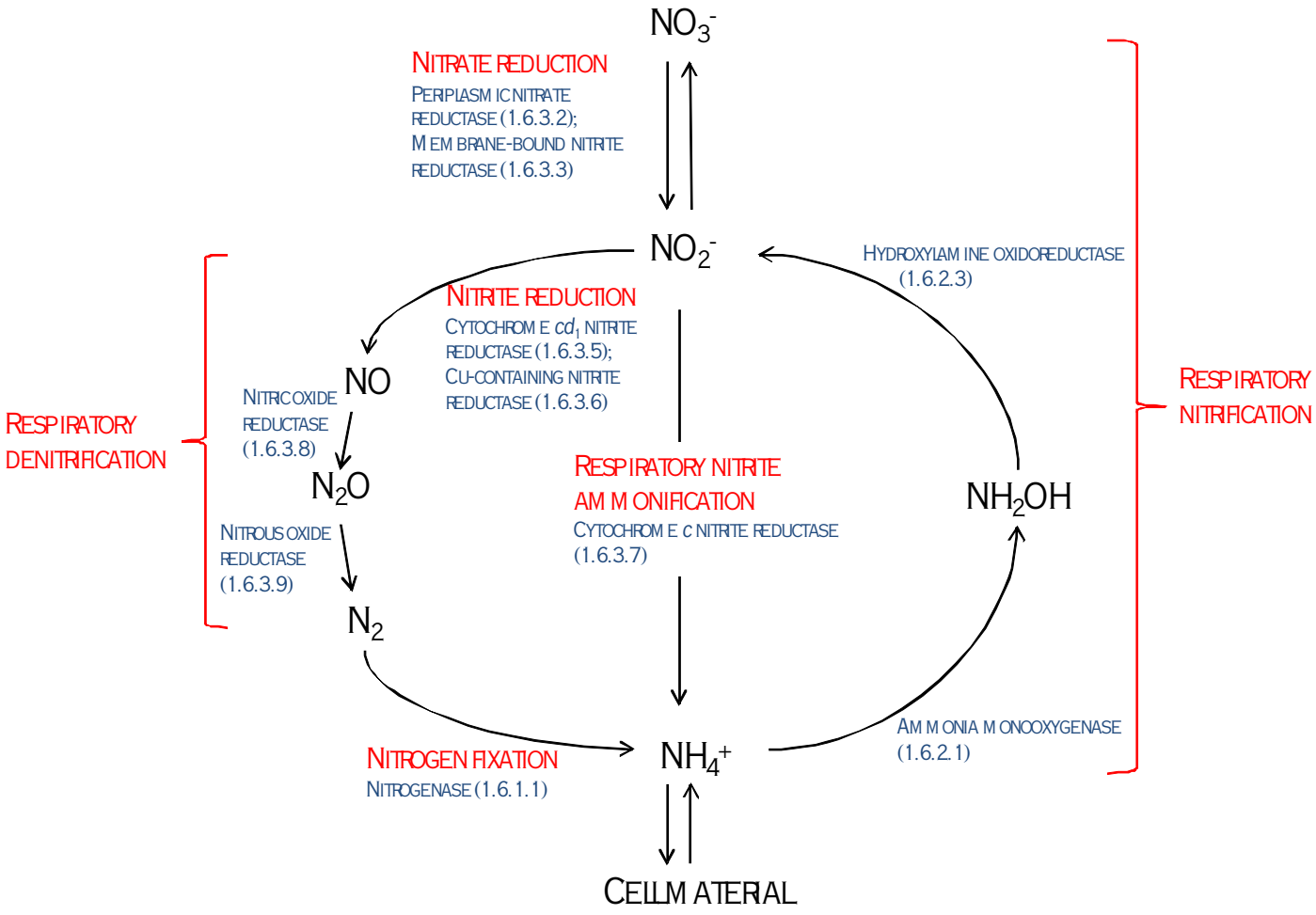

these metalloenzymes have been elucidated and their roles will be discussed. In the context of this thesis, the pentaheme nitrite reductases (NrfA) and hydroxylamine oxidoreductase (HAO) are of particular relevance, and their characteristics will be more fully explored.

The bacterial redox reactions (excepting nitrogen fixation) that occur in the biological nitrogen cycle are associated with the electron transport systems of cytoplasmic membranes. There are three oxidation reactions, converting ammonia to hydroxylamine to nitrite to nitrate, in which electrons are donated to oxygen via membrane-bound electron transport systems. The five reduction reactions, in which nitrate is reduced to nitrite, nitric oxide, nitrous oxide, nitrogen and finally ammonia, require the receipt of electrons through electron-transport chains.

### 1.6.1 Nitrogen fixation

Nitrogen fixation describes the process by which atmospheric nitrogen gas is converted to ammonia. This reaction may be carried out chemically, using the Haber reaction for example, or by bacteria that contain the highly oxygen-sensitive nitrogenase system.

#### 1.6.1.1 The Nitrogenase System

The nitrogenase enzyme is essential to the process of biological nitrogen fixation and catalyses the ATP-dependent reduction of dinitrogen to ammonia. It has been extensively researched and has been found to be a challenging subject for study (Rees *et al*, 2000).

The nitrogenase complex is comprised of two proteins, the Fe protein and the MoFe protein. The Fe protein contains a [4Fe-4S] cluster and transfers electrons from a donor protein (such as flavodoxin) to the MoFe protein. The active site for the binding and reduction of nitrogen is in the MoFe protein, which contains two novel types of iron-sulfur clusters; the P-cluster is an [8Fe-7S] cluster and the FeMo cofactor contains molybdenum in a [Mo-3Fe-3S] cluster bridged to a [4Fe-4S] cluster. The P-cluster mediates electron transfer from the [4Fe-4S] cluster of the Fe protein to the active site cofactor in the MoFe protein. However, although a

**Figure 1.12: The structure of the nitrogenase MoFe cofactor.**

*From Einsle et al, 2002. The six iron atoms and nine sulfur atoms in the central cavity of the MoFe cofactor lie on two concentric spheres in the active site.*

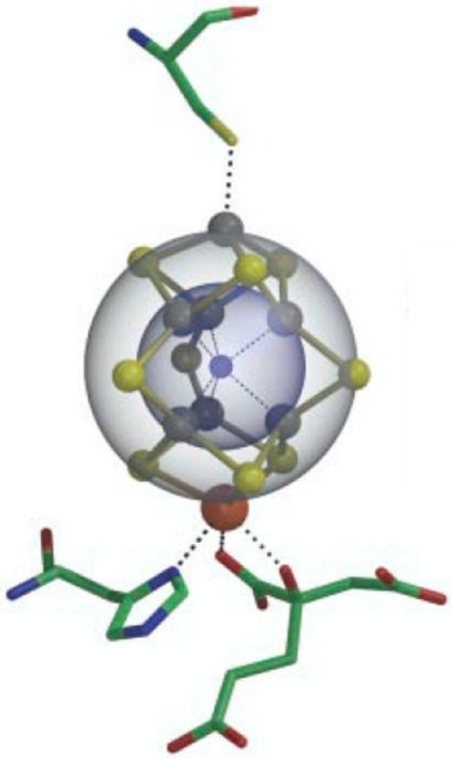

high resolution structure of nitrogenase (Figure 1.12; Einsle *et al*, 2002) is available, the mechanism of nitrogen binding and reduction remains unclear.

In addition to this, a novel nitrogenase system from *Streptomyces thermoautotrophicus* has been characterised (Ribbe *et al*, 1997). This nitrogenase is of special interest as it is the only such system yet studied that tolerates oxygen, and even utilises the highly reactive superoxide as its source of electrons. This *Streptomyces* organism is isolated from the soil covering burning charcoal piles, where superoxide is generated as a result of the oxidation of carbon monoxide. The superoxide is oxidised by a Mn-containing superoxide oxidoreductase that donates electrons to the nitrogenase system. This nitrogenase is similar to the other more commonly encountered nitrogenases, in that it also contains the FeS and Mo clusters, but it differs in its inability to reduce acetylene (a common nitrogen fixation assay) and lower ATP consumption per nitrogen reduced.

### 1.6.2 Nitrification

Nitrification is a key process in the biological nitrogen cycle. Although ammonia itself can be incorporated into biological materials, in soils it is oxidised sequentially to nitrite and nitrate. Soil nitrate is then used as a nitrogen source for plant cell growth.

The nitrification reactions contained in the cycle (the oxidation of ammonia to hydroxylamine, nitrite and finally nitrate) have traditionally been difficult to examine for two main reasons. Firstly, the bacteria involved in these reaction are difficult to culture to sufficient cell densities and secondly, the membrane-bound ammonia monooxygenase enzyme (which catalyses the

conversion of ammonia to hydroxylamine; $NH_3 + O_2 + [2H] \rightarrow NH_2OH + H_2O$) has been hard to purify reproducibly due to its lability. However, the characterisation of hydroxylamine oxidoreductase (HAO) has been successful and this enzyme will be examined in more detail in section 1.6.2.3.

#### 1.6.2.1 Ammonia monooxygenase:

Attempts to deduce the structure of ammonia monooxygenase and perform a characterisation of this enzyme have been challenging due to issues with culturing and purification, as mentioned previously. However, it is currently thought that the catalytic site contains a polynuclear copper centre (Ensign *et al*, 1993).

In order for the membrane-bound ammonia monooxygenase to function, a source of electrons is required, in addition to ammonia ($NH_3$) and oxygen ($O_2$). These electrons must be obtained from the oxidation of hydroxylamine ($NH_2OH$) to nitrite ($NO_2^-$), which produces four electrons. Two of these electrons must be utilised in the conversion of ammonia to hydroxylamine by the membrane-bound ammonia monooxygenase under discussion, while the remaining two are passed along the electron transport chain to $O_2$ (Ferguson *et al*, 1998).

#### 1.6.2.2 Anaerobic ammonium oxidation (ANAMOX)

In addition to the processes discussed thus far, the oxidation of ammonia to nitrite or nitrate to produce nitrogen can also be achieved anaerobically by mixed microbial populations in a

process known as ANAMOX (anaerobic ammonium oxidation, $NH_4^+ + NO_2^- \rightarrow N_2 + 2H_2O$). The bacteria involved in this process are able to grow under chemolithoautotrophic conditions and use ammonia as an electron donor and nitrite as an electron acceptor (Van der Graf *et al*, 1998). Cytochromes have been found to be abundant in the cultures involved in this reaction and novel reactions have been proposed, including the reaction of ammonium with hydroxylamine to yield hydrazine (Iverson *et al*, 1998).

#### 1.6.2.3 Hydroxylamine oxidoreductase (HAO)

Hydroxylamine oxidoreductase (HAO) is a water-soluble periplasmic enzyme that has been studied with much interest due to its possession of an unusual P460 heme centre, so called due to the characteristic spectroscopic absorbance of the reduced enzyme (Anderson *et al*, 1984). HAO is located in the periplasm and catalyses the four electron oxidation of hydroxylamine to nitrite ($NH_2OH + H_2O \rightarrow NO_2^- + 5H^+ + 4e^-$).

The structure of HAO from *Nitrosomonas europaea* was solved to 2.8 Å resolution in 1997 (Figure 1.13; Igarashi *et al*, 1997) and revealed the protein to be trimeric (200 kDa). Each monomer (67 kDa) of the trimer contains eight hemes, seven of which are conventional *c*-type hemes and one of which is the novel P460 centre (heme 4). The P460 heme has been shown to bind carbon monoxide, indicating that it is five-coordinate, high-spin and so expected to be involved in catalysis (Hooper *et al*, 1983). The remaining seven conventional hemes are thought to be involved in electron transfer between the P460 active site and the physiological electron acceptor cytochrome $c_{554}$ (Arciero *et al*, 1991).

The eight heme centres in each monomer are arranged in four clusters; a tricluster containing the P460 and two of the *c*-type hemes (hemes 6 and 7), two diclusters (containing hemes 1 and 2, and 3 and 5) and one magnetically isolated heme (heme 8) (Arciero *et al*, 1998). The hemes in each cluster are found to be positioned essentially parallel to one another. Examination of the trimer reveals that the hemes are all located towards the "bottom" of the structure, where a ring of eighteen *c*-type hemes can be seen (hemes 2-3 and 5-8. Hemes 1 are not positioned in the ring) with the active site P460 hemes found above. EPR studies of the hemes have indicated that they interact strongly with one another (Hendrich *et al*, 2001)

**Figure 1.13: The structure of hydroxylamine oxidoreductase (HAO) from *Nitrosomonas europaea*, determined to 2.8 Å resolution.**

*From Igarashi et al, 1997. The three subunits are coloured in green, purple and blue and the hemes are shown in red. The trimeric structure can be seen from two different angles.*

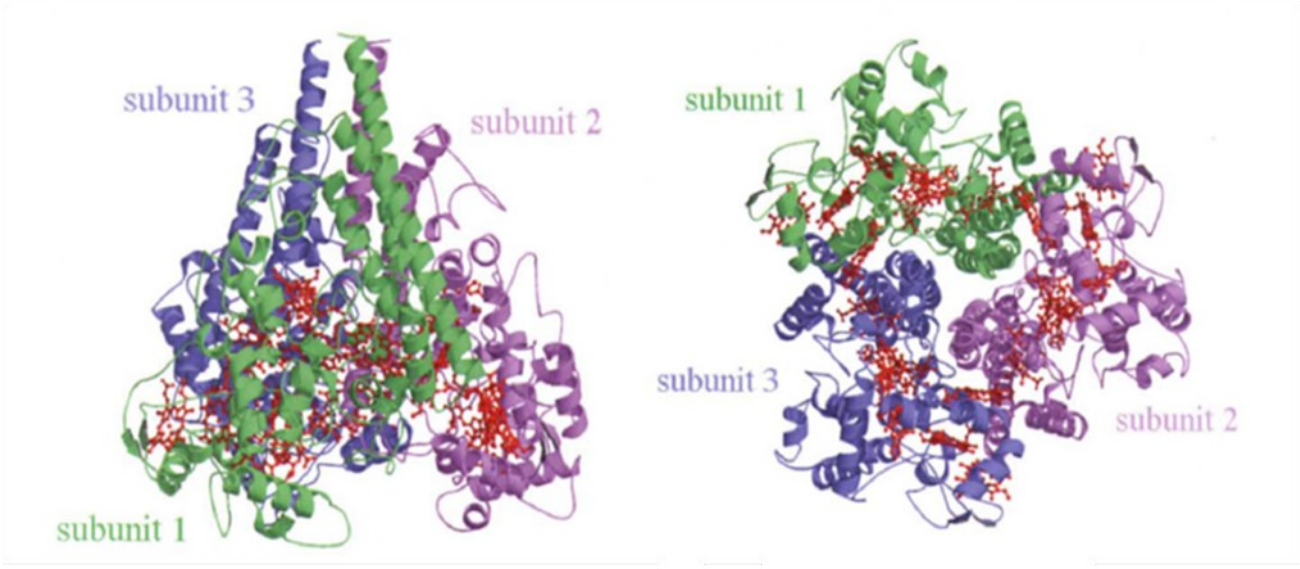

and the inter-heme distances within the four clusters of the monomer are small (between ~3.8 Å and ~4.1 Å). The penta-coordinate P460 cytochrome is the active site for hydroxylamine binding. The oxidation of hydroxylamine occurs via two sequential abstractions of electron pairs with the release of five protons.

The structure of the active site shows that the P460 heme is covalently attached to a tyrosine residue (Tyr467) from an adjacent subunit and it is thought that this linkage is required in order to form the physiological trimer. The vacant site of the pentacoordinate P460 iron has been shown to bind hydroxylamine and it has been suggested that a number of residues adjacent to the active site are involved in catalysis (aspartate (Asp257), histidine (His268) and tyrosine (Tyr334)), acting as proton acceptors in the nitrite-forming reaction.

The oxidation of hydroxylamine to nitrite involves the release of four electrons as two separate two-electron oxidations (Figure 1.14). Two of these electrons are used to reduce ammonia monooxygenase (AMO), which then converts ammonia into hydroxylamine, while the remaining two are used in respiration. This means that HNO is the only bound intermediate to the HAO enzyme and this intermediate must be rapidly oxidised in order to prevent the production of either of the two toxic species, nitrous oxide or nitric oxide, instead of nitrite. In this respect, an important feature of the structure is the location of the two hemes (6 and 7) close to the P460 active site. These hemes are thought to be so located in order to rapidly accept the pair of electrons released from the substrate which are not utilised by AMO and transfer them to the diheme clusters, in order to leave hemes 6 and 7 free to accept the second pair of electrons from P460. This rapid transfer of electrons may help to prevent the slower single electron transfer that might result in the release of $N_2O$ or NO. Electrons are removed from HAO by cytochrome $c_{554}$, a unique tetraheme protein with no significant

sequence homology to other proteins, which is thought to dock in a cavity in the HAO trimer (Andersson *et al*, 1986).

**Figure 1.14: Arrangement of hemes within a hydroxylamine oxidoreductase monomer and possible routes of electron transfer.**

*From Igarashi et al, 1997. The orange ellipsoids represent the hemes of one monomer, while the dashed lines are hemes from adjacent monomers. The yellow arrows indicate the direction of major electron flow.*

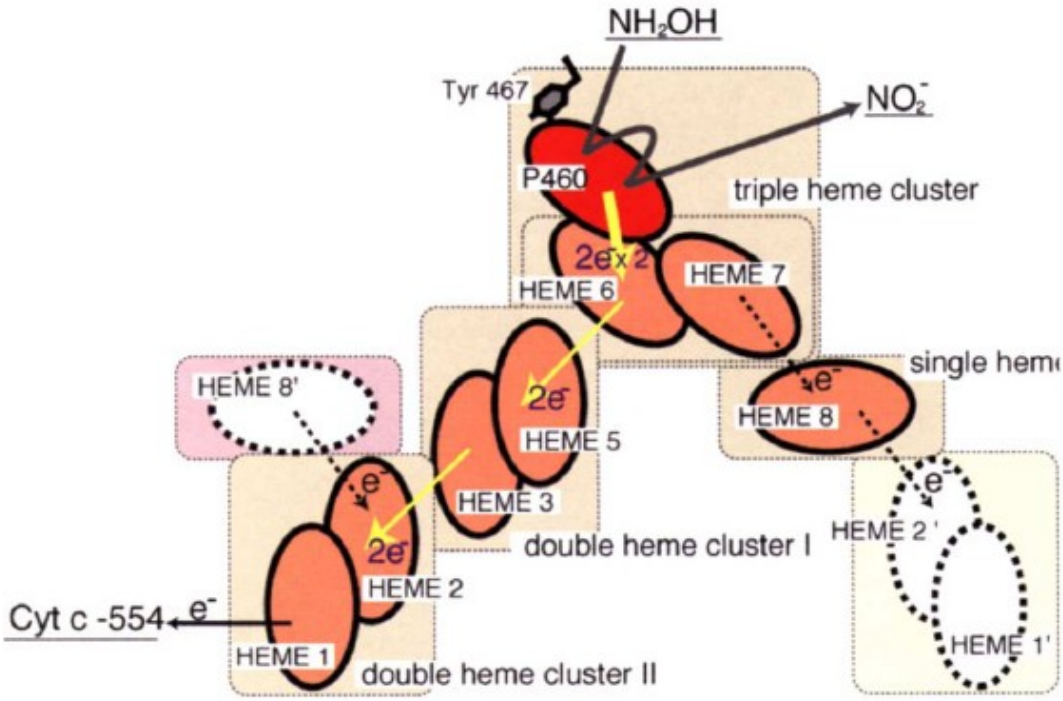


### 1.6.3 Denitrification

Denitrification describes the processes by which nitrate is successively reduced to nitrogen gas via nitrite, nitric oxide and nitrous oxide. These reactions are carried out almost exclusively by

bacteria, although it has been determined that some ecological contribution is made by certain species of fungi.

### 1.6.3.1 The Nitrate reductases

The nitrogen cycle involves two types of nitrate reductases, both of which catalyse the reduction of nitrate to nitrite ($NO_3^- + 2H^+ + 2e^- \rightarrow NO_2^- + H_2O$). One of these types of nitrate reductase is located in the periplasm (Nap), and the other is found in the cytoplasmic membrane (Nar).

### 1.6.3.2 Periplasmic Nitrate Reductase (Nap)

The periplasmic nitrate reductase enzymes (Nap) can be classified into two groups. The first group contains heterodimeric Nap, which purifies as a two-subunit complex containing a small 16 kDa diheme subunit (NapB) and a larger 90 kDa subunit (NapA) that binds a [4Fe-4S] cluster and a molybdenum-containing cofactor. The second group contains monomeric Nap, which consists only of the [4Fe-4S] and molybdenum cofactor-containing NapA. The molybdenum cofactors found in these enzymes are coordinated by two molybdopterin guanine dinucleotide (MGD) groups.

The structures of these enzymes have been solved (heterodimeric NapAB from *Rhodobacter sphaeroides* (Arnoux *et al*, 2003) and monomeric NapA from *Desulfovibrio desulfuricans* (Dias *et al*, 1999)) and in all cases it appears that NapA folds into four domains. One of these

domains is composed of an N-terminal part of the polypeptide and binds the [4Fe-4S] cluster and the other three domains fold around the molybdenum cofactor, providing a number of H-bonds to the MGD moieties.

#### 1.6.3.3 Membrane-bound Nitrate Reductase (Nar)

Several structures of the membrane-bound nitrate reductase (Nar) have been reported (Bertero *et al*, 2003 and Jormakka *et* al, 2004) and have indicated that the enzyme is composed of three polypeptide chains, forming the complete NarGHI heterotrimer (Figure 1.15). Of these chains, NarG (140 kDa) and NarH (kDa) are soluble, while the NarI chain (20 kDa) is located in the cytoplasmic membrane and anchors the other two subunits through mainly hydrophobic interactions.

The structure of the enzyme is such that the C-terminal tail of NarI interacts with both NarG and NarH, forming a "flower-shaped" structure (Bertero *et al*, 2003). NarG contains an unusual [4Fe-4S] cluster and the molybdenum-containing MGD cofactor active site. NarI contains two *b*-type hemes and a quinol binding site that receives electrons from the quinol pool. NarH contains three [4Fe-4S] clusters and one [3Fe-4S] cluster that together form a molecular wire through which electrons are transferred from Nar I to Nar G. The distance between one of the *b*-type hemes of NarI and the [3Fe-4S] cluster of NarH is 8.9 Å, permitting rapid electron transfer between the two.

In addition to this, single subunit (NarB) assimilatory systems have also been found in cyanobacteria. In this case, the electron donor is reduced ferredoxin.

**Figure 1.15: The overall three-dimensional structure of the membrane-bound nitrate reductase, Nar GHI, from *E. coli* K12.**

*Figure from González et al, 2006. The location of the enzyme in the membrane is shown. Each of the subunits and metal cofactors is identified.*

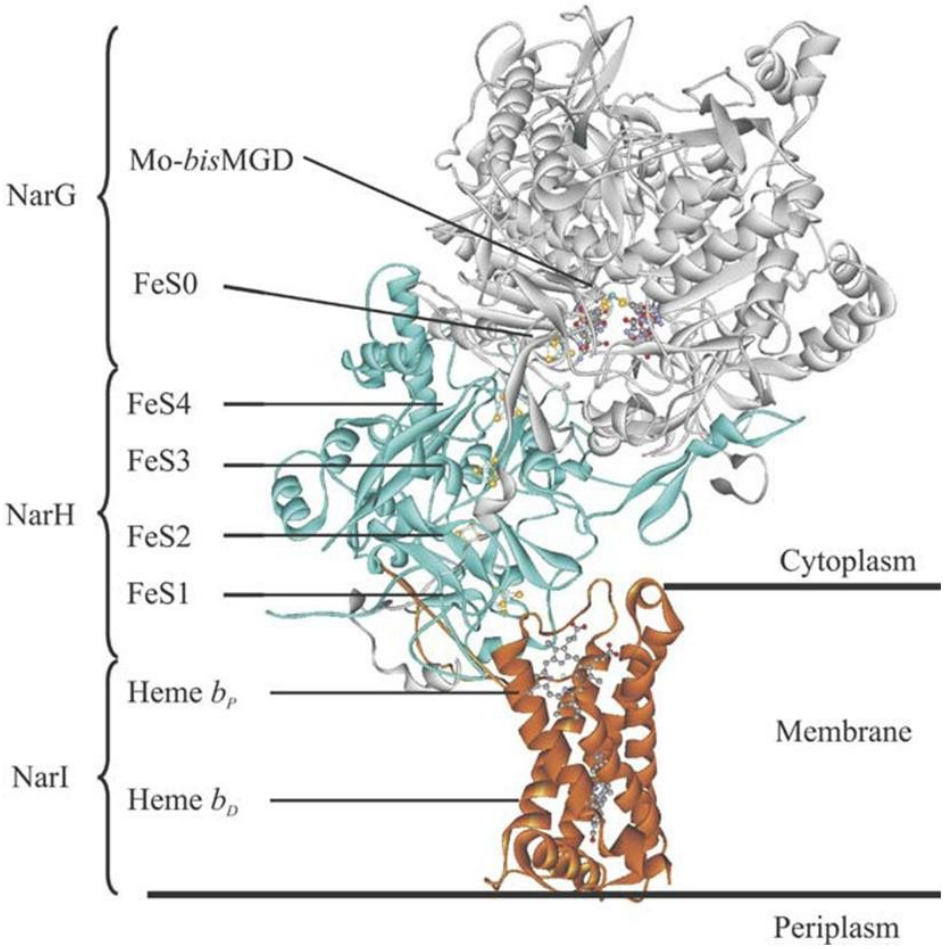


### 1.6.3.4 The Nitrite Reductases

There are three types of respiratory nitrite reductases which catalyse the reduction of nitrite to either nitric oxide or ammonium. These nitrite reductases are located in the periplasm of Gram-negative bacteria and it is thought that no species expresses more than one type. In addition to this, a cytoplasmic siroheme nitrite reductase that reduces nitrite to ammonium in nitrite

assimilation or detoxification is found fungi and plants, although this enzyme is expected to show significant similarity to the related siroheme sulfite reductases (Richardson *et al*, 1998).

### 1.6.3.5 Cytochrome $cd_1$ Nitrite Reductase ($cd_1$Nir)

The reduction of nitrite to nitric oxide ($NO_2^- + 2H^+ + e^- \rightarrow NO + H_2O$) is catalysed by cytochrome $cd_1$ nitrite reductase. Several structures have been solved, including those from *Paracoccus pantotrophus* (Fig. 1.16; Fulop *et al*, 1995) and *Pseudomonas aeruginosa* (Nurizzo *et al*, 1997). The active sites of the enzymes are the $d_1$ hemes, which are located in an eight bladed β-propeller structure. However, there appear to be some differences between the two structures; the coordination of the $d_1$ hemes in the different structures is inconsistent and additional differences are observed in the cytochrome *c* domain. The reasons for these structural differences are yet to be elucidated.

### 1.6.3.6 Copper-containing Nitrite Reductase (CuNir)

The copper-containing nitrite reductases also catalyse the reduction of nitrite to nitric oxide. These are homotrimeric enzymes which bind three type I and three type II copper centres (Godden *et al*, 1991, Dodd *et al*, 1998). In the type I centres the protein-derived ligands coordinating the copper are cysteine, methionine and two histidines. The type II copper centres are found at the subunit-subunit interface and are ligated by three histidine residues, of which two are derived from one subunit and the other from the adjacent subunit. The

**Figure 1.16: The structure of cytochrome $cd_1$ nitrite reductase from *Paracoccus pantotrophus*.**

*Figure from Fulop et al, 1995. The protein chain is rainbow coloured, starting in blue at the N-terminus and finishing at the C-terminus in red. The protein is dimeric in structure.*

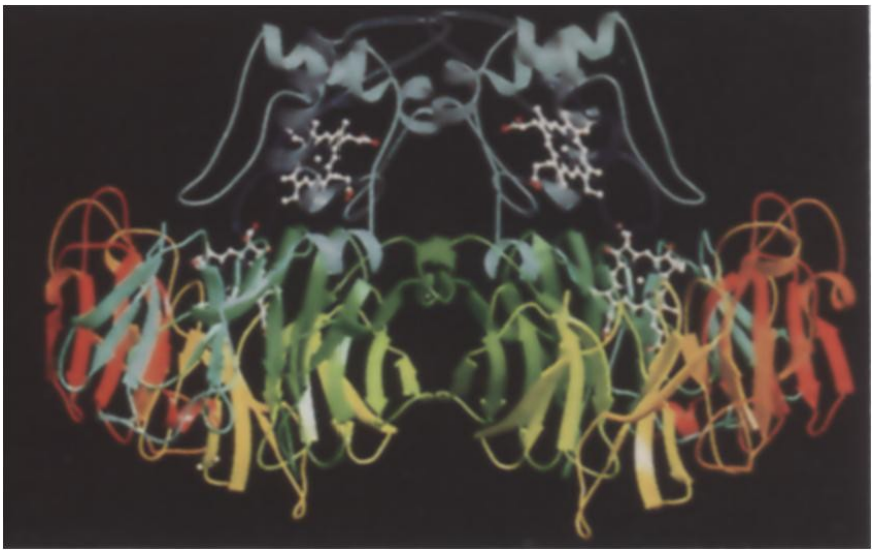

tetrahedral coordination sphere of the type II centres is completed by a water or hydroxide molecule.

The type II centre is the active site of the enzyme and nitrite has been observed bound here in crystals from several sources (Murphy *et al*, 1997, Dodd *et al*, 1998 (Fig. 1.17)). The type I copper centres are involved in electron transfer from soluble electron donors to the active site (Kukimoto *et al*, 1995).

### 1.6.3.7 Cytochrome *c* Nitrite Reductase (*cc*NiR/NrfA)

Cytochrome *c* nitrite reductase catalyses the six electron reduction of nitrite to ammonia ($NO_2^-$ + $8H^+$ + $6e^-$ → $NH_4^+$ + $2H_2O$). This reaction occurs without the release of any intermediates, in contrast to the process of respiratory denitrification. The crystal structure of the enzyme has been obtained from a number of sources, including the sulfur-reducing bacterium *Sulfurospirillum deleyianum* (Einsle *et* al, 1999), the rumen bacterium *Wolinella succinogenes* (Einsle *et al*, 2000) and the enteric bacterium *Escherichia coli* (Bamford *et al*,

**Figure 1.17: The structure of the copper-containing nitrite reductase from *Alcaligenes xylosoxidans.***

*Figure from Dodd et al, 1998. The two domains of the monomer are shown, domain I in green and domain II in red. The two domains are linked by a twelve residue peptide, shown in blue.*

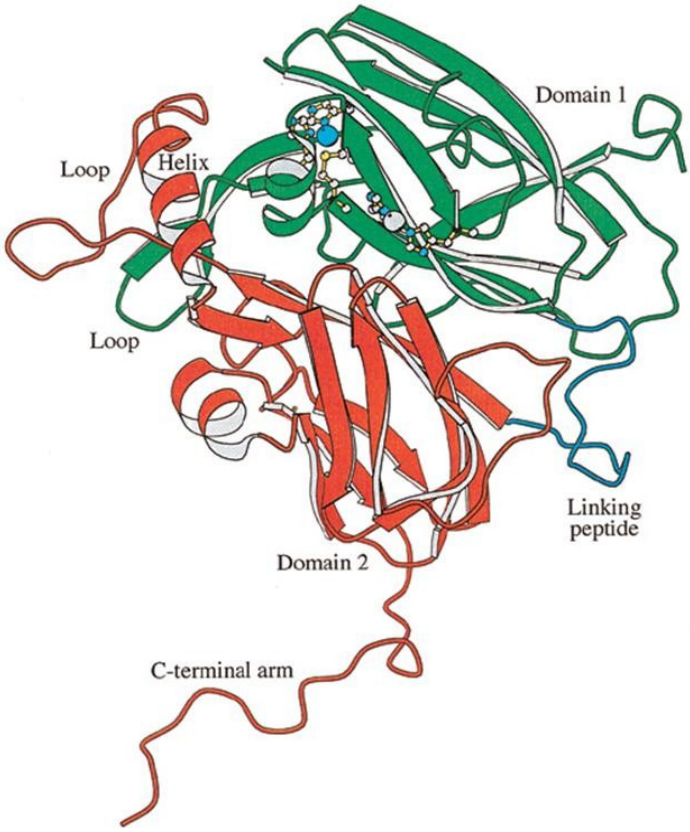

2002a). In each case the enzymes have a highly conserved 3-dimensional structure and are either soluble periplasmic proteins or are bound to the periplasmic face of the cytoplasmic membrane. The cytochrome *c* nitrite reductases are encoded by a single gene (*nrfA*) and have masses of 52-65 kDa.

In each of the structures listed above NrfA is a compact homodimer of pentahemes (Figure 1.18), indicating that they are members of a family of homologous NrfA proteins. The protein is folded compactly and dominated by three long α-helical segments, two of which are involved in dimer formation through a mainly hydrophobic surface.

**Figure 1.18: The homodimeric structure of cytochrome *c* nitrite reductase, NrfA, from *Desulfovibrio desulfuricans*, determined to 2.3 Å.**

*(Figure from Cunha et al, 2003) The orientation of the heme groups is visible towards the base of the structure, on either side of the dimer interface.*

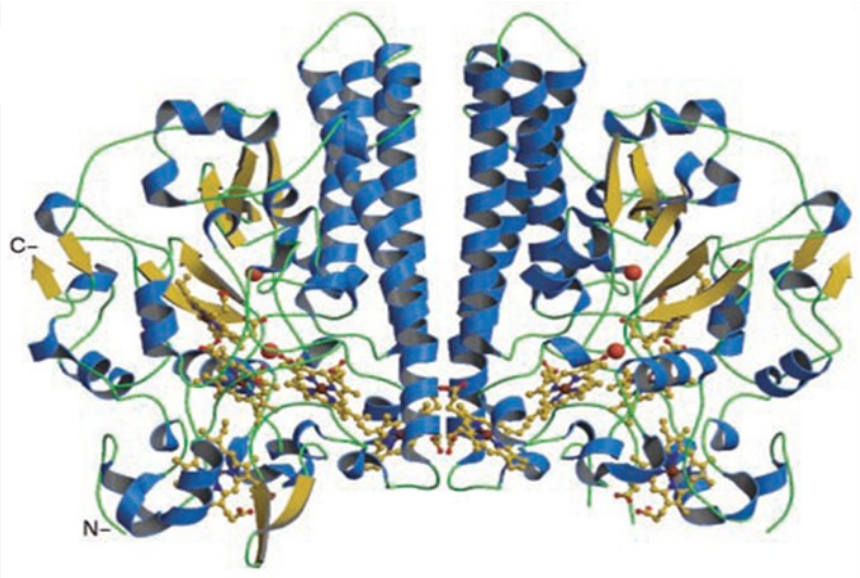

**Figure 1.19: The arrangement of the heme groups in the dimeric NrfA enzyme.**

*The hemes are numbered in their order of occurrence in the protein sequence and the distances between the iron atoms are given in Å. Heme 1 is the active site. The right hand side monomer shows the superposition of the arrangements of hemes in the monomers of NrfA from S. deleyianum (red), W. succinogenes (blue) and E. coli (green) (Cunha et al, 2003).*

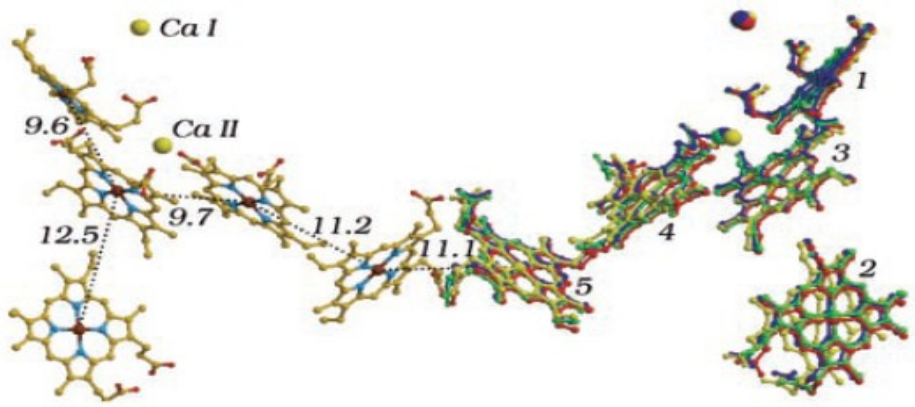


Each pentaheme monomer contains five hemes which are closely packed in near-parallel and near-perpendicular heme pairs (Figure 1.19), in a similar manner to that observed in hydroxylamine oxidoreductase. Hemes 1, 3 and 4 form one clustered and almost co-planar group, with hemes 2 and 5 slightly further apart.

The active-site heme (Heme 1) is notable for its novel ligation, in which a lysine ligand is co-ordinated to the heme iron. This unusual co-ordination is the result of the presence of a CXXCK amino acid motif in the protein sequence, leading to the amine nitrogen of the lysine residue acting as the proximal ligand (Lys134 in *W. succinogenes* NrfA, Lys126 in *E. coli* NrfA and Lys133 in *S. deleyianum* NrfA). This heme also has a distal oxygen ligand that is probably donated from a water or hydroxide molecule (as indicated in the structure from *E. coli*), although this ligand has been observed as sulfate in the structures from *W. succinogenes* and *S. deleyianum*, and also as azide in the structure from *W. succinogenes*. Additionally, NrfA

from *W. succinogenes* has been crystallised in the presence of nitrite and also hydroxylamine, the presumed intermediate of the nitrite reduction reaction (Einsle *et al*, 2002). Substrate access to the active site at heme 1 has been shown to be through two narrow channels from the surface of the protein.

Heme 2 has been proposed as the site of entry for electrons to the enzyme. Hemes 2-5 are conventionally bound by CXXCH motifs and are *bis*-histidinyl coordinated. These hemes are probably used by the enzyme to store and transfer electrons to the active site. The distances separating the closely-packed hemes (the edge-to-edge distances indicate that the hemes are as close as 4 Å) are sufficiently short to allow direct electron transfer between them and this is also the case between both Hemes 5 at the dimer interface, leading to the postulate that electronic interaction between the monomers may be functionally relevant (Schumacher *et al*, 1994).

The electrostatic potential at the surface of the NrfA dimer has also been mapped (Figure 1.20). The potential map is dominated by a positively charged region around the channel leading to the active site, thought to be the substrate inlet channel. A negative potential is visible around the proposed product efflux channel. These electrostatic features are conserved in NrfA family enzymes and are considered important to attract negatively charged nitrite ions to the active site and drive positively charged ammonium ions to the exterior of the enzyme.

**Figure 1.20: The electrostatic potential mapped at the dimer surface of the cytochrome *c* nitrite reductase, NrfA, from *Desulfovibrio desulfuricans*.** *The arrows indicate the substrate inlet in each monomer and the product outlet in the left hand side monomer (Figure from Cunha et al, 2003).*

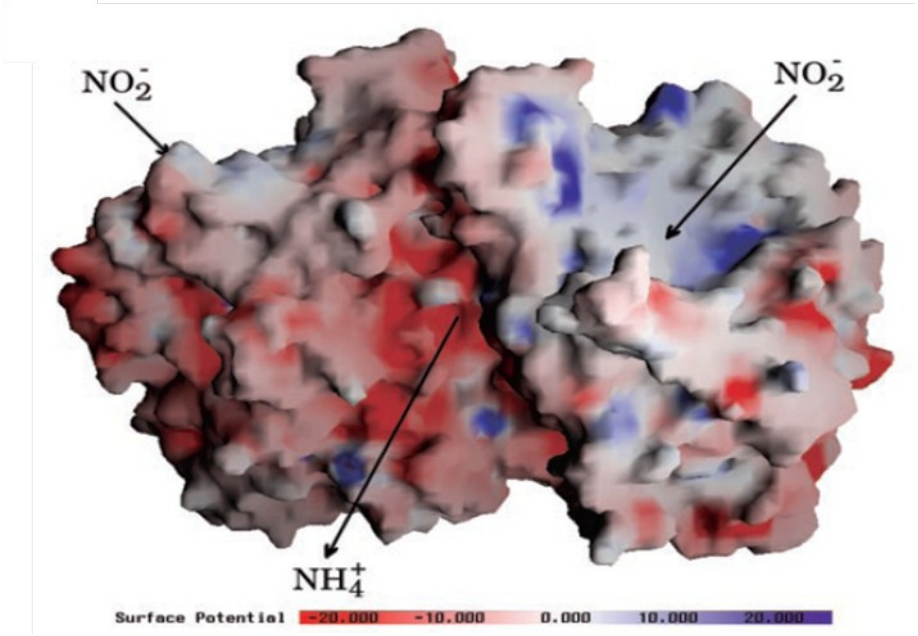


In addition to nitrite, the NrfA enzymes have been shown to reduce hydroxylamine and nitric oxide to ammonia, although at reduced specific activities of ~1 % and ~50 % of nitrite respectively (Stach *et al*, 2000).

The mechanism of the six-electron reduction of nitrite to ammonia by the cytochrome *c* nitrite reductases has been investigated using structural and density functional theoretical methods (Figure 1.21; Einsle *et al*, 2002). The first step of the reaction is the binding of nitrite to the active site heme of the reduced enzyme and the reaction then proceeds without the production of any intermediates. The first N-O bond is cleaved heterolytically and two one-electron reductions and one protonation follow to yield $Fe^{(II)}$-HNO. This species is reduced by two further electrons, thus generating the hydroxylamine intermediate $Fe^{(II)}$-

**Figure 1.21: Proposed mechanism for the reduction of nitrite to ammonium by cytochrome *c* nitrite reductase.**

*Figure from Einsle et al, 2002. Nitrite binds to the water-bound resting state of cytochrome c nitrite reductase, starting the reaction cycle. The first N-O bond is heterolytically cleaved, followed by two one-electron reductions and a protonation, yielding Fe(II)-HNO. This species*

*is readily reduced by two electrons to Fe(II)-$H_2NOH$. A further reduction leads to the dissociation of the second water molecule and the product, ammonia, finally dissociates.*

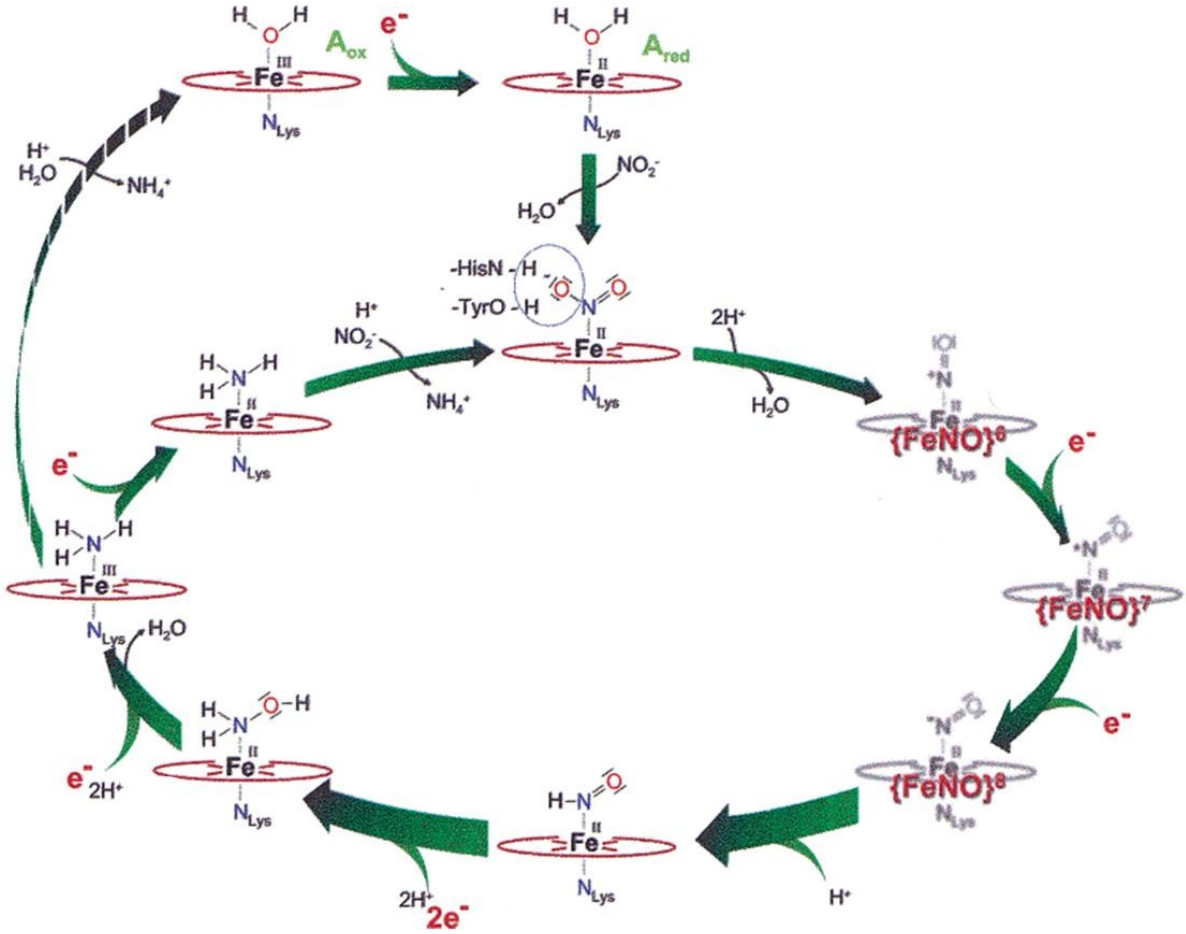


$H_2NOH$. This intermediate in turn undergoes a one-electron reduction, releasing water, and a final reduction step results in the dissociation of ammonia.

The described mechanism has three main features:

1. The mechanism is composed of reduction and protonation steps. Following each reduction, the affinity of the bound intermediate for protons increases. Subsequent protonation, in turn, increases the electrophilicity of the intermediate. Thus, the reaction is driven by a continuous supply of electrons, which is thermodynamically favourable. This sequence of reduction and protonation is key in order to reduce the nitrite N=O double bond, leading to the formation of hydroxylamine and subsequent cleavage yielding ammonia.

2. The spin state of the active site iron (heme 1) changes from high to low with the binding of nitrite. This permits the remainder of the reaction to occur without any additional spin-state changes.

3. The activation of the second N-O bond is increased by the ability of the NO π*-orbitals to accept two electrons.

Study of the cytochrome *c* nitrite reductases has revealed that bacteria show two distinct types of *nrfA* gene clusters, which appear to correlate to differences in the transfer of electrons from the quinone pool to the enzymes:

The first type of cluster is found in organisms including *W. succinogenes* and *S. deleyianum*, where the operon containing *nrfA* also contains *nrfH*, the gene encoding the a membrane-bound protein NrfH. NrfH is a tetraheme cytochrome *c* and is a member of the NapC quinol dehydrogenase family (Einsle *et al*, 2000; Simon *et al*, 2000). Mutation studies in the operon encoding cytochrome *c* nitrite reductase in *W. succinogenes* have indicated that the NrfH subunit functions as a membrane anchor for NrfA and also acts to mediate electron transfer

between NrfA and the membranous menaquinone pool (Simon *et al*, 2000). The soluble NrfA is the catalytic subunit of a NrfHA nitrite reductase complex, thought to occur physiologically in an $\alpha_2\beta_2$ arrangement, although this is yet to be confirmed.

The second type of cluster occurs in organisms including *E. coli*, in which *nrfA* is located in a cluster with *nrfB*, *nrfC* and *nrfD*. NrfB is a periplasmic pentaheme cytochrome that exists as a ~40 kDa homodimer and this reduced dimer has been shown to transfer electrons to the NrfA dimer. NrfC is a [4Fe-4S] ferredoxin also located in the periplasm, while NrfD is a membrane-integral quinol dehydrogenase, thus indicating that the *nrfABCD* operon in *E. coli* is related to a significantly different electron transfer process to that occurring in the *nrfAH* operon described above.

#### 1.6.3.8 The Nitric Oxide Reductases (NOR)

Bacterial nitric oxide reductase is a membrane-bound enzyme that catalyses the conversion of nitric oxide to nitrous oxide ($2NO + 2H^+ + 2e^- \rightarrow N_2O + H_2O$), a two electron reduction involving the formation of an N-N bond. The enzyme is composed of two subunits; NorC is a 17 kDa subunit containing a *c*-type heme centre and NorB is a 53 kDa subunit containing two *b*-type hemes and a non-heme iron. The active site of the enzyme is a dinuclear centre which consists of one of the *b*-type hemes and the non-heme iron (Hendriks *et al*, 1998), while the *c*-type centre is thought to accept electrons from donor proteins.

In addition to this, it has been found that a number of fungi contain a partial denitrification system which is involved in the biological nitrogen cycle. The end product of this partial

system is nitrous oxide, rather than dinitrogen as in the bacterial system. A crystal structure has been obtained for the nitric oxide reductase from *Fusarium oxysporum* (Parks *et al*, 1997). This enzyme is completely different to the bacterial enzyme; fungal NOR is a soluble cytochrome P450 molecule.

#### 1.6.3.9 Nitrous Oxide Reductase (NOS)

Nitrous oxide reductase catalyses the final denitrification step of the biological nitrogen cycle, reducing nitrous oxide to dinitrogen gas ($N_2O + 2H^+ + 2e^- \rightarrow N_2 + H_2O$). Nitrous oxide reductase structures from *Pseudomonas nautica* (Fig 1.22; Brown *et al*, 2000a,b) and *Paracoccus denitrificans* (Haltia *et al*, 2003) have shown the enzyme to be a homodimer of a 65 kDa copper-containing subunit. This subunit is composed of a $Cu_A$ domain and a $Cu_Z$ domain. The dinuclear $Cu_A$ is an electron entry site, while the tetranuclear $Cu_Z$ is the active site, found enclosed in a seven-bladed β-propeller structure. The two subunits are arranged head-to-toe so that inter-dimer electron transfer occurs between the $Cu_A$ centre of one monomer and the $Cu_Z$ centre of the other.

**Figure 1.22: The structure of nitrous oxide reductase from *Pseudomonas nautica*.**

*Figure from Brown et al, 2000b.One monomer of the dimer is shown in grey, with the other in colour. The β-strands of the propeller surrounding the $Cu_Z$ active site are in dark green.*

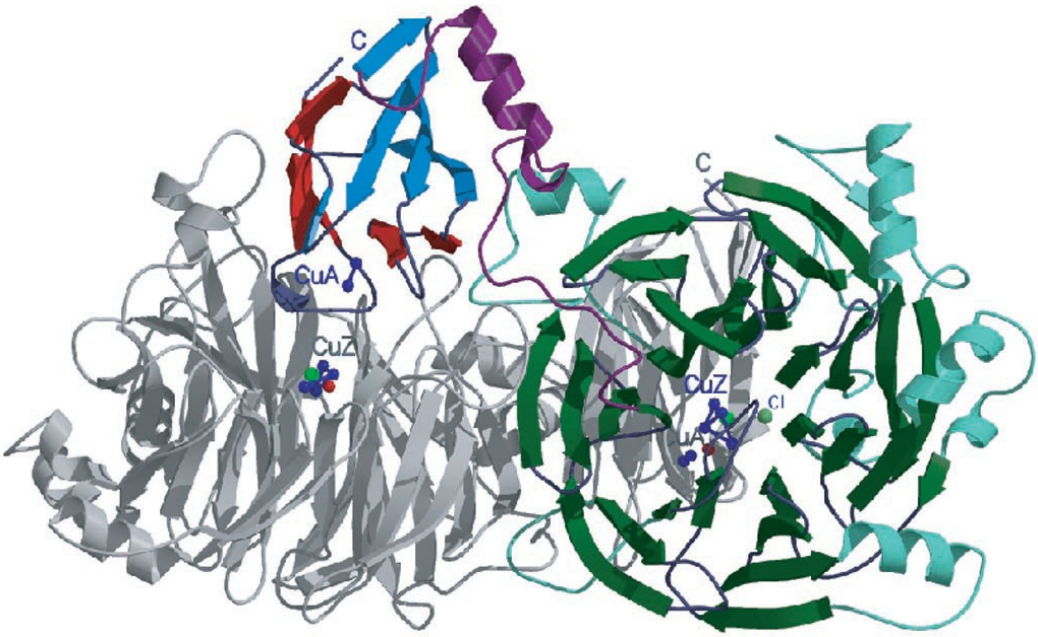


The $Cu_Z$ centre is a novel type of metal cluster, in which four copper ions are coordinated by seven histidines, two hydroxides and a bridging inorganic sulphide. It is though that $N_2O$ binds to the $Cu_Z$ centre via a single copper ion, while the remaining coppers act as an electron reservoir in order to facilitate fast electron transfer and minimise the formation of dead-end products (Brown *et al*, 2000a,b).

## 1.7 *SHEWANELLA*

Bacteria of the genus *Shewanella* are classified as Gram-negative γ-proteobacteria. *Shewanella* was initially isolated from rancid butter and designated *Achromobacter putrefaciens* (Derby *et al*, 1931). This taxon was subsequently reclassified as *Pseudomonas putrefaciens* (Long *et al*, 1941a,b), but distinctions between this organism and others of the *Pseudomonas* genus resulted in a further reclassification as *Alteramonas putrefaciens* (Baumann *et al*, 1972).

In 1985, the *Shewanella* genus was established and included the bacteria *Shewanella putrefaciens*, *Shewanella benthica* and *Shewanella hanedai* (MacDonell *et al*, 1985).

*Shewanella* strains have been isolated globally from a wide range of environments including Antarctic sea ice (*S. gelidimarina*, Bowman *et al*, 1997), Arctic marine sediment (*S. hanedai*, Jensen *et al*, 1980), North American freshwater lakes (*S. oneidensis*, Myers *et al*, 1988), the North Sea, (*S. frigidimarina*, Reid *et al*, 1999) and the sub-tropical freshwaters of the Amazon River Delta (*S. amazonensis*, Venkataswaran *et al*, 1998).

In addition to this wide variety of mainly silt deposit or mud flat environments, *Shewanella* strains have also been isolated from a diverse range of hosts, including human clinical samples (*S. putrefaciens*, Chen *et al*, 1997 and Dhawan *et al*, 1998; *S. alga* and *S. putrefaciens*, Khashe *et al*, 1998), rotting fish (*S. colwelliana*, Weiner *et al*, 1988; *S. marinintestina*, *S. schlegeliana*, *S. sairae*, Masataka *et al*, 2003) and deep-sea oil pipelines (*S. putrefaciens*, Pickard *et al*, 1993).

The incredible diversity of environments and hosts in which *Shewanella* species can exist is thought to be a reflection of the wide range of substrates upon which they have been found to respire. At least fifteen terminal electron acceptors used for respiration by *Shewanella* have so far been identified (Table 1.1).

**Table 1.1: Known terminal electron acceptors used in anaerobic respiration by *Shewanella* species**

| Metal | Nitrogen | Sulfur | Organic |
|---|---|---|---|
| Mn(IV) | $NO_2^-$ | $SO_3^{2-}$ | Fumarate |
| Fe(III) | $NO_3^-$ | $S_2O_3^{2-}$ | Mesaconate |
| U(IV) | TMAO | DMSO | Glycine |
| Cr(VI) | | Elemental S(0) | Crotonate |

### 1.7.1 *Shewanella oneidensis* MR-1

*Shewanella oneidensis* MR-1 is a facultative freshwater anaerobe and was isolated from Lake Oneida, NY, USA. This bacterium was initially classified as *Shewanella putrefaciens*, but has been subsequently reclassified as the strain *Shewanella oneidensis*-MR1 (Reid *et al*, 1999). The genome has been sequenced and published (Heidelberg *et al*, 2002), allowing for detailed analysis.

Analysis of the genome sequence has indicated that the bacterium contains 39 genes encoding *c*-type cytochromes, many of unknown function, 14 of which contain four or more hemes (Meyer *et al*, 2004). Although these figures are relatively small compared to those determined for *G. sulfurreducens*, they remain significant as the second largest number of *c*-type cytochromes found in any organism sequenced thus far. It is thought that, as in the case of *G.*

*sulfurreducens*, this abundance of putative cytochromes confers upon the organism the ability to utilise a wide range of terminal electron acceptors during anaerobic respiration. This range includes nitrate, nitrite, sulfate, thiosulfate, elemental sulfur, fumarate and metal ions such as Fe(III) and Mn(IV).

Functions have been proposed for some of the putative proteins encoded in the *S. oneidensis* genome. Several of the tetraheme proteins have been proposed to have a novel role in the reduction of amino acids (Heidelberg *et al*, 2002) and some others have been implicated in iron reduction (Gordon *et al*, 2000). Some of the eight decahemes have also been demonstrated to be involved in the processes of insoluble metal oxide reduction, including the periplasmic MtrA (Beliaev *et al*, 1998; Pitts *et al*, 2003) and the outer membrane proteins OmcA and OmcB (Myers *et al*, 2001). The remainder of the *c*-type heme-containing proteins predicted by the genome sequence are of unknown function and sequence alignments of many of these proteins show very little homology with enzymes of known or predicted function. The majority of these unidentified cytochromes (~ 80%) contain periplasmic leader sequences and hydrophobicity plots of the amino-acid sequences predicted indicate there to be no large regions of hydrophobic amino acids (www.tigr.com), suggesting there to be no membrane-anchor regions of polypeptide. Therefore, these proteins are predicted to be soluble and located in the periplasm. A number of respiratory complexes have been identified and found to be the same as those from *Escherichia coli*, including succinate dehydrogenase, formate dehydrogenase, fumarate reductase and nitrite reductase (Yankovskaya *et al*, 2003; Jormakka *et al*, 2003; Iverson *et al*, 1999; Bertero *et al*, 2003). These complexes are all found to be membrane-bound and have active sites facing the cytoplasm (with the exception of formate dehydrogenase), indicating that the respiratory system of *Shewanella oneidensis* is unusual in construction and arrangement.

A number of multiheme cytochromes from *S. oneidensis* have been more fully characterised, including a periplasmic flavocytochrome *c* fumarate reductase (Taylor *et al*, 1999), CymA, OmcA, MtrA and octaheme tetrathionate reductase. The NapC/NirT homologue, CymA, is a membrane-bound tetraheme protein that has been revealed to play a role in the respiration of Fe(III), nitrate, nitrite, fumarate and dimethyl sulfoxide (Myers *et al*, 1997; Schwalb *et al*, 2003).Studies of the outer membrane decaheme OmcA have indicated that it is implicated in the reduction of insoluble Fe(III) species (Field *et al*, 2000). Conversely, MtrA, a periplasmic decaheme, is involved in the reduction of soluble Fe(III) species (Pitts *et al*, 2003).

### 1.7.2 Octaheme Tetrathionate Reductase (OTR)

Analysis of the genome sequence of *Shewanella oneidensis* MR-1 revealed the presence of a single octaheme protein (SO4144), located in an open reading frame (ORF gsp260) that also contains a number of other potential proteins, including a monoheme cytochrome (SO4142) which may function as the physiological electron donor to the octaheme (although this is yet to be confirmed).

The octaheme protein was predicted to have a novel protein sequence with no known homologs. The sequence of 442 amino acid residues contains eight CXXCH conventional *c*-type heme attachment motifs, hence identifying the protein as an octaheme. The gene has a periplasmic leader sequence, which is then cleaved as the protein is processed within the cell. Genomic analysis predicts that a large number of *c*-type cytochromes are periplasmically-

located in *S. oneidensis* and it is thought that many are involved in the diverse and complex respiratory processes of which this bacterium is capable.

The octaheme protein has been cloned and over-expressed in the *Shewanella frigidimarina* Δ*fcc*$_3$ strain EG301, allowing the isolation of the protein. The molecular weight of the protein was found to be 54.5 kDa, its crystal structure determined to 2.2 Å resolution (Fig 1.23; Mowat *et al*, 2004) and the protein shown to be enzymatic. The amino acid sequence of the octaheme is shown in Appendix I. The ability of the enzyme to reduce tetrathionate and oxidise thiosulfate was identified and the relevant kinetic parameters determined (Table 1.2; Rothery, 2003).

**Table 1.2: Steady-state kinetic data for the reduction of tetrathionate and oxidation of thiosulfate by the octaheme tetrathionate reductase (OTR) from *Shewanella oneidensis*.** *Data recorded at 25 °C, pH 7.0, I = 0.1 M (Rothery, 2003).*

| Substrate | $k_{cat}$ ($s^{-1}$) | $K_M$ (μM) | $k_{cat} / K_M$ ($M^{-1} s^{-1}$) |
|---|---|---|---|
| Tetrathionate reduction | 19.9 ± 0.6 | 70 ± 9 | $2.9 \times 10^5$ |
| Thiosulfate oxidation | 16.8 ± 0.9 | 7100 ± 2500 | $2.4 \times 10^3$ |

Examination of these data shows that the reduction of tetrathionate is the more efficient reaction, leading to the designation of the enzyme as an octaheme tetrathionate reductase (OTR), according to Equation 1.7.

$$S_4O_6^{2-} + 2e^- \rightarrow 2S_2O_3^{2-} \qquad \textbf{Equation 1.7}$$

This presented a novel type of tetrathionate-reducing enzyme, as the only previously identified tetrathionate reductase enzyme is a membrane-bound molybdoenzyme from *Salmonella typhimurium* (Hensel *et al*, 1999).

### 1.8.2.1 Analysis of the Crystal Structure of OTR

The crystal structure of OTR shows very little structural similarity to any other structure deposited in the Protein Data Bank (http://www.rcsb.org/pdb; Berman *et al*, 2000). Analysis of this structure (Figure 1.23) has determined that the protein possesses a novel fold. The eight heme groups (shown in red) are arranged along one side of the protein and are numbered in accordance with their appearance in the amino acid sequence. The N-terminal region (residues 1-240) is mainly α-helical and forms a framework upon which hemes I-VII are located (shown in yellow), the rest of the protein (residues 241-442) being mostly folded into a large β-sheet. The top of the protein (as oriented in Figure 1.23) is comprised of part of the β-sheet, forming a cap over the substrate binding pocket (shown in green) and appearing to block solvent access to heme II. A small, predominantly helical area of polypeptide (gold-yellow) encloses the active site.

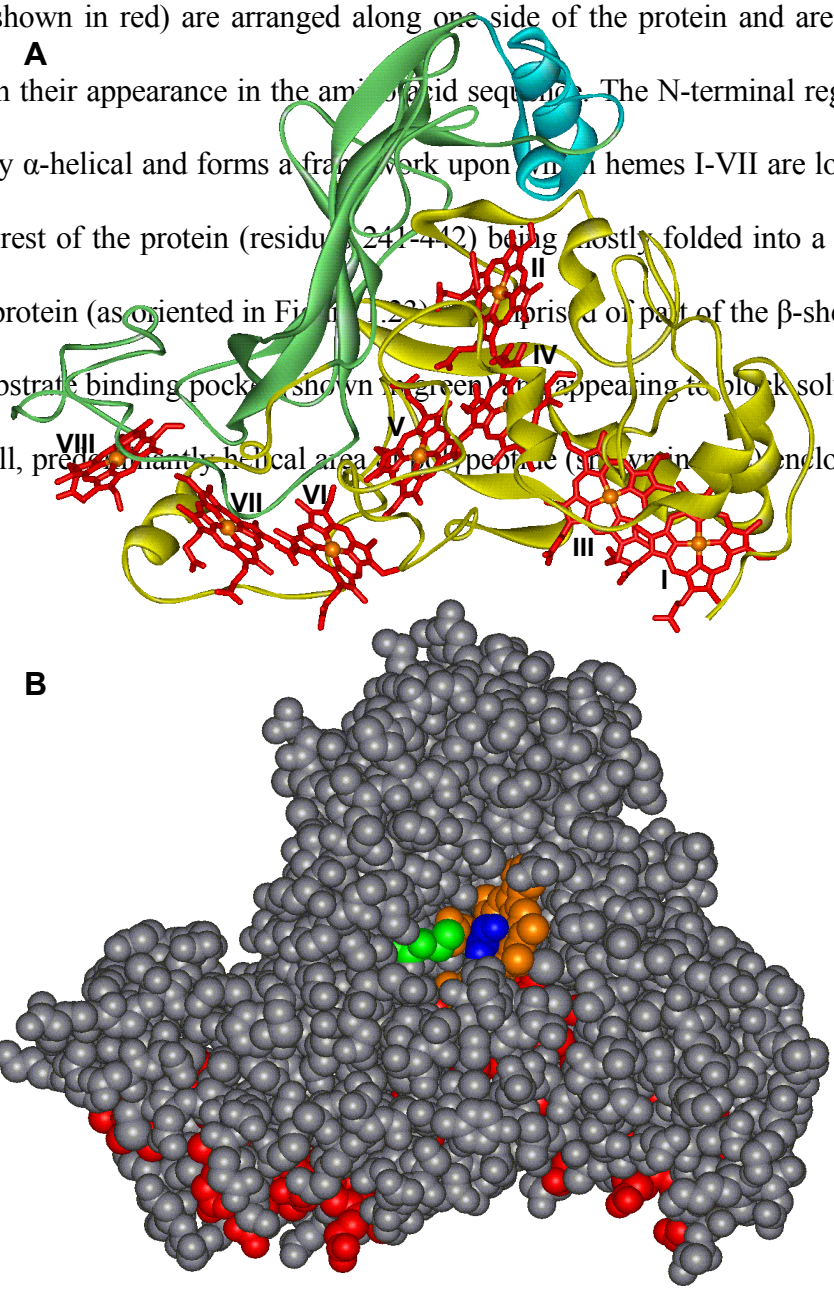


**Figure 1** **TR) from**

***Shewane***

*From Mo* *chitecture.*
*The heme* *in yellow.*
*Heme II* *olypeptide*
*enclosing* *he crystal*
*structure* *be slightly*
*surface e* *val of six*

*amino acid residues between Gly146 (in blue) and Lys153 (green) from the model. The missing residues are GGGDAV.*

#### 1.7.2.2 The Structure of the Active Site

Further examination of the structure reveals the presence of an unusually-ligated heme at the active site, heme II (Figure 1.24). Despite the identification of eight histidinyl heme attachment amino acid motifs in the protein sequence, heme II was shown to be five-coordinate with a lysine residue (Lys56) axially-ligated to the heme. This ligation had only previously been identified in the active site heme of the pentaheme cytochrome *c* nitrite reductase, NrfA,

although interestingly in that case the ligating lysine is contained in an unusual CXXCK heme attachment motif. The ligating lysine (Lys56) in OTR is found remotely in the sequence to the heme-binding cysteine residues (Cys74 and Cys77) and the anticipated histidine ligand (His78) of the motif. In fact, His78 is found to be directed away from the active site, with a tryptophan residue (Trp41) located between it and Lys56.

The sixth ligand to the active site heme of OTR is thiocyanate, found as a consequence of the presence of 150 mM potassium thiocyanate in the crystallisation solution. While the presence of thiocyanate is not physiologically relevant, it may indicate the role of the proximal heme face. The putative substrate binding pocket is located above heme II, where the only cysteine residue in the protein sequence which is not involved in thioether linkages to hemes (Cys64) is located at a distance of 7.5 Å from the heme. If thiocyanate is not present the proximal heme face consists of a cavity that could potentially be filled by a number of exogenous ligands. This cavity at the heme proximal face is also seen in the pentaheme nitrite reductases and is the proposed site of nitrite reduction. The atypical ligation at heme II leads to a change in the electronic distribution around the active site heme, as compared to that found for the conventionally ligated hemes. It is this altered distribution that results in the reactivity of the heme.

**Figure 1.24: The structure of the active site heme of octaheme tetrathionate reductase (OTR).**

*Panel A shows the electron density around the conventionally bis-histidine ligated hemes I and III-VIII. Panel B shows the electron density around the unusually ligated active site heme II, with a lysine ligand at one face of the heme and an exogenous thiocyanate ligand at the active site face. Panel C shows the structure of the active site in detail. Lysine 56 is able to ligate because the expected heme ligand, histidine 78, has moved away from the heme. A $SCN^-$ ion appears within the active site, ligating the heme, and the active site cysteine 64 has been modelled as a persulfide derivative.*

An additional indication as to the role of the protein is given by the presence of the cysteine

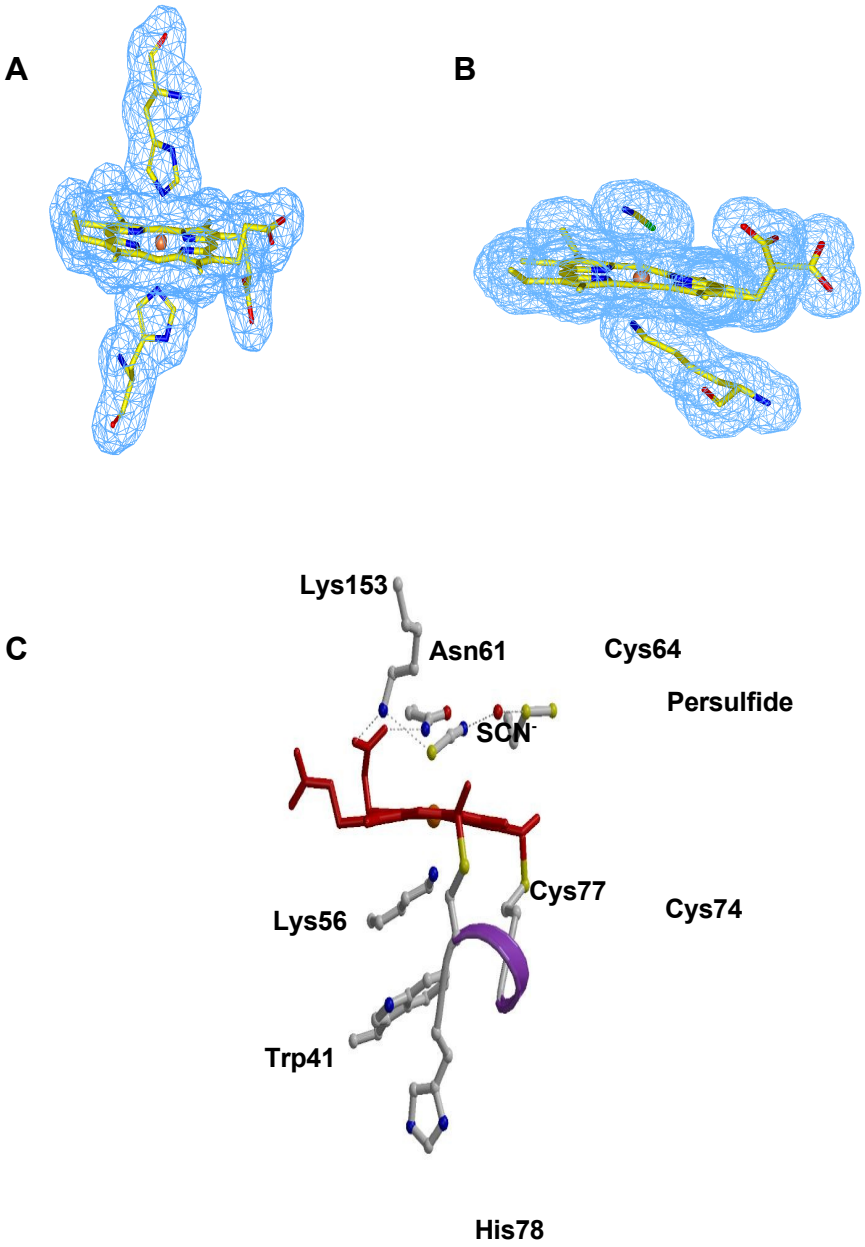


residue close to the proximal face of heme II. OTR contains seventeen cysteine residues, all but one of which are involved in the binding of the *c*-type hemes. The remaining cysteine (Cys64)

is located above the proximal face of heme II, with the cysteinyl sulfur positioned at a distance of 9.2 Å from the heme iron.

The cysteine 64 residue appears to have undergone a post-translational modification. A region of unexplained electron density has been found in the region of the terminal sulfur atom of cysteine 64 using Fourier maps calculated using the fully refined structural model. Refinement of the density reveals that the derivative is probably a cysteine persulfide or cysteine sulfenic acid and these modifications have been previously identified in other protein crystal structures (Clairborne *et al*, 1999; Bordo *et al*, 2000; Bamford *et al*, 2002). The additional atom has not yet been identified, but the residue is shown in Figure 1.24(C) as a cysteine persulfide post-translational modification, forming what appears to be a "dead-end" complex.

The cavity formed by the absence of an amino acid ligand to the proximal face of heme II easily accommodates the thiocyanate ion seen in the crystal structure. The distance between the unknown atom attached to the cysteinyl sulfur and the sulfur atoms of thiocyanate is 8.5 Å. This indicates that the natural substrate of OTR may contain a chain of atoms with sulfur or oxygen atoms separated by a similar distance at either end.

#### 1.7.2.3 Similarities with Other Multiheme Structures

Octaheme tetrathionate reductase shows no fold similarity to other known protein structures, however the arrangement of heme groups does show similarity to those of hydroxylamine

oxidoreductase from *Nitrosomonas europaea* and the pentaheme nitrite reductase from *Wolinella succinogenes* (Mowat *et al*, 2005). The hemes in OTR are arranged into a three-heme cluster (active site heme II, hemes IV and V), two heme pairs (hemes I and III, VI and VII) and a single heme (heme VIII) (Figure 1.25).

The triheme clusters of OTR and HAO are almost identical and both contain the active site heme, Heme II and P460 respectively. The structures of OTR and HAO also contain the two heme pairs, which are organised in a similar manner, as well as the single hemes.

**Figure 1.25: Overview of the heme arrangement in OTR.**
*From Mowat et al, 2005. Hemes are grouped into clusters, in a similar manner to those found in HAO.*

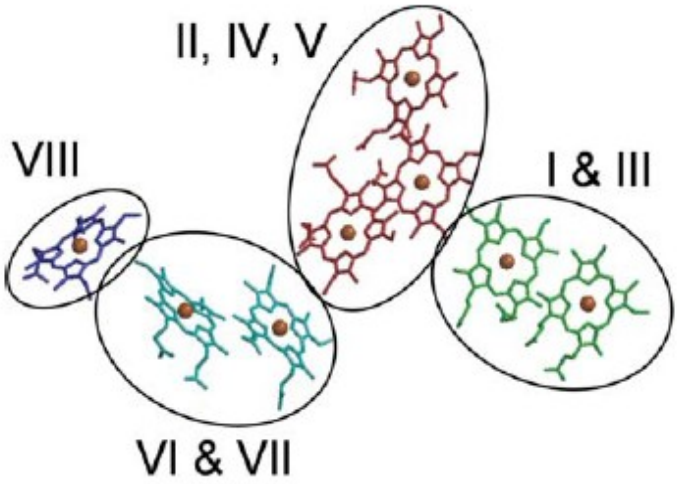


It is possible to superimpose seven of the eight hemes in OTR and HAO (Figure 1.26), although it can be seen that despite the identity of the active site triheme clusters it is necessary that the active sites heme II and P460 are oriented on either side of the heme chain in order for the other seven hemes to overlay correctly. In addition to this, HAO is a functional trimer and

there is thought to be significant interaction between the heme groups of neighbouring monomers. There is no evidence of any multimeric character in OTR.

A similar overlay of the five hemes of NrfA with OTR can also be achieved (Figure 1.26). In this case it is notable that each of the five hemes of NrfA is positionally related to hemes II to VI of OTR. The unusually lysine-ligated hemes, heme 1 and heme II respectively may be directly superposed, with this superposition extending even to the positions of the active site lysines and the substrate binding sites. However, as is the case for HAO, there is no overall fold similarity between OTR and NrfA.

#### 1.7.2.4 Proposed mechanism of tetrathionate reduction

A possible mechanism for tetrathionate reduction by OTR has been proposed by Rothery (2003), in which Cys64 undergoes a disulfide exchange with tetrathionate, followed by a two electron reduction at heme II. The modification of a cysteine residue to a sulfenic acid has been identified in the mechanisms of a number of enzymes (Claiborne *et al*, 2001), and this also has a precedent in the thiosulfate oxidising enzyme SoxAX from *Rhodovulum sulfidophilum* (Bamford *et al*, 2002b), in which a persulfide modification is found. There is currently no conclusive evidence to confirm this mechanism, although the crystal structure shows that the side chain sulfur atom of Cys64 is modified. The electron density map

**Figure 1.26: Comparison of the heme arrangements of OTR (in red), HAO (left, in blue) and NrfA (right, in green).**

*From Atkinson et al, 2007. The active site P460 heme of HAO is shown in light blue. It can be seen that only the active site hemes are excluded from the superposition. Although the heme architecture is similar, there is no fold similarity between the three enzymes.*

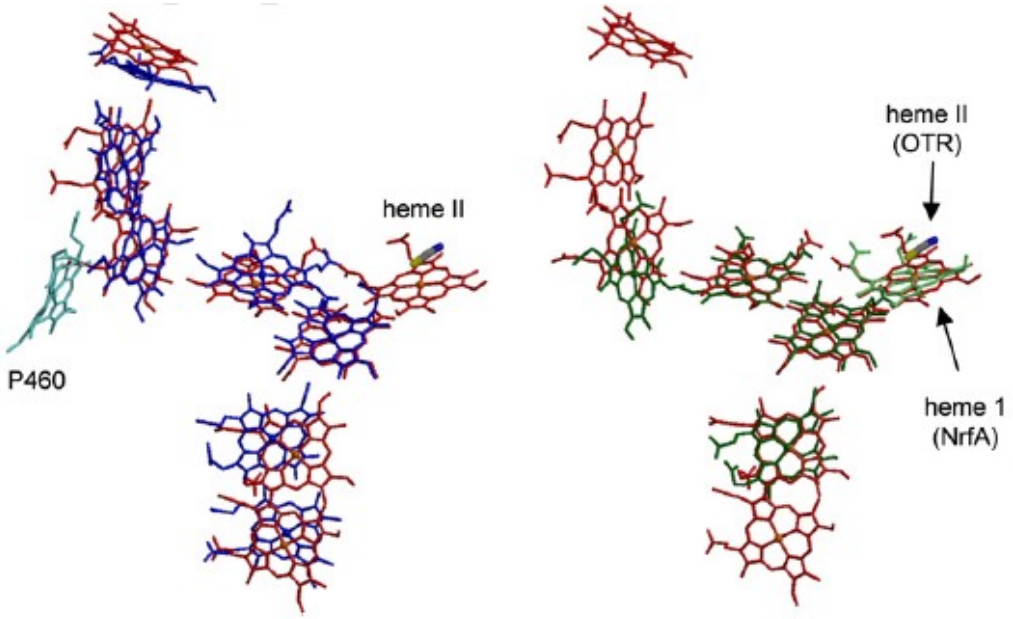


indicates the possible presence here of a second bound sulfur or oxygen atom; however, these possibilities cannot be distinguished from one another in the current structure.

The discovery of this novel tetrathionate reduction activity and unprecedented heme ligation in OTR from *Shewanella oneidensis* is exciting, although much is still to be discovered about this interesting enzyme.

## 1.8 *GEOBACTERACEAE*

Organisms of the genus *Geobacteraceae* are members of the δ-proteobacteria (Lovley *et al*, 1993), a group containing many phylogenetically diverse species which are all capable of

dissimilatory sulfate reduction under anoxic conditions. *Geobacteraceae* are rod-shaped, Gram-negative cells. Cells are non-motile and do not form spores. They are chemoautotrophs that are able to completely oxidise a number of organic substrates to carbon dioxide with Fe(III) as the terminal electron acceptor. Reduction of Fe(III) oxide by these species can, under certain conditions, result in the extracellular accumulation of ultrafine-grain magnetite. The type species of this genus is *Geobacter metallireducens*, the closest relative to *G. sulfurreducens* by 16S rRNA phylogenetic analysis.

*Geobacter* species are of great interest for study due to their novel electron transfer capabilities and also because they serve as a model for a variety of environmental phenomena associated with iron reduction, such as the oxidation of natural and contaminant organic matter, the magnetisation of aquatic sediments, the release of phosphate, trace metals and dissolved iron into ground and drinking waters, and the dissimilatory reduction of other metals with multiple redox states (e.g. Mn(IV) and U(IV)) (Lovley, 2003).

### 1.8.1 *Geobacter sulfurreducens* PCA

The bacterial species G*eobacter sulfurreducens* PCA was initially isolated from the surface sediments of a hydrocarbon-contaminated ditch in Norman, Oklahoma (Caccavo *et al*, 1994). The bacteria are anaerobic chemoorganotrophs which are able to oxidise acetate with Fe(III), S(0), Co(III), fumarate or malate as electron acceptor and both acetate and hydrogen may be used as electron donors for Fe(III) reduction. Upon discovery, the ability to couple the oxidation of both acetate and hydrogen to the reduction of Fe(III) was found to be unique to this species.

*G. sulfurreducens* is an important component of subsurface environments and is capable of energy generation using a range of different terminal electron acceptors. Further to this, the species also has the ability to couple the precipitation of soluble metals to insoluble forms (e.g. U(VI) to U(IV)), to the oxidation of organic compounds to carbon dioxide. Studies of this organism are therefore of great interest for a number of reasons. The ability of *Geobacter* species to remove potentially harmful metal ions and organic contaminants from the environment has potential use in the bioremediation of contaminated land and ground water. Additionally, the capability of these species to transfer electrons onto the surface of electrodes has led to the possibility of the design of novel microbial fuel cells which can efficiently convert waste organic matter into electricity (Bond *et al*, 2003).

Analysis of the complete genome of *G. sulfurreducens* PCA (Methé *et al*, 2003) has revealed 3466 predicted open-reading frames, of which 111 are putative *c*-type cytochromes (as defined by the presence of the *c*-type heme attachment motif, CXXCH; Figure 1.27). This unprecedented number of cytochromes highlights the importance of electron transport to the organism and reflects the flexibility in its electron-transfer pathways that is required for the reduction of such a diverse range of metal ions. Of the 111 *c*-type cytochromes identified, 73 are predicted to contain more than one heme, with a significant number containing 8 or more hemes (Table 1.3). Many of these multiheme cytochromes are being found to have associated enzymatic activities.

**Figure 1.27: Circular representation of the genome of *Geobacter sulfurreducens.***

*From Methé et al, 2003 (Supporting Material). Predicted c-type cytochromes are shown in pink in the third circle from the outside.*

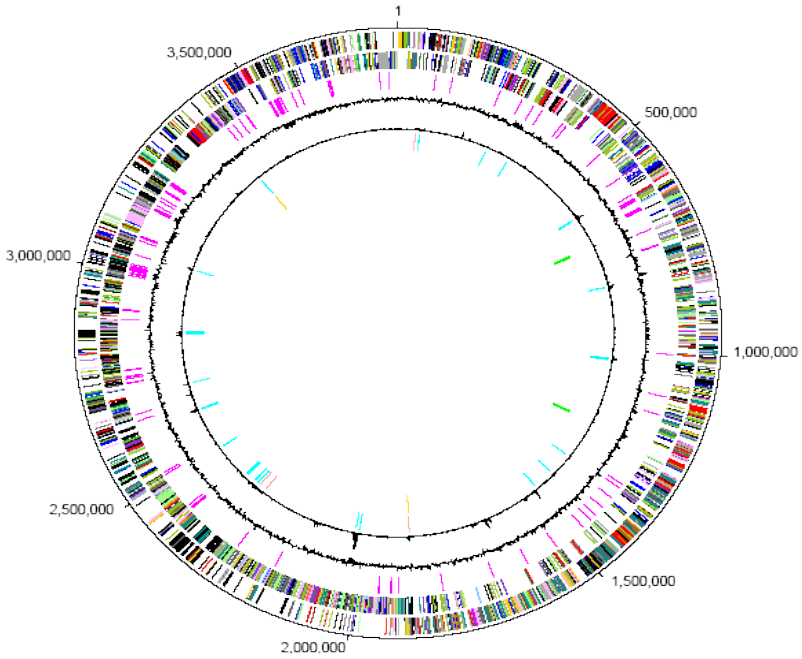


As a result of the publication of the genome sequence of *G. sulfurreducens* PCA (Methé *et al*, 2003), a number of potentially interesting multiheme cytochromes have been isolated and characterised. Many of these cytochromes are thought to be involved in the reduction of metals, such as Cr(VI), Fe(III) and U(VI), and may be involved in important biogeochemical processes.

For example, the periplasmic triheme cytochrome $c_7$, known as PpcA, has been isolated and characterised from a number of sources, including *Desulfuromonas acetoxidans* (where the protein is known as cytochrome $c_{551.5}$) and *G. sulfurreducens* (Pokkuluri *et al*, 2004b). PpcA has been shown to reduce metal ions, such as Fe(III), U(VI) and Cr(VI) (Assfalg *et al*, 2002) and the *D. acetoxidans* protein has been implicated in sulfur reduction (Pfennig *et al*, 1976).

**Table 1.3: Table showing the number of predicted *G. sulfurreducens* *c*-type cytochromes containing 8 or more heme groups.**

*The following table was complied by Dr. E.L. Rothery and Dr. C.S. Miles (University of Edinburgh) following analysis of the G. sulfurreducens genome sequence. Potential multiheme*

*cytochromes were identified using the heme-binding CXXCH amino acid sequence. This table shows the number of proteins expected to contain each stated number of heme groups; for example, the genome sequence predicts that G. sulfurreducens will contain three decaheme proteins. Multiheme proteins containing less than 8 hemes are not shown in this table.*

| **No. of hemes per protein** | **Predicted no. of proteins** |
|---|---|
| 8 | 8 |
| 9 | 1 |
| 10 | 3 |
| 11 | 1 |
| 12 | 8 |
| 15 | 1 |
| 16 | 1 |
| 17 | 1 |
| 18 | 1 |
| 23 | 1 |
| 26 | 1 |
| 27 | 4 |
| 34 | 1 |
| 35 | 1 |

PpcA from *G. sulfurreducens* (Figure 1.28) has been similarly shown to directly reduce soluble species which enter the periplasm, but has additionally shown the ability to transfer electrons to a terminal Fe(III)-oxide reductase found on the outer membrane of the cell (Lloyd *et al*, 2003). This diversity of reactions has led to debate as to the physiological role of PpcA, as has the observation that the packing of PpcA in the crystal structures of both *D. acetoxidans* and *G. sulfurreducens* leads to the close interaction of the hemes of adjacent molecules. In the *D. acetoxidans* PpcA, hemes I and IV of adjacent molecules are closely located and heme IV is found to be near-parallel to heme III of the molecule alongside. This arrangement of hemes is frequently found in electron transport proteins (Iverson *et al*, 1998), leading to the suggestion that these interactions between the PpcA $c_7$ molecules may form an intermolecular electron transport pathway (Czjzek *et al*, 2001).

**Figure 1.28: The structure of cytochrome $c_7$ PpcA from *Geobacter sulfurreducens.***

*From Pokkuluri et al, 2004b. The polypeptide backbone is shown in blue and the hemes are shown in green with their oxygen atoms coloured red. A molecule of deoxycholic acid is shown towards the bottom of the structure. Deoxycholic acid is required for crystallisation and is not found in the periplasm of G. sulfurreducens, however its position may reflect a small molecule binding site.*

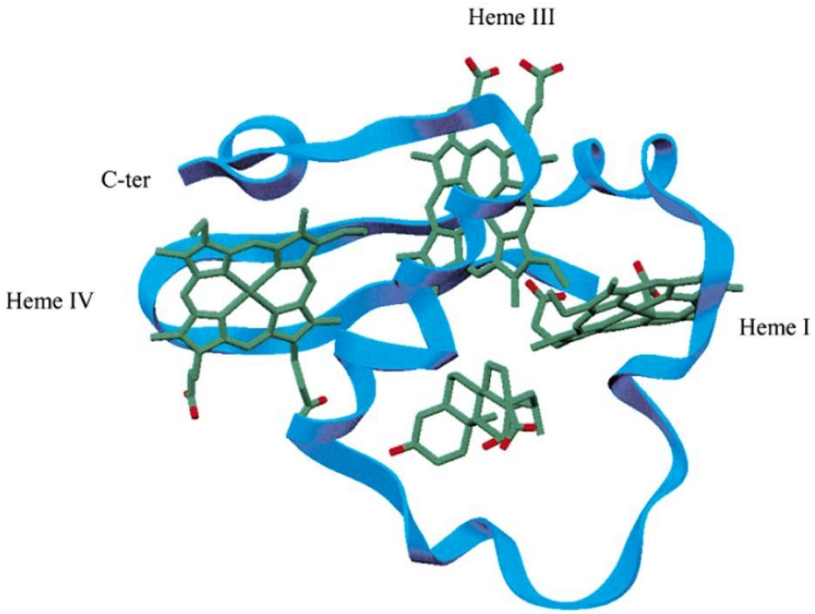


In the PpcA from *G. sulfurreducens*, the molecules are found similarly packed, with intermolecular heme I-heme IV distances as small as 7 Å, only ~ 1 Å greater than intramolecular heme-heme distances. This leads to the postulate that a "chain" of PpcA "modules" could potentially form, resulting in an unbroken polypeptide.

This interesting proposition has also been considered in relation to a number of other multiheme cytochromes from *G. sulfurreducens*. Examination of the genome sequence has revealed the presence of three other cytochromes that are polymers of $c_7$ domains (two dodecahemes (tetramers of $c_7$ units) and a nonamer of 27 hemes). GSU1996 is one such dodecaheme and work has been carried out cloning the protein as four domains, for one of which the crystal structure has been obtained (Pokkuluri *et al*, 2004a).

### 1.8.2 GSU0357

Investigation of the genome sequence of *G. sulfurreducens* has led to the identification of a number of potential target proteins which may be of interest for study. One intriguing target is GSU0357, which has been identified as an octaheme homologue of the pentaheme cytochrome *c* nitrite reductases previously described.

GSU0357 contains seven conventional CXXCH *c*-type cytochrome attachment motifs and one unconventional CXXCK motif (Figure 1.29). The theoretical mass of the protein is 56,405 Da and its theoretical pI is 9.03.

**Figure 1.29: The amino acid sequence of GSU0357.**

*The signal sequence is indicated in blue, CXXCH motifs in red and CXXCK motif in green.*

GSU0357

MWKKRLAVLAVAAGAAVALSIPALSTAAKGKPAATGAKGDGRETCYGCHEEVKALKEGSK
HARLACDSCHDKLKEHLANYETKPGTNLDPAKCGSCHKNEYSSFFTVNYDAQPRKEKGIP
TGRSPMQDKLLAGHGFTFEHNEPRGHAFMVVDQFIVDRFQGGRFQYKKGAWGMDATGKAW
DILTDTGKKLPETAMAGNPTCIQCKTSDHILKWKFMGDKDPKATWDRSSDIVAVAKDTQN
PVGCIHCHDPHGTQPRVVRDGLIQAIEKDPTANIFAKNGKTDLKVISFRDGFRKIGVMEK
TDSRLMCAQCHVEYNCNAGSQWSDGQKVGYDDQRTNHFPLKNAKDLLAHYKKLDFYDFKH
AITGARLVKLQHPEAETYAGSVHDRAGVGCADCHMPRMKGKDGKMFKSHGVIRPAHHVKE
ACLGCHPKSTVEQKSYQIEGTRNYIRGKMRKAEYWLGQLIDTYAAAKRMGIGEDVLAKAR
EKHEEAHVLWEYWTAENSDGFHNPELARDSLTSSIAASKAGVKLLNDAMEPKK

GSU0357 shows the closest sequence alignment to the cytochrome *c* nitrite reductases, such as the nitrite reductase from *Desulfovibrio desulfuricans* ATCC 27774 (Cunha *et al*, 2003; similarity 37%; see Appendix III for sequence alignment). Therefore, it might be expected that GSU0357 will have a similar structure and role as a nitrite reductase. The *D. desulfuricans* enzyme is isolated as a 61 kDa 5-heme monomer and adopts a homodimeric structure in the active enzyme (Figure 1.18), as previously described.

However, the key difference between this enzyme and the enzymes previously discussed is of particular interest; the sequence of GSU0357 contains eight predicted hemes, as opposed to five. This enzyme could therefore be the first known octaheme cytochrome *c* nitrite reductase. It is not known what effect the addition of three hemes would have on the structure and properties of the enzyme, and conversely the extra hemes may have no influence. NrfA from *D. desulfuricans* functions with a redox partner, NrfH, and it may be the case that the three additional hemes encoded in the GSU0357 sequence removes the requirement for a NrfH-like physiological redox partner. Additionally, the postulate that this enzyme functions as a nitrite reductase may be disproved; it is possible that the enzyme may be found to have a different, or even multiple, substrates and may catalyse a range of reactions.

A putative octaheme oxoanion polyreductase with high sequence identity to GSU0357 has been isolated from the extremophile bacterium *Thioalkalivibrio nitratireducens* (Polyakov *et al*, 2003). *Thioalkalivibrio* species are haloalkaliphilic obligately chemolithoautotrophic sulfur-oxidizing bacteria, isolated from soda lakes globally (Foti *et* al, 2006). Soda lakes are extremely alkaline environments, maintaining stable pH values of 9.5-11. It is known that the sulfur cycle is one of the most active microbial processes occurring in soda lakes and, although until recently the potential of aerobic chemolithoautotrophic sulfur-oxidising bacteria to grow in extremely alkaline conditions had not been identified, more than 100 isolates of such bacteria have been cultured from the sediments of various soda lakes.

The octaheme enzyme from *Thioalkalivibrio nitratireducens* reduces a number of oxoanions, including nitrate, nitrite, bromate, chlorate and catalyses peroxidase and haloperoxidase reactions (Polyakov *et al*, 2003). However, no data have yet been published on this enzyme.

## 1.9 FOCUS OF THIS THESIS

The work reported in this thesis examines the two multiheme enzymes, octaheme tetrathionate reductase and GSU0357, which have been isolated from the dissimilatory metal-reducing bacteria *Shewanella oneidensis* and *Geobacter sulfurreducens* respectively.

Previous work on octaheme tetrathionate reductase (OTR) has allowed its over-expression, isolation and structure determination, in addition to some characterisation of its reactions. The work in this thesis includes an improved purification protocol for this enzyme and seeks to extend the existing characterisation by examining a series of further potential substrates and investigating the possibility, as suggested by homology of heme arrangement with other multiheme *c*-type cytochromes, that OTR may in fact be a nitrogen cycle enzyme. In addition to this, a programme of site-directed mutagenesis has been initiated, in order to probe the role of the unexpected lysine ligand to the active site heme.

Sequence analysis has predicted that GSU0357 contains 7 conventionally- and one unconventionally-ligated heme groups. The binding motif of the unconventional heme suggests that a lysine residue may be a heme ligand. This inclusion of a lysine in the binding motif is unusual and has only previously been observed in the pentaheme cytochrome *c* nitrite reductases, with which GSU0357 shows some sequence homology. It is hence proposed that GSU0357 may function as an enzyme in the nitrogen cycle. The putatively octaheme GSU0357 therefore presents an interesting and novel target for study.

The aim of this work was to purify and characterise the novel octaheme nitrite reductase GSU0357 from *Geobacter sulfurreducens*. Culture of the species has been optimised to maximise the yield of bacterial cells and a purification scheme to allow the isolation of pure protein is under development. This purification has proved to be non-trivial and a range of different methods have been employed and will be discussed. Some characterisation of a potential substrate for GSU0357 will also be examined.

# *CHAPTER 2*

# *MATERIALS AND METHODS*

# 2 MATERIALS AND METHODS

## 2.1 BACTERIAL GROWTH

Bacterial cultures were grown in Luria Bertani (LB) Broth (Table 2.1) which had been autoclaved at 121 °C for 20 mins in a Kestral autoclave and then supplemented with antibiotics once cooled. Agar plates were prepared by the addition of agar to the media prior to autoclaving.

**Table 2.1: Media components.**

| Medium | Component | Mass |
|---|---|---|
| Luria Bertani Broth | Tryptone Extract | 10 g $l^{-1}$ |
| | NaCl | 10 g $l^{-1}$ |
| | Yeast | 5 g $l^{-1}$ |
| Agar | 15 g $l^{-1}$ dissolved in LB broth | |

### 2.1.1 Growth of Octaheme Tetrathionate Reductase from *Shewanella oneidensis* MR-1

Recombinant octaheme tetrathionate reductase (OTR) was prepared by Dr. M. Doherty and Dr. L. McIver, Department of Chemistry, University of Edinburgh, using the broad-host-range controlled-expression vector pMMB503EH (Figure 2.1; Overbye Michel,

1995) in the *Shewanella frigidimarina fcc*$_3$ knockout strain EG301 (NCIMB 400; Rif$^R$, Δfcc:ahp, Km$^R$), as described by Mowat *et al*, 2004 (see Supplementary Methods). The intrinsic signal sequence of the target was used. Bacterial strains were stored as 7 % DMSO stocks (-80°C).

### 2.1.2 Growth of K56A Octaheme Tetrathionate Reductase from *Shewanella oneidensis* MR-1

The site-directed mutant of OTR, K56A, was generated by Dr. C.S. Miles, Institute for Structural and Molecular Biology, University of Edinburgh, using the QuikChange XL Site-Directed Mutagenesis Kit (Stratagene). The template for the reaction was pMD2 (*SO4144*/pMMB503EH). Oligonucleotides were designed to incorporate the lysine 56 to alanine change and were complementary to the same sequence on both strands of the plasmid. The oligonucleotide sequences were:

K56AFor (5' GAACCGTGGTTCGGGGTGCGAAAAACAGTATTAATAAC)

K56ARev (5' GTTATTAATACTGTTTTTCGCACCCCGAACCACGGTTC).

Mismatches are underlined. Screening for the required mutation was carried out by DNA sequencing and the OTR K56A coding sequence was checked to verify that no secondary mutations had been introduced. The resulting plasmid, pCM178, was used to transform the mobilising *E. coli* strain SM10 and was subsequently transferred into the *Shewanella oneidensis* MR-1 octaheme knockout strain (constructed by Dr. L. McIver, Department of Chemistry, University of Edinburgh) by conjugation.

**Figure 2.1: The plasmid vector pMMB503EH**

*Figure from Overbye Michel et al, 1995.*

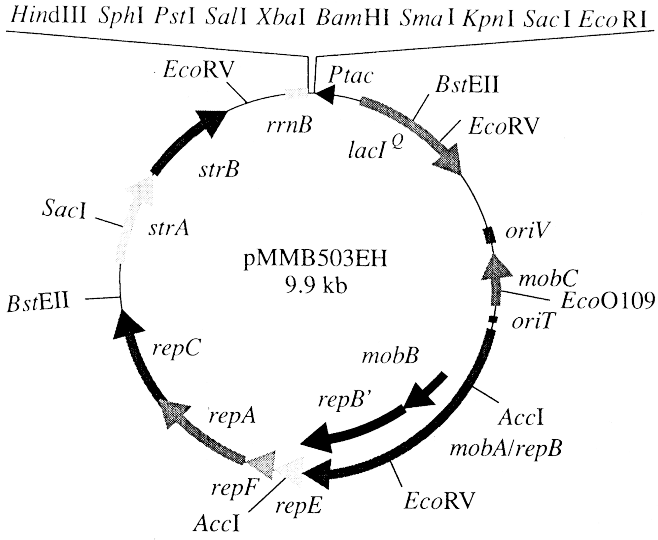


Starter cultures which had been inoculated with single colonies from an agar plate were grown in 75ml flasks of sterile media containing the antibiotics Kanamycin (25 mg $l^{-1}$) and Streptomycin (50mg $l^{-1}$) for 15 hours at 23 °C, 150 rpm, in an orbital shaker (Innova 4330, New Brunswick Scientific).

5 ml aliquots of starter culture were inoculated into 0.5 l LB broth in 1 l non-baffled conical flasks and grown for 13 hours under the same conditions. The culture was then induced with IPTG (isopropyl-β-D-thiogalactopyranoside) at a final concentration of 250 mg $l^{-1}$ and the shaker speed increased to 200 rpm. After a further 8 hours of growth, cells were harvested by centrifugation at 8,000 rpm, 4 °C for 1 hour using a Sorval RC26Plus refrigerated centrifuge.

### 2.1.3 Growth of GSU0357 in *Shewanella frigidimarina* and *Escherichia coli*

*Shewanella frigidimarina* EG301 and *Escherichia coli* JM109 (DE3) cells expressing recombinant GSU0357 were prepared by Dr. C.S. Miles, ISMB, University of Edinburgh. In both cases the intrinsic signal sequences of the targets were used. These constructs were prepared and their proteins purified simultaneously in order to determine which route would most readily allow the GSU0357 protein to be obtained. Bacterial strains were stored at -80 °C as 7% DMSO stocks.

#### 2.1.2.1 Expression of GSU0357 in *Shewanella frigidimarina* EG301

The DNA sequence encoding GSU0357 was amplified from *Geobacter sulfurreducens PCA* genomic DNA using the polymerase chain reaction (PCR). The primers

GB0357For (5' CACGAATTCATGTGGAAGAAACGACTGGCTGTACTG)
and GB0357Rev (5' CTGAAGCTTTTACTTCTTGGGTTCCATGGCGTCGTTC)

were used to incorporate an *Eco*RI restriction endonuclease site immediately upstream of the ATG start codon and a *Hin*dIII site immediately downstream of the TAA stop codon, respectively. The PCR product was initially cloned into the pGEM-T vector (Promega) and the GSU0357 coding sequence verified by DNA sequencing. The GSU0357 coding sequence was excised from pGEM-T using the introduced *Eco*RI and *Hin*dIII restriction enzyme sites and cloned into the pMMB503EH expression plasmid (cut with the same restriction enzymes). The resulting plasmid, pCM260, was

transferred to the mobilising *E. coli* strain SM10 and subsequently transferred to the *Shewanella frigidimarina* strain EG301 by conjugation.

#### 2.1.2.2 Expression of GSU0357 in *Escherichia coli* JM019(DE3)

To enable expression of GSU0357 in *E. coli*, the pETBlue-1 expression vector (Novagen; Figure 2.2) was used. The GSU0357 coding sequence was amplified from *Geobacter sulfurreducens* PCA genomic DNA by PCR. The primers used were

GB0357PBFor (5' ATGTGGAAGAAACGACTGGCTGTACTG)

and GB0357Rev (5' CTGAAGCTTTTACTTCTTGGGTTCCATGGCGTCGTTC).

The forward primer was designed to encode an ATG start codon at the 5' end to enable cloning into the pETBlue-1 vector (at the pre-cut *Eco*RV site). There were no restrictions on the design of the reverse primer so an existing GSU0357 PCR primer (see above) was used. Cloning of the PCR fragment into pETBlue-1 was carried out as per the manufacturer's protocol. Screening by digestion was carried out to select for constructs with the insert in the correct orientation. The GSU0357 coding sequence of the selected construct was then sequenced to verify that no mutations had been introduced during the PCR. The resulting plasmid, pCM261, was transferred to the *E. coli* expression strain JM109(DE3) along with the pEC86 plasmid (Arslan, 1998). pEC86 expresses the *E. coli* cytochrome *c* maturation genes (*ccmABCDEFGH*) constitutively.

**Figure 2.2: The pETBlue-1 vector (Novagen)**

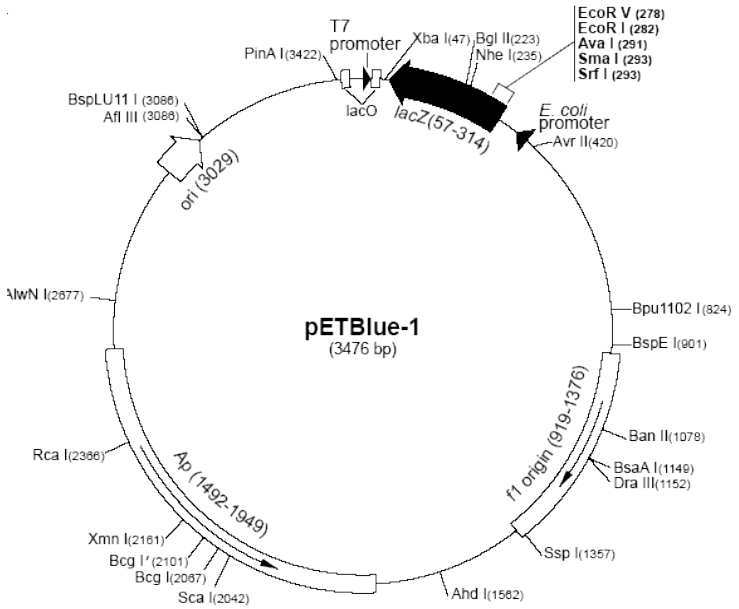


For both the *S. frigidimarina* and *E. coli* expression systems, agar stocks were inoculated using DMSO cell stocks and allowed to grow at room temperature (*ca*. 22 °C), out of direct sunlight, for 50 hours. A single colony from the cultured plate was used to inoculate 75 ml LB broth, and these starter growths were incubated under the appropriate conditions (Table 2.2) for 24 hours.

**Table 2.2: GSU0357 growth conditions.**

| | ***Shewanella frigidimarina*** | ***Escherichia coli*** |
|---|---|---|
| Antibiotics ($l^{-1}$) | 50 mg Kanamycin<br>25 mg Streptomycin | 50 mg Carbenicillin<br>50 mg Chloramphenicol |
| Flask type | Non-baffled | Baffled |
| Temperature (°C) | 23 | 37 |
| Shaking speed (rpm) | 140 | 150 (pre-induction)<br>200 (post-induction) |

5 ml aliquots of starter growth were then used to inoculate 0.5 l broth in 1 l conical flasks and grown for 8 hours. Cultures were then induced with IPTG at a final

concentration of 250 mg $l^{-1}$. After 15 further hours growth the cells were harvested by centrifugation at 8000 rpm, 4 °C for 15 minutes.

## 2.2 PROTEIN PURIFICATION

The following buffers were used during the purification of the enzymes (Table 2.3):

**Table 2.3: Purification buffers.**

| Buffer | Description | pH |
|---|---|---|
| **A** | 10 mM Tris.HCl, 10 mM NaCl | 8.4 |
| **B** | 10 mM Tris.HCl, 500 mM NaCl | 8.4 |
| **C** | 10 mM Tris.HCl, 100 mM NaCl | 8.4 |
| **D** | 50 mM Tris.HCl, 5 mM EDTA, 10 mM NaCl | 8.0 |
| **E** | 20 mM $Na_2HPO_4$, 20 mM NaCl, 5mM EDTA, 25 % (w/v) sucrose | 7.2 |

### 2.2.1 Purification of Wild Type and K56A Octaheme Tetrathionate Reductase

OTR was purified using a sequence of weak anion exchange chromatography, hydroxyapatite chromatography and strong anion exchange chromatography (Figure

2.3), as detailed below and in Section 3.1. The K56A OTR mutant was purified using the same procedure. The progress of the purification was followed using SDS-PAGE after each stage. These gels are shown in Sections 3.1, while the SDS-PAGE gel of pure wild type OTR is shown in Figure 2.6.

#### 2.2.1.1 Cell lysis

After centrifugation, cells were resuspended in Buffer A. Cell lysis was initiated by incubating the suspension with egg white lysozyme (Sigma) for 30 mins and completed by ultrasonication (10 x 20 seconds at 10 microns amplitude, with cooling between sonications, Sanyo Soniprep 150) on ice. Cell debris was removed by centrifugation at 20,000 rpm, 4°C, 60 mins) and the supernatant collected.

#### 2.2.1.2 Weak anion exchange chromatography

Column chromatography was conducted at 4 °C. Pre-swollen DE-52 anion exchange resin (Whatman) was suspended in buffer A and a 4 cm x 20 cm column was poured and equilibrated.

**Figure 2.3: Overview of wild type and K56A OTR protein purification from *S. frigidimarina*.**

*The cell free extract obtained from S. frigidimarina cells was purified using weak and strong anion exchange and hydroxyapatite chromatography.*

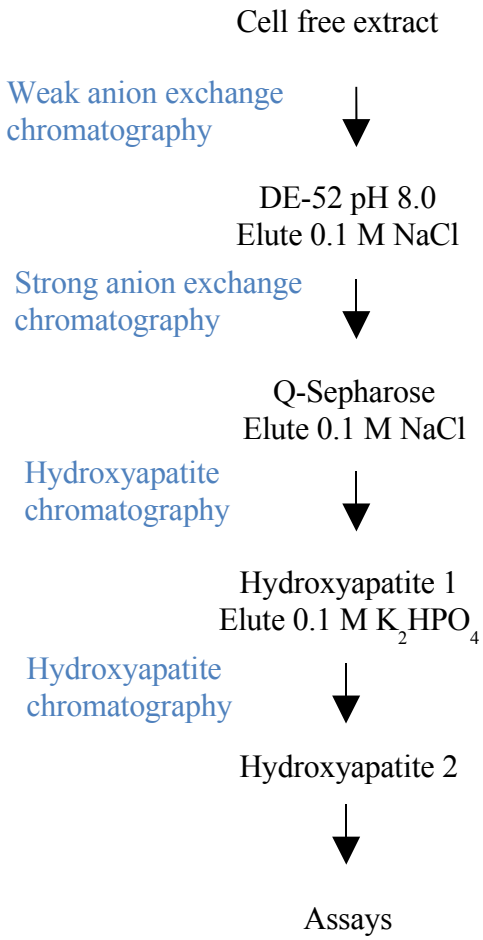


The supernatant was applied to the top of the column and the bound proteins formed a red band at the top. The column was then washed with 5 column volumes of buffer A and subsequently eluted using a stepwise NaCl gradient, with 100 mM increments. OTR was found to elute at 100 mM NaCl. Protein fractions for further purification were pooled and dialysed against 2 x 4 l of buffer A.

#### 2.2.1.3 Strong anion exchange chromatography

Purification using Q-Sepharose strong anion exchange resin was performed using an FPLC (Fast Protein Liquid Chromatography) system using a 60 ml HiLoad 26/10 Q-

Sepharose column equilibrated in buffer A. The protein solution was passed through a 0.45 μm filter, loaded on to the column and washed with 5 column volumes of buffer A. The column was eluted using a linear gradient of increasing NaCl concentration from 0 – 100 % buffer B (100 – 0 % buffer A) and the fractions analysed for OTR content using gel electrophoresis. The protein fractions for further purification were pooled and dialysed against 2 x 4 l of buffer A.

### 2.2.1.4 Hydroxyapatite chromatography

Hydroxyapatite resin (Bio-Rad Chemicals) was prepared by suspension in buffer A and fines removed by washing with buffer. A 3 cm x 8 cm column was poured and equilibrated in buffer A.

The protein solution was applied to the top of the column and washed with 5 column volumes of buffer A. The protein bound in a tight red band at the top of the column. The column was eluted using 100 mM $K_2HPO_4$. The protein fraction for further purification was dialysed against 2 x 4 l of buffer A.

This hydroxyapatite chromatography step was then repeated to improve the purity of the sample, as discussed in Section 3.1. The purity of the sample was then assessed using SDS-PAGE (Section 2.3), as indicated in Figures 2.6 and 3.4 (wild type OTR), and 4.3 (K56A OTR).

### 2.2.1.5 Concentration and storage

The protein was concentrated to *ca.* 100 μM using centrifugation (Amicon Centriprep, 80 kDa MWCO) and stored at -20° C in 0.5-ml aliquots.

### 2.2.2 Purification of GSU0357

As detailed in Section 2.1.2, recombinant GSU0357 was expressed in both *Shewanella frigidimarina* EG301 and *Escherichia coli* JM109(DE3) cells. The procedures used to purify protein from each system are summarised in Figures 2.4 and 2.5 and fully described in Sections 2.2.2.1 and 2.2.2.2 respectively.

**Figure 2.4: Overview of GSU0357 protein purification from *S. frigidimarina* EG301.**

*The cell free extract obtained from S. frigidimarina cells was subjected to weak and strong anion exchange chromatography, followed by ammonium sulfate precipitation and size exclusion chromatography to yield a partially pure sample of GSU0357 which was used in preliminary activity assays.*

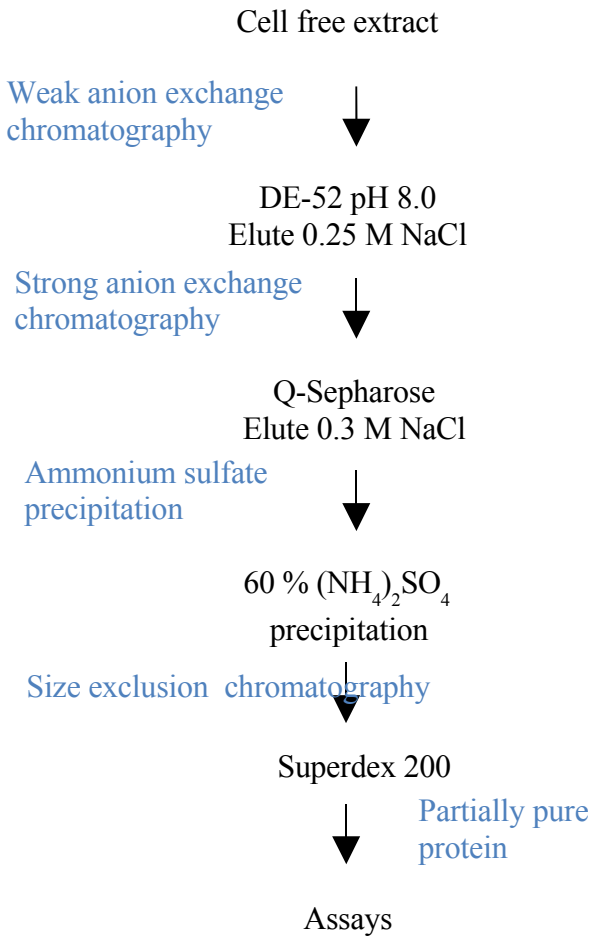


**Figure 2.5: Overview of GSU0357 protein purification from *E.coli* JM109(DE3).**

*The cell free extract obtained from E. coli cells was not found to contain any significant amount of GSU0357 protein and so the membrane fraction was treated using an inclusion body-type procedure in which the insoluble material was unfolded and refolded. Size exclusion chromatography was performed on the resulting sample, yielding a partially pure sample of GSU0357 which was used in preliminary activity assays.*

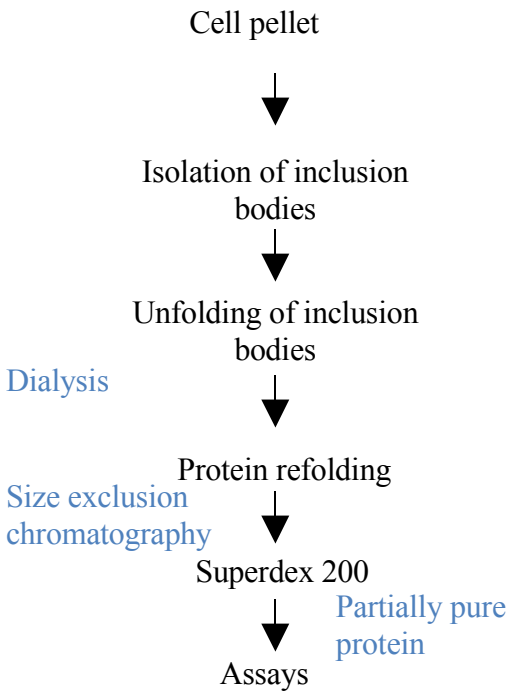


### 2.2.2.1 Purification of GSU0357 from *Shewanella frigidimarina*

GSU0357-containing cells were resuspended in Buffer A and lysed as described in Section 2.2.1.1.

#### 2.2.2.1.1 Weak anion exchange chromatography

The cell free extract was applied to a DE-52 weak anion exchange chromatography column and eluted using a stepwise NaCl gradient (as described in Section 2.2.1.2). GSU0357 was found to elute at 0.25 M NaCl. Protein fractions for further purification were pooled and dialysed against 2 x 4 l of buffer A.

#### 2.2.2.1.2 Strong anion exchange chromatography

Purification using Q-Sepharose strong anion exchange resin was performed as described in Section 2.2.1.3. The column was eluted using a linear gradient of increasing NaCl concentration from 0 – 100 % buffer B (100 – 0 % buffer A) and the fractions analysed for GSU0357 using gel electrophoresis. GSU0357 was found to elute at 0.3 M NaCl. Protein fractions for further purification were pooled and dialysed against 2 x 4 l of buffer A.

#### 2.2.2.1.3 Ammonium sulfate precipitation

The protein-containing fractions were taken to 60 % $(NH_4)_2SO_4$ (Fisher) saturation (395 g $l^{-1}$) and stirred for one hour. Precipitated proteins were removed by centrifugation (20,000 rpm, 20 mins, 4 °C) and the pellet resuspended in Buffer A. The ammonium sulfate was removed from the solution by dialysis against 3 x 4 l Buffer A. To ensure complete diffusion of the ammonium sulfate from the solution, the system was allowed to equilibrate overnight at 4 °C.

#### 2.2.2.1.4 Gel filtration chromatography

Size exclusion chromatography was performed using an FPLC system with a 320 ml HiPrep 26/60 Superdex 200 column equilibrated in Buffer C. The protein solution was passed through a 0.45 μm filter and loaded on to the column. The column was eluted isocratically using buffer C. Protein fractions were analysed using SDS-PAGE and fractions of interest were dialysed against 2 x 4 l of buffer A and concentrated as described in Section 2.2.1.5.

#### 2.2.2.2 Purification of GSU0357 from *Escherichia coli* JM109(DE3)

##### 2.2.2.2.1 Cell lysis

Approximately 50 g wet weight of cell pellet was resuspended in 150 ml buffer D and 1.5 ml of 100 mM PMSF and 16 μl of 50 mg/ml lysozyme were added to the resuspension. The solution was placed in a water bath at 37 °C until it became viscous and then sonicated (10 x 20 s at 10 microns, with cooling between sonications) on ice. Cell debris was removed by centrifugation at 20,000 rpm, 30 mins, 4 °C.

##### 2.2.2.2.2 Isolation and refolding of inclusion body material

The cell pellet was resuspended in 150 ml Buffer E and 1.5 ml of 100 mM PMSF and 1.5 ml Triton-X added. This solution was centrifuged at 20,000 rpm, 30 mins, 4 °C, and the resulting centrifugation pellet contained the inclusion body-type protein. In order to

unfold this protein the pellet was dissolved in ~100 ml 8 M urea containing 10 mM DTT. This solution was dialysed against 5 x 4 l 50 mM Tris/HCl, pH 8.5, over the course of three days and then centrifuged at 20,000 rpm, 30 mins, 4 °C. The supernatant, containing the inclusion body protein, was concentrated.

#### 2.2.2.2.3 Gel filtration chromatography

Gel filtration was perfomed as described in Section 2.2.2.1.4 and the resulting fractions of interest dialysed against 2 x 4 l Buffer A and concentrated as described in Section 2.2.1.5.

## 2.3 SDS-PAGE

SDS-PAGE (sodium dodecyl sulphate polyacrylamide gel electrophoresis) was used to assess the purity of the protein and estimate molecular weight. All gels were first heme- and then Coomassie-stained in order to distinguish proteins containing heme from those that did not.

### 2.3.1 Sample preparation

Samples for electrophoresis were made up to 20 µl with 25 % v/v NuPAGE LDS sample buffer (Invitrogen) and boiled for 5 minutes to denature the polypeptide chain.

### 2.3.2 Gel Loading and Electrophoresis

15 µl of sample was loaded on to a pre-poured 4-12 % Bis-Tris gel (Invitrogen) and 5 µl of pre-prepared molecular weight marker (SeeBlue Plus2, Invitrogen; Table 2.4) was loaded alongside. The gel was run for 1 hour at 150 V in NuPage MES SDS running buffer (Invitrogen).

**Table 2.4: Approximate molecular weights (kDa) of protein bands in SeeBlue Plus2 Pre-Stained Molecular Weight Standards in NuPAGE MES buffer.**

*The molecular weights of these marker proteins are used to estimate the molecular weights of the proteins observed experimentally on an SDS-PAGE gel.*

| Marker protein | Molecular weight (kDa) |
|---|---|
| Myosin | 188 |
| Phosphorylase | 98 |
| BSA | 62 |
| Glutamic dehydrogenase | 49 |
| Alcohol dehydrogenase | 38 |
| Carbonic anhydrase | 28 |
| Myoglobin red | 17 |
| Lysozyme | 14 |
| Aprotinin | 6 |
| Insulin, B chain | 3 |

### 2.3.3 Heme Staining

*C*-type hemes are covalently bound to the protein backbone and so are not lost in the denaturation of the sample by boiling. Therefore, any *c*-type cytochromes present in the

sample can be visualised using a hydrogen peroxide/TMBZ heme stain (Goodhew *et al*., 1984).

The staining process occurs as a result of the heme peroxidase activity of heme-containing proteins with the oxidizable substrate TMBZ in the staining solution, the product of which is an insoluble blue precipitate in the gel. The result of this staining technique is inconsistent for cytochromes *b* and the cytochromes P450 as the denaturing conditions employed during electrophoresis mean that only a variable portion of the heme is retained in the protein. However, as a consequence of the covalent attachment of the heme to the protein in *c*-type cytochromes, staining is consistent and heme-staining is a valuable technique in the purification of these proteins.

The SDS-PAGE gel was incubated in equilibration buffer (Table 2.5) for 30 mins with shaking at 125 rpm. Developing solution was added and the gel incubated for a further 30 mins at 125 rpm in the dark. The hydrogen peroxide was then added and the gel allowed to develop for 5 minutes. *C*-type cytochromes appeared as dark blue bands on the gel (Figure 2.6).

**Table 2.5: SDS-PAGE solutions.**

| **Stain** | **Purpose** | **Component** | **Quantity** |
|---|---|---|---|
| Heme Stain | Equilibration | $dH_2O$ | 60 ml |
| | | 2.5 M Sodium Acetate | 10 ml |
| | | Methanol | 30 ml |
| | Developing | TMBZ | 10 mg |

| | | | |
|---|---|---|---|
| | | Hydrogen peroxide (100 vol) | 1 ml |
| Coomassie Stain | Staining | $dH_2O$ | 50 ml |
| | | Methanol | 40 ml |
| | | Acetic Acid | 10 ml |
| | | Coomassie Brilliant Blue | 1 ml |
| Destain | Destaining | $dH_2O$ | 50 ml |
| | | Methanol | 40 ml |
| | | Acetic Acid | 10 ml |

**Figure 2.6: Heme-stained SDS-PAGE analysis of OTR**

*Lane MW is SeeBlue Plus2 molecular weight marker with corresponding molecular weights indicated at the right hand side of the diagram. Lanes 1-4 show purified OTR (MW = 54,450 Da)*

.

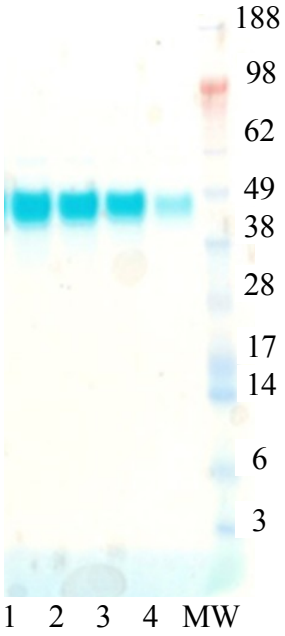


### 2.3.3 Coomassie Staining

Coomassie is used to stain for total polypeptide content in the samples run on the gel.

Following heme-staining, the gel was equilibrated in Coomassie stain (Table 2.5) for 30 mins at 125 rpm and then destained with several changes of solution until bands were clearly visible.

## 2.4 PROTEIN CHARACTERISATION

The wild type and K56A OTR proteins were assessed using UV/visible spectrophotometry to determine their purity and concentration, and a number of techniques including steady-state kinetic analysis, pH-activity dependence assays, solvent kinetic isotope effects and an ammonium detection assay were used to characterise their reactions.

The crude extracts containing GSU0357 proteins obtained by over-expression in *S. frigidimarina* and *E. coli* were tested for nitrite reductase activity using steady state kinetic analysis.

### 2.4.1 UV/Visible spectrophotometry

UV/visible spectra were routinely collected to analyse the identity, purity and concentration of the OTR proteins (Figure 2.7). Spectra were collected between 800 nm and 240 nm with a Shimadzu UV-2101 spectrophotometer, using a quartz cell of 1 cm path length.

### 2.4.2 Concentration determination

The concentration of the OTR protein sample was determined from the spectrum of the reduced protein.

**Figure 2.7: UV/visible spectra of wild type OTR**

*The oxidised spectrum is shown in black and the reduced spectrum in red. The absorbance ratio of this sample $A_{408}/A_{270}$ = 4, indicating that the enzyme is of sufficient purity for use in assays.*

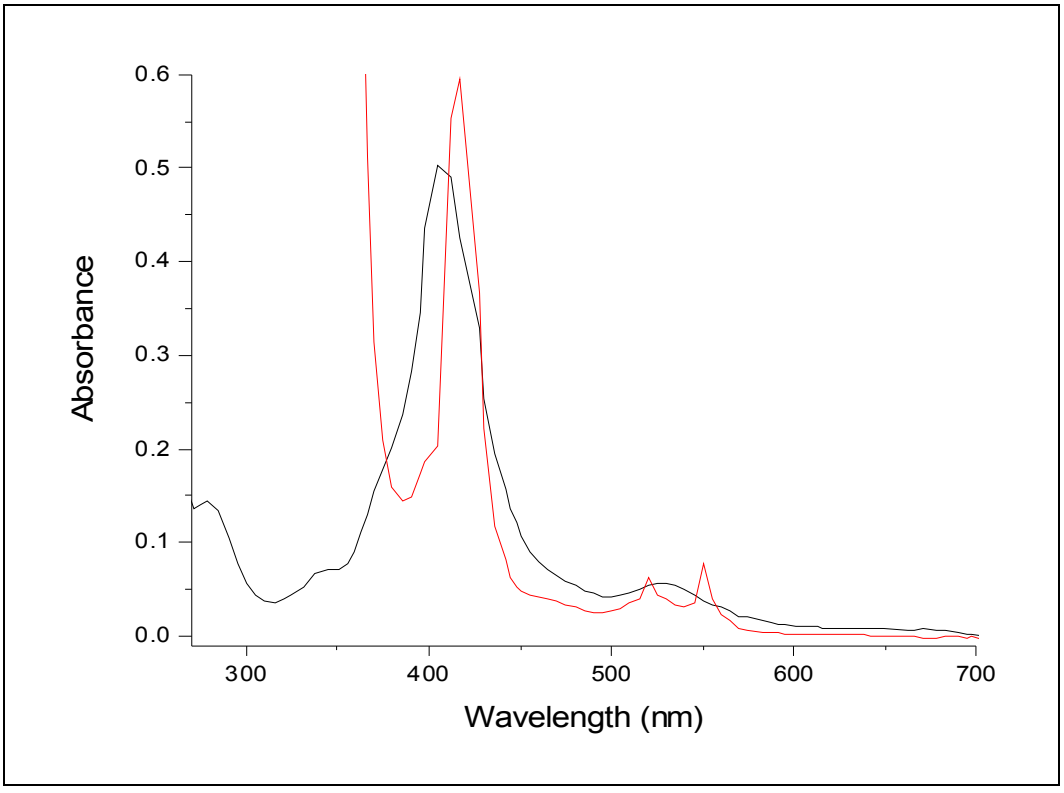


A protein sample of approximately 1 µM was prepared in 10 mM Tris.HCl, 10 mM NaCl (pH8.40) buffer and reduced by the addition of solid $Na_2S_2O_4$ until no further change in the spectrum was observed. The concentration of OTR was then determined from the absorbance of the reduced Soret band at 420 nm by the Beer-Lambert Law, using the extinction coefficient for OTR ($\varepsilon_{420}$ = 1226.6 $mM^{-1}$ $cm^{-1}$; Rothery, 2003).

### 2.4.3 Purity determination

The purity of the wild type and K56A OTR proteins was monitored using UV/visible spectrophotometry as follows:

An approximately 1 μM protein sample was prepared in 10 mM Tris/HCl 10 mM NaCl pH 8.4 buffer (Buffer A) and UV/visible spectra of the protein obtained. The relative absorbance ratio of the heme Soret band to the peak at 270 nm was determined. The 270 nm peak is due to absorbance by the aromatic residues of the protein and is indicative of the protein concentration in the sample. The Soret peak at 408 nm is a result of absorbance by the heme groups.

OTR protein with a spectral ratio of $A_{408}/A_{270} > 4$ was considered to be an acceptably pure sample for use in assays (Figure 2.7).

## 2.5 STEADY-STATE KINETIC ANALYSIS

### 2.5.1 Peroxidase activity

Steady state kinetic analysis of the peroxidase activity of wild type and K56A OTR was carried out using a colorimetric assay which monitored the oxidation of the dye o-dianisidine (Section 3.2.1).

The substrate-dependent oxidation of the dye was monitored at 460 nm using a Shimadzu UV-2101 spectrophotometer and the substrates hydrogen peroxide and cumene hydroperoxide. Assays were conducted at 25 °C using an assay buffer containing 100 mM $KP_i$, pH 7.5 and an ~ 8 mM solution of o-dianisidine in EtOH.

An assay solution comprised of 50 µl o-dianisidine solution [~8 mM], a known concentration of the peroxide substrate and assay buffer, to a total volume of 980 µl, was placed in a cuvette. 20 µl of enzyme was placed on the inside of the lid of the cuvette and the cuvette sealed. The reaction was initiated by the inversion of the cuvette and consequent mixing of its contents and monitored spectrophotometrically at 460 nm. All assays were performed in triplicate.

The kinetic parameters $K_M$ (the Michaelis constant) and $k_{cat}$ (turnover number) were determined from steady state results, over a range of substrate concentrations, fitted to the Michaelis-Menten equation by a least squares regression analysis (Microcal Origin software).

### 2.5.2 Reduction of substrate

The ability of the OTR and GSU0357 proteins to reduce a variety of nitrogenous substrates was investigated. The substrates tested for reduction by wild type and K56A

OTR were nitrite, hydroxylamine, nitric oxide and nitrous oxide, while the substrate tested for GSU0357 was nitrite.

The steady state reduction of the above substrates was assayed using an adaptation of the technique described by Turner *et al*, 1999 (Section 3.2.2). The substrate-dependent reoxidation of reduced methyl viologen was monitored at 600 nm using a Shimadzu UV-PC 1501 spectrophotometer. To ensure anaerobicity, the spectrophotometer was housed in a Belle Technology glove box under a nitrogen atmosphere ($[O_2] < 5$ ppm).

Prior to assaying, bulk reduction of methyl viologen was carried out in anaerobic conditions at 25 °C as a 5 mM solution in 1.5 M NaCl. Platinum electrodes were used with an Ag/AgCl reference electrode. The potential of the solution was held at -550 mV *vs* SHE using an Autolab PGSTAT10 potentiostat until reaction completion was indicated by cessation of current flow.

Each substrate (nitrite and hydroxylamine) was prepared as a series of stock solutions in deionised water at a range of concentrations (0 – 500 mM) for use in the assay (Table 2.6).

Assays were conducted at 25 °C using 50 mM Tris-HCl, pH 7.0 as the assay buffer. Reduced methyl viologen was added to the assay buffer so that a reading of ~1

**Table 2.6: Table of stock solutions and volumes used in substrate reduction assays.**

*Nitrite and hydroxylamine stock solutions were prepared in a range of concentrations (1 – 100 mM) for use in the assay. This table shows the volume of each stock solution to be added to the assay mixture to achieve the substrate concentration required in the final assay solution (total assay volume 1 ml).*

| Final [substrate] in assay solution (µM) | Stock solution (mM) | Volume of substrate added (µl) |
|---|---|---|
| 1 | 1 | 3 |
| 5 | 1 | 15 |
| 10 | 1 | 30 |
| 20 | 10 | 6 |
| 50 | 10 | 15 |
| 100 | 10 | 30 |
| 250 | 100 | 7.5 |
| 500 | 100 | 15 |
| 1000 | 100 | 30 |

absorbance unit was obtained (corresponding to ~80 µM). A known concentration of enzyme was added to the assay solution and the reaction initiated by the addition of the substrate to be tested at a range of substrate concentrations (0 – 1000 mM), such that the final volume of the assay mixture was 1 ml (Table 2.6; Figure 2.8). All assays were performed in triplicate.

Steady state thiosulfate oxidation was assayed under the same buffer conditions using ferricyanide as the electron acceptor. Thiosulfate oxidation is observed as a decrease in absorbance at 420 nm as ferricyanide ($\varepsilon_{420} = 1.01$ $mM^{-1}cm^{-1}$) is reduced by the enzyme.

The rate of substrate reduction over a range of substrate concentrations was fitted to the Michaelis-Menten equation by a least squares regression analysis (Microcal Origin software) and the kinetic parameters $K_M$ (dissociation constant for the formation of the Michaelis complex) and $k_{cat}$ (turnover number) were determined.

**Figure 2.8: Activity profile of a steady-state turnover assay**

*The reduction of substrate is observed in the assay as the oxidation of reduced methyl viologen. Initially, the UV/visible absorbance of the assay mixture is high due to the presence of reduced methyl viologen. The reaction is initiated by the addition of substrate and the observed decrease in absorbance is due to the oxidation of methyl viologen as the substrate is reduced. The activity of the enzyme is determined by measuring the change in absorbance of the assay mixture per unit time.*

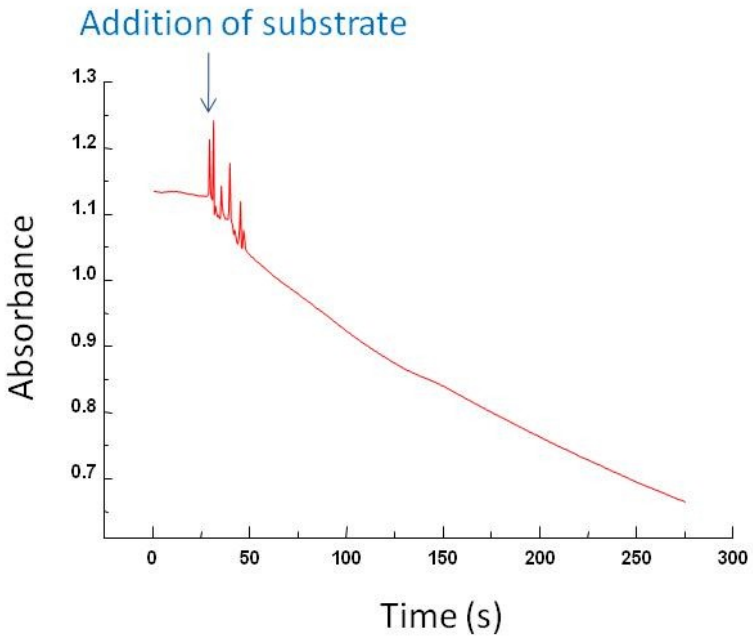


## 2.6 pH-DEPENDENCE OF ACTIVITY

The effect of pH on the catalytic rate of the enzyme was examined by measurement of activity at saturating substrate concentrations over the pH range 5.5 – 10.0 at 0.5 pH unit intervals, as indicated in Table 2.7. The pH profiles obtained were fitted by least squares regression to a single p$K_a$ value using Microcal Origin software.

**Table 2.7: pH-dependence of activity buffers:**

| Buffer | p$K_a$ | pH range | Component | Quantity |
|---|---|---|---|---|
| 50 mM MES.NaOH | 6.1 | 5.5 - 6.7 | $dH_2O$ | 500 ml |

| | | | | |
|---|---|---|---|---|
| (450 mM NaCl) | | | 1 M NaOH<br>NaCl | 50 ml<br>26.3 g |
| 50 mM Tris.HCl<br>(450 mM NaCl) | 8.1 | 7.0 - 9.0 | $dH_2O$<br>1 M NaOH<br>NaCl | 500 ml<br>50 ml<br>26.3 g |
| 50 mM CHES.NaOH<br>(450 mM NaCl) | 9.3 | 8.6 - 10.0 | $dH_2O$<br>1 M NaOH<br>NaCl | 500 ml<br>50 ml<br>26.3 g |

## 2.7 SOLVENT KINETIC ISOTOPE EFFECTS

The effect of solvent deuteration on the rate of substrate turnover was studied using the steady-state assay as previously described (Section 2.5.2). Methyl viologen, buffer and substrate solutions were prepared in $H_2O$ and $D_2O$ as for the standard solutions, using DCl or NaOD where required.

The pD of the deuterated solution was calculated according to Equation 2.1, in order to correct for the acidity of the pH electrode itself (Glascoe *et al*, 1960):

$$pD = \text{pH meter reading} + 0.4 \qquad \textbf{Equation 2.1}$$

The stock protein solution was prepared in $H_2O$ and concentrated so that the addition of the protonated enzyme solution was less than 0.05 % of the total assay volume.

The percentage of $D_2O$ in the assay components was varied between 0 and 100 % by adjusting the proportions of deuterated and protonated buffer added to the assay cuvette. The protein solution was permitted to equilibrate with the deuterated buffer for

30 s prior to the initiation of the assay by the addition of a saturating concentration of substrate. The solvent isotope effect was calculated using the ratio $k_H/k_D$.

## 2.8 AMMONIUM DETECTION ASSAY

The substrate reduction assay mixtures were analysed for ammonium ions using a modified version of the indophenol method (HMSO, Department of the Environment, 1981) using a Kone Specific Delta Discrete Analyser. In this method, hypochlorite ions are generated *in situ* by the alkaline hydrolysis of sodium dichloroisocyanurate and then react with ammonium ions to form monochloramine. Monochloramine reacts with salicylate ions in the presence of sodium nitroprusside to form a blue indophenol complex which is detected colorimetrically at 660 nm.

A 3 ml sample of the steady-state kinetic assay mixture (Section 2.5.2) was analysed after the reduction of either nitrite or hydroxylamine had been observed. This mixture was placed in a sealed vial immediately following the reaction. Negative control samples were prepared containing the assay components individually and in combination, as were positive control samples containing the assay components spiked with 100 μM $NH_4Cl$.

The salicylate/citrate reagent was prepared by dissolving 65 g each of sodium salicylate and tri-sodium citrate in 500 ml of a 20 mM sodium nitroprusside solution. The sodium dichloroisocyanurate reagent was prepared by adding 1 g of sodium dichloroisocyanurate to 500 ml of a 0.2 M NaOH solution. These solutions are stable for one month when kept in darkness.

Each of these two reagents was added to 25 ml boats in the Analyser instrument. The instrument was calibrated using stock solutions of $NH_4Cl$ as the formation of the indophenol complex was monitored at 660 nm. Assay mixture samples of 0.5 ml were analysed in triplicate and compared to the calibration data.

# *CHAPTER 3*

# *CHARACTERISATION OF OCTAHEME TETRATHIONATE REDUCTASE*

# 3 CHARACTERISATION OF OCTAHEME TETRATHIONATE REDUCTASE

Our current knowledge of the structure, properties and possible function of the octaheme tetrathionate reductase (OTR) from *Shewanella oneidensis* is described in detail in Section 1.7.2.

## 3.1 PURIFICATION OF OTR FROM *SHEWANELLA FRIGIDIMARINA*

An improved purification protocol to that described by Rothery (2003) has been developed, resulting in improved yields and purity. Rothery's protocol involved the growth and lysis of the *Shewanella* cells as indicated in Sections 2.1.1 and 2.2.1 respectively. Following this, the lysate was then sequentially subjected to weak anion exchange diethylaminoethyl chromatography, strong anion exchange Q-sepharose chromatography, hydroxyapatite chromatography and finally Superdex 200 gel filtration chromatography. In this process, it was observed that a significant proportion of the OTR protein appeared to be lost at the gel filtration stage. After trying a number of different approaches to solve this problem, it was found that the most efficient clean-up method was to replace the gel filtration step with a second hydroxyapatite column.

An improved purification protocol has been developed, as described in Section 2.2.1. The following more fully indicates the purifications made at each stage of this process (Note that buffers are as defined in Chapter 2, Table 2.3):

**Column 1:** Weak anion exchange chromatography - DEAE column:

The cell free extract was applied to a 4 x 10 cm DE-52 column, which had been previously equilibrated with Buffer A, and the column washed with Buffer A until no further protein fractions eluted. The bound proteins form a narrow red band at the top of the column which does not migrate on washing. A step-wise NaCl gradient was applied to the column and OTR eluted at 100 mM NaCl. Fractions containing OTR were pooled and dialysed against 2 x 4 l Buffer A.

**Figure 3.1: Heme-stained SDS-PAGE gel of DE fractions obtained in the purification of OTR.**

*Lane M = molecular weight marker, P = cell pellet, S =cell free extract, FT = column flow through, 0.1 = 0.1 M NaCl fraction, 0.2 = 0.2 M NaCl fraction, 0.5 = 0.5 M NaCl fraction. OTR elutes at 0.1 M NaCl and is highlighted in the red circle.*

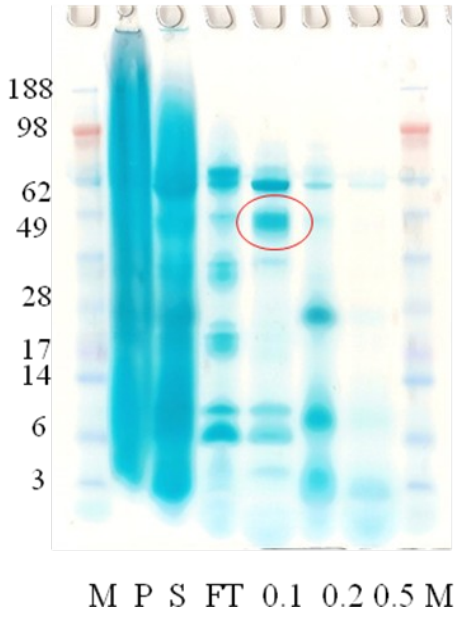

**Column 2:** Strong Anion Exchange Chromatography - Q-Sepharose column:

Purification was performed using an FPLC system and a 60 ml HiLoad 26/10 Q-Sepharose column which had been equilibrated with Buffer A. The protein solution was filtered using a 0.45µm filter, applied to the column and the column washed with Buffer A. A linear gradient of increasing [NaCl] was applied from 0 - 100 % Buffer B (100 – 0 % Buffer A). OTR eluted at approximately 0.15 M NaCl. Fractions containing OTR were pooled and dialysed against 2 x 4 l Buffer A.

**Figure 3.2: Heme-stained SDS-PAGE gel of Q-Sepharose fractions obtained in the purification of OTR.**

*Lane M = molecular weight marker, FT = flow through, lanes 1-16 are sequentially eluted protein fractions at increasing [NaCl] from left to right. The OTR band is highlighted in the red circle. At this point the protein was estimated to be approximately 50 % pure.*

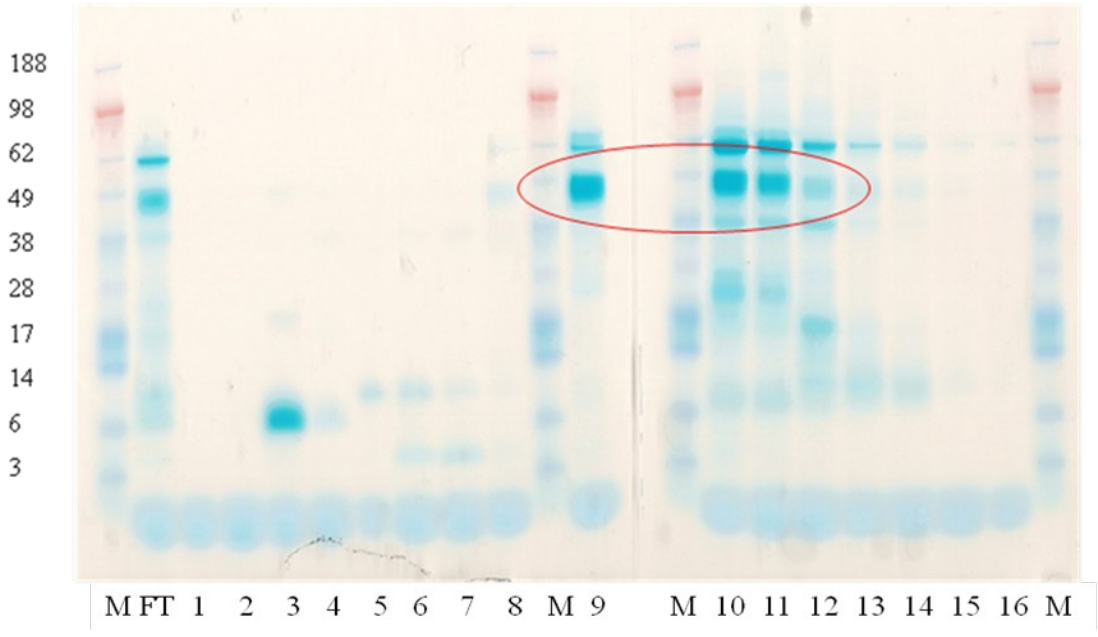

**Column 3:** Hydroxyapatite column 1:

The protein fraction was loaded onto a 3 x 8 cm hydroxyapatite column, which had been previously equilibrated using Buffer A**.** The column was washed with Buffer A and OTR eluted using a single step of 100 mM $K_2HPO_4$. The protein-containing fraction was dialysed against 2 x 4 l Buffer A. Both the heme- and Coomassie-stained (Figure 3.3) SDS-PAGE gels of the protein fractions at this point show only these two bands, indicating that only OTR and a protein of ~ 60 kDa molecular weight remain in the protein solution.

**Figure 3.3: Coomassie stained SDS-PAGE gel of hydroxyapatite fractions obtained in the purification of OTR.**

*M = molecular weight marker, lanes 1-8 are protein fractions sequentially eluted at 0.1 M $K_2HPO_4$. The OTR band is indicated by the arrow and in lane 3 is estimated to be >80 % pure.*

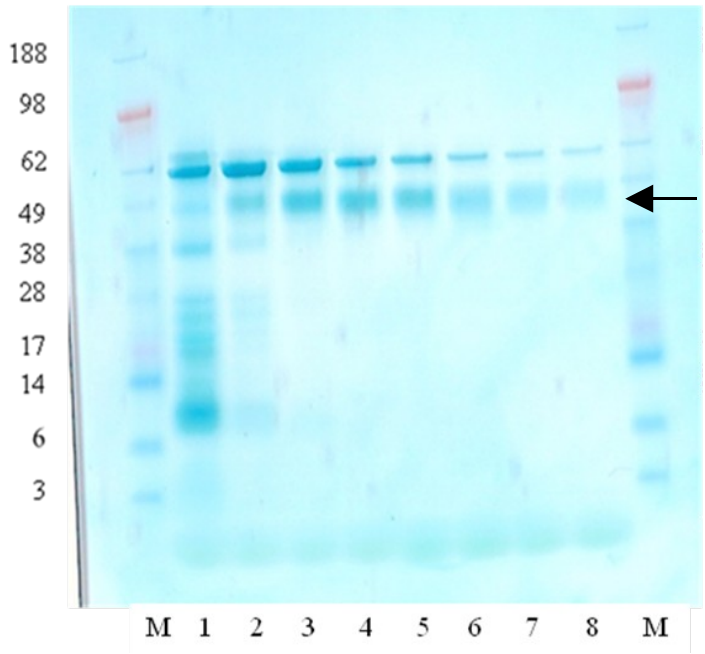


**Column 4:** Hydroxyapatite column 2:

The previous hydroxyapatite column was repeated, resulting in a significantly more pure sample, as indicated by SDS-PAGE (Figure 3.4). Purity was confirmed with an experimental spectrum (Figure 3.5) and an absorbance ratio $A_{408}/A_{270} > 4$.

**Figure 3.4: Heme-stained SDS-PAGE gel showing the hydroxyapatite fractions obtained in the purification of OTR.**

*M = molecular weight marker, lanes 1-4 show protein fractions eluted at 0.5 M $K_2HPO_4$, lanes 5- show protein fractions eluted at 0.1 M $K_2HPO_4$. The band containing OTR is indicated. Protein in lanes 9-12 is estimated to be >95 % pure.*

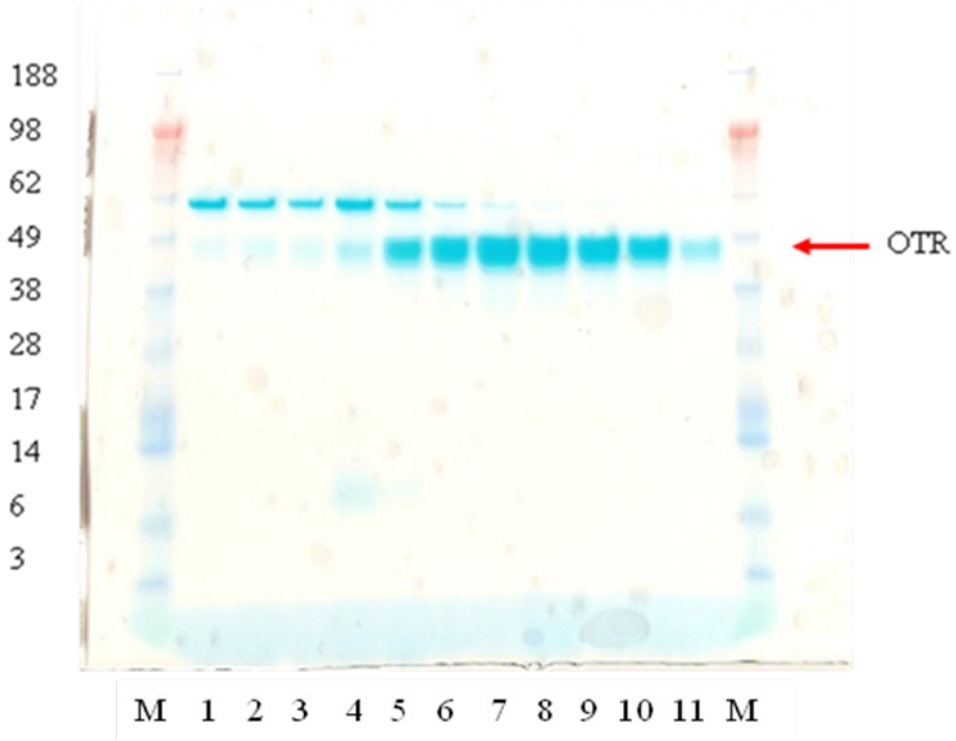


**Figure 3.5: UV/visible spectra of wild type OTR**

*The oxidised spectrum is shown in black and the reduced spectrum in red. The absorbance ratio of this sample $A_{408}/A_{270}$ = 4, indicating that the enzyme is of sufficient purity for use in assays.*

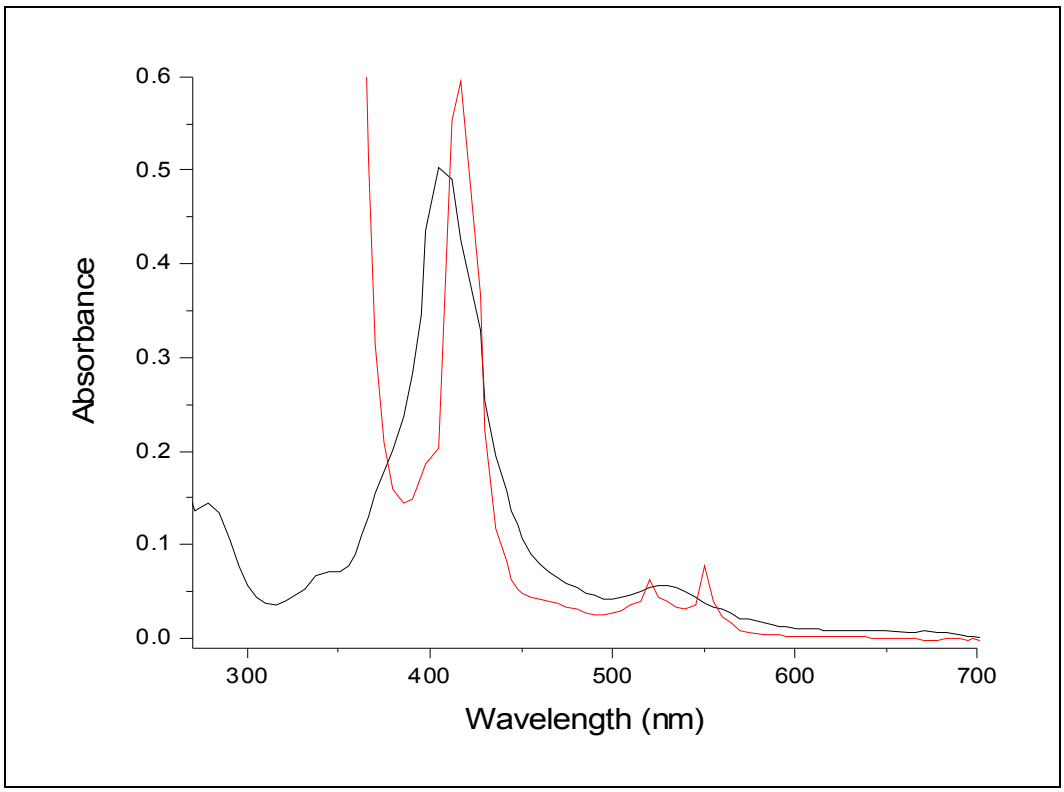


This improved protocol resulted in an average yield of approximately 0.34 mg $l^{-1}$ culture, representing a significant improvement of ~ 20 % as compared with the original purification scheme (average yield ~ 0.28 mg $l^{-1}$; Table 3.1). The improved protocol is also more straightforward in that it does not require an additional gel filtration step, with an additional hydroxyapatite column performing the final clean-up of the sample. There is no difference in the activity of OTR purified using each procedure.

**Table 3.1: Comparison between initial and improved OTR purification protocols**

*The stages, yields and purity of the wild type OTR protein obtained using Rothery's purification protocol (Rothery, 2003) and the improved method as described in this thesis. Protein yield is expressed in mg of protein per litre of culture and purity is monitored using the UV/visible absorbance ratio $A_{408}/A_{270}$. Rothery's protocol contains no published yield or purity data and so the values stated here are experimental.*

| | **Rothery's protocol** | **Improved protocol** |
|---|---|---|
| **Stages** | Weak anion exchange<br>Strong anion exchange<br>Hydroxyapatite chromatography<br>Gel filtration | Weak anion exchange<br>Strong anion exchange<br>Hydroxyapatite chromatography x2 |
| **Average protein yield (mg $l^{-1}$)** | 0.28 | 0.34 |
| **Absorbance ratio ($A_{408}/A_{270}$)** | 4.1 | 4.3 |

## 3.2 KINETIC ANALYSIS OF OTR

The ability of OTR to catalyse reactions with substrates known to be utilised by other heme-containing enzymes was investigated. The results are reported in the following sections.

### 3.2.1 Determination of peroxidase activity

The ability of OTR to act as a peroxidase was confirmed by monitoring the conversion of the colourless, reduced form of the dye o-dianisidine (Figure 3.6) to its coloured, oxidised form in solution. In addition to investigating peroxidase activity using hydrogen peroxide, cumene hydroperoxide (Figure 3.7) was also assayed as this organic substrate is less damaging to the protein. Assays were carried out over the substrate concentration range 0 – 20 mM and OTR was found to act as a peroxidase with both hydrogen peroxide and cumene hydroperoxide.

Observed rates of reaction were calculated using the extinction coefficient of o-dianisidine, $\varepsilon_{460}$ = 11.3 $mM^{-1}$ $cm^{-1}$ (Worthington, 1988). Michaelis curves were then used to determine the kinetic parameters of the reactions (Figures 3.8 and 3.9, Table 3.2). All assays were carried out in triplicate and each point shown in Figures 3.8 and 3.9 represents the average of these.

**Figure 3.6: o-dianisidine, shown in its reduced form**

*The reduced, colourless, form of the dye o-dianisidine is used as an electron donor in the detection of peroxidase activity. As the peroxidase reaction occurs the dye becomes oxidised and coloured. The appearance of this colour corresponds to the rate of the reaction.*

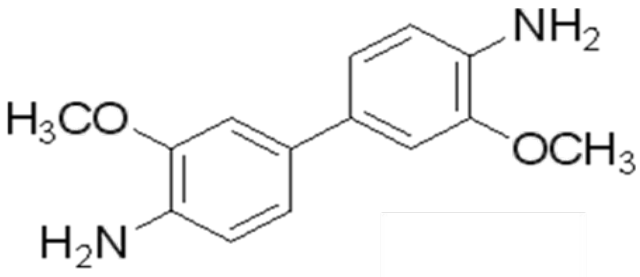


**Figure 3.7: Cumene hydroperoxide**

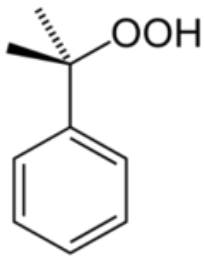


The ability of OTR to turn over hydrogen peroxide with a catalytic efficiency approximately five times greater than that for cumene hydroperoxide is probably a function of the relative size of these substrates. Cumene hydroperoxide is significantly larger and more bulky than the small hydrogen peroxide molecule and it is therefore likely that its access to the active site of OTR is more restricted, reducing turnover.

The ability of OTR to function as a peroxidase is perhaps not surprising as this reaction is characteristic of many hemoproteins. However, as a comparison, cytochrome *c* peroxidase from *Paracoccus denitrificans* has a turnover number of 1033 $s^{-1}$ and a Michaelis constant of 3.3 μM (Gilmour *et al*, 1994) and so is considerably more efficient as a peroxidase than OTR.

**Table 3.2: Kinetic parameters for the peroxidase activity of OTR.**

*Parameters determined at pH 7.0, 25 °C, I = 0.1 M.*

| **Substrate** | $K_M$ **(mM)** | $k_{cat}$ **($s^{-1}$)** | $k_{cat}$ **/** $K_M$ **($M^{-1}$ $s^{-1}$)** |
|---|---|---|---|
| **Hydrogen peroxide, $H_2O_2$** | 15.8 ± 0.5 | 17.5 ± 0.6 | 1.11 x $10^3$ |
| **Cumene hydroperoxide, $C_9H_{11}OOH$** | 9.2 ± 1.8 | 2.2 ± 0.5 | 2.39 x $10^2$ |

**Figure 3.8: Michaelis curve showing the steady state peroxidase activity of OTR with hydrogen peroxide.** *Parameters determined at pH 7.0, 25 °C, I = 0.1 M.*

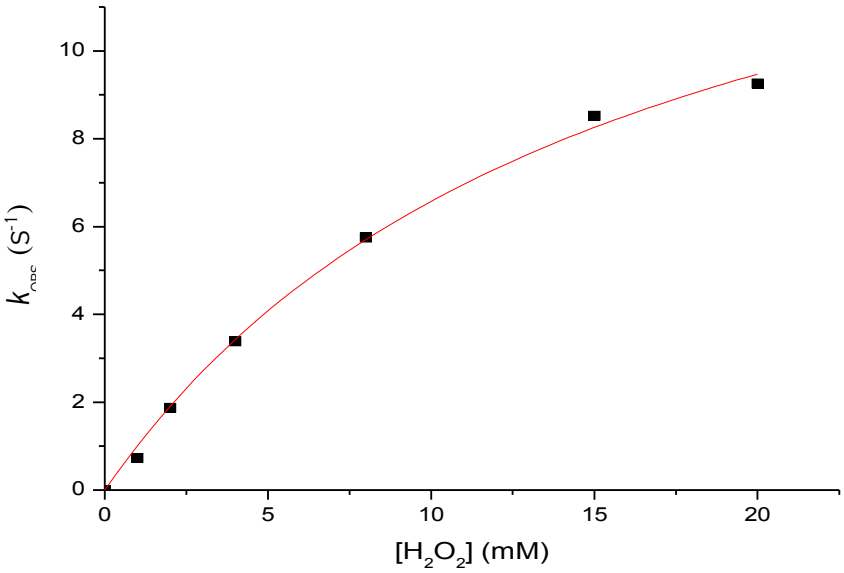


**Figure 3.9: Michaelis curve showing the steady state peroxidase activity of OTR with cumene hydroperoxide.** *Parameters determined at pH 7.0, 25 °C, I = 0.1 M.*

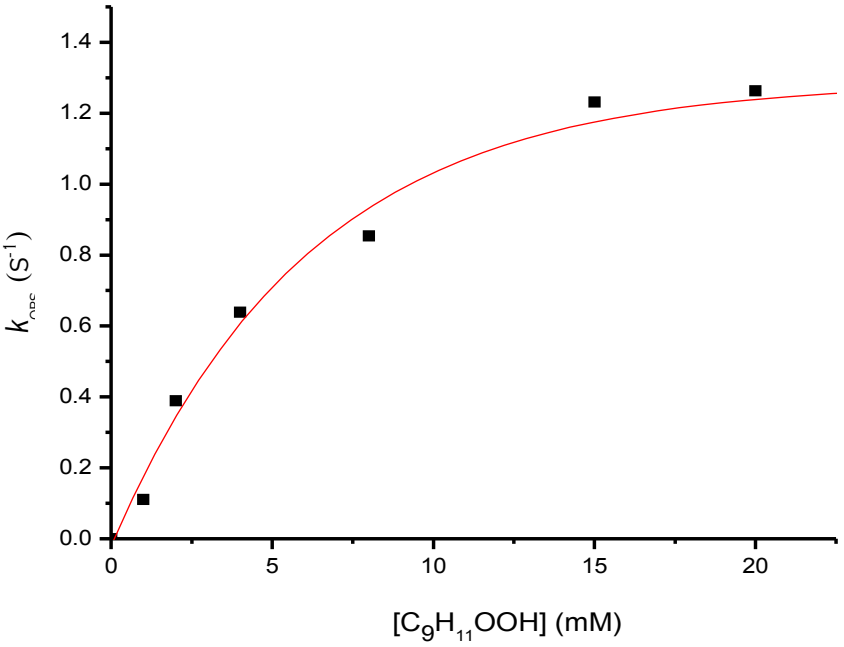


### 3.2.2 Substrate-dependent reductase activity

The basis of the substrate reduction assay is the reduction and oxidation of the dye methyl viologen (Figure 3.10). When methyl viologen is reduced (electrochemically or by the addition of sodium dithionite) it absorbs strongly in the blue region of the visible spectrum. On oxidation the dye becomes colourless, hence the extent of the conversion from oxidised to reduced methyl viologen can be quantitatively monitored at 600 nm ($\varepsilon_{600}$ = 13,700 $M^{-1}cm^{-1}$).

**Figure 3.10: Methyl viologen, shown in its oxidised form**.

*Electrochemical reduction or the addition of sodium dithionite reduces viologen to its radical form which releases electrons in the presence of the substrate and substrate reductase enzyme.*

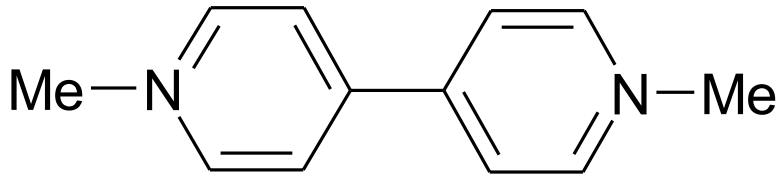


The ability of the enzyme to catalyse the reduction of nitrite was determined at pH 7.0, 25 °C, *I* = 0.1 M and methyl viologen was used as the electron donor in the reaction. Methyl viologen was reduced electrochemically, in preference to reduction by the common reductant sodium dithionite, in order to avoid the addition of any potentially reactive sulfur-containing products to the assay. The reaction was initiated by the addition of enzyme to the cuvette containing the substrate and reduced methyl viologen and the change in absorbance measured as a function of time (Figure 3.11).

The ability of OTR to catalyse the reduction of a range of substrates was assayed. Initially, assays were conducted using sulfur-containing substrates such as sulfate, sulfite, tetrathionate and trithionate, however no activity was observed other than with tetrathionate. In addition to this, thiosulfate oxidation was detected, as observed by Rothery (2003).

**Figure 3.11: An example of the absorbance trace obtained in a methyl viologen-linked steady state kinetics experiment.**

*At the start of the experiment, methyl viologen is in its reduced state and the absorbance of the assay mixture at 600 nm is high. Addition of the enzyme initiates the reaction. The enzyme reduces the substrate using electrons from methyl viologen, which is in turn oxidised, becoming colourless.*

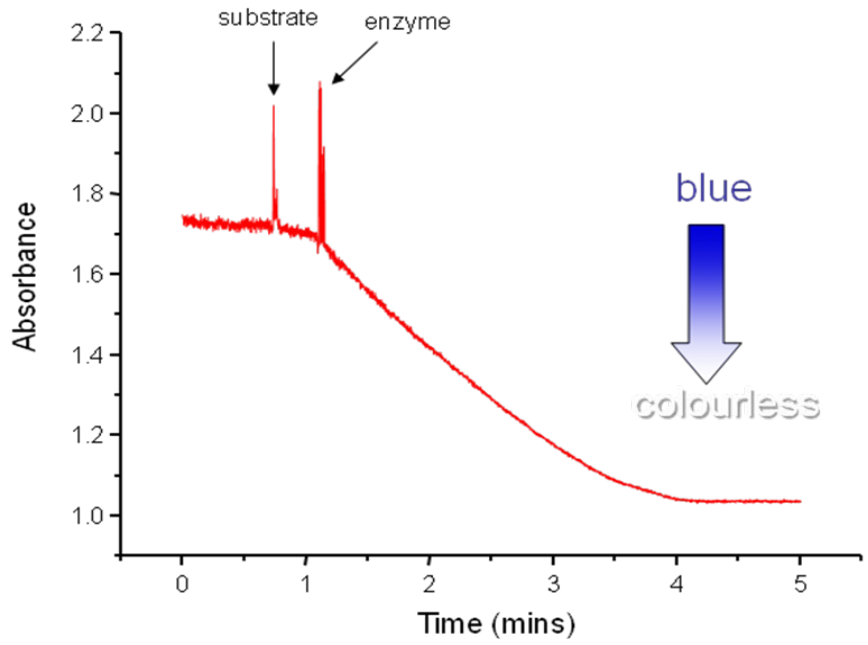


In view of the structural similarities between OTR and the nitrogen cycle enzymes cytochrome *c* nitrite reductase and hydroxylamine oxidoreductase (Section 1.7.2.3), substrate reduction assays (Section 2.5.2) were conducted using a range of nitrogenous substrates, including nitrite,

hydroxylamine, nitric oxide and nitrous oxide. In all cases these species were found to be substrates for reduction by OTR. The reductions of nitrite and hydroxylamine by OTR were easily observed as a gradual decrease in absorbance at 600nm (corresponding to the oxidation of methyl viologen in the assay mixture) on the timescale examined, however the reductions of nitric oxide and nitrous oxide appeared to occur instantaneously so although these reactions could be seen to occur it was not possible to obtain accurate kinetic data. The Michaelis curves for the reductions of nitrite and hydroxylamine by OTR are shown in Figures 3.12 and 3.13 respectively and the kinetic parameters for these reactions are summarised in Table 3.3. All assays were carried out in triplicate and each point shown in Figures 3.11 and 3.12 represents the average of these. The errors stated in Table 3.3 are calculated from the standard deviation of the three data sets. The low errors associated with this data suggest that this assay is reliable and the data has been found to be reproducible using different batches of protein.

The products of these reactions were analysed using the modified indophenol method (Sections 2.8 and 3.3)

**Figure 3.12: Michaelis curve showing the steady state reduction of nitrite by OTR.** *Parameters determined at pH 7.0, 25 °C, I = 0.1 M.*

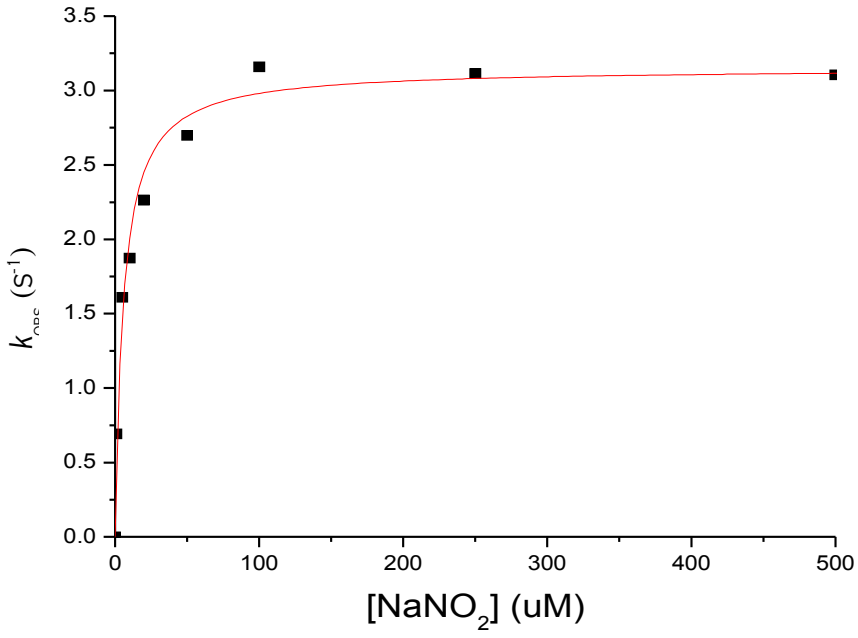


**Figure 3.13: Michaelis curve showing the steady state reduction of hydroxylamine by OTR.** *Parameters determined at pH 7.0, 25 °C, I = 0.1 M.*

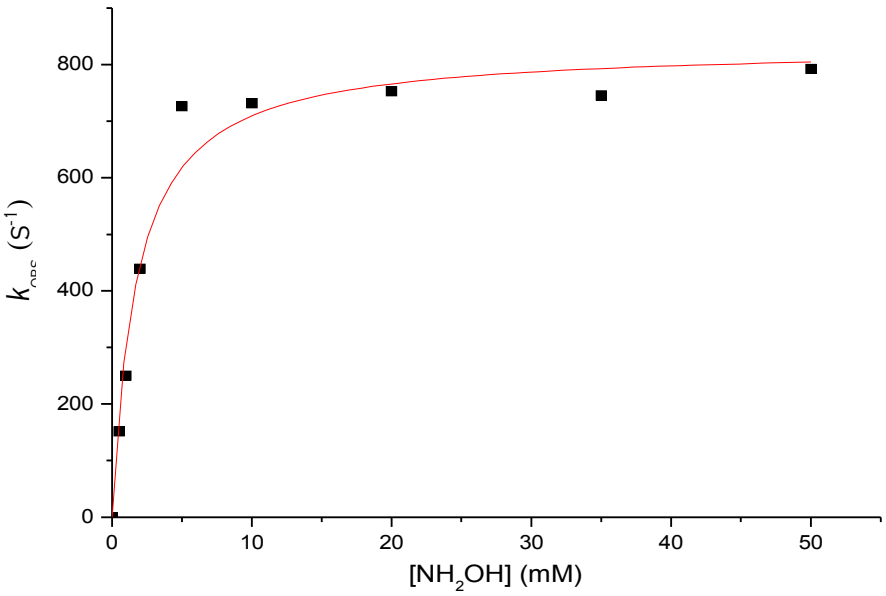


**Table 3.3: Kinetic parameters for the reduction of nitrite and hydroxylamine by OTR.**

*Data for tetrathionate reduction (Rothery, 2003) is included for comparison. Parameters determined at pH 7.0, 25 °C, I = 0.1 M. The errors stated are calculated from the standard deviation of three data sets.*

| **Substrate** | $K_M$ **(mM)** | $k_{cat}$ **($s^{-1}$)** | $k_{cat}$ **/** $K_M$ **($M^{-1}$ $s^{-1}$)** |
|---|---|---|---|
| **Nitrite, $NO_2^-$** | 0.0052 ± 0.0010 | 2.8 ± 0.4 | $5.3 \times 10^5$ |
| **Hydroxylamine, $NH_2OH$** | 2.2 ± 0.4 | 849 ± 7 | $3.9 \times 10^5$ |
| **Tetrathionate** | 0.070 ± 0.009 | 19.9 ± 0.6 | $2.9 \times 10^5$ |

OTR has been demonstrated to function effectively as both a nitrite and hydroxylamine reductase. The low value of the Michaelis constant for the reduction of nitrite suggests that nitrite is a good substrate for the enzyme, while the rate of hydroxylamine reduction is significant. The product of these reactions was expected to be ammonium, as further discussed in Section 3.3.

These results are comparable with data obtained for the reduction of nitrite and hydroxylamine by the pentaheme cytochrome *c* nitrite reductases. For example, the Michaelis constants for these two reactions when carried out by the nitrite reductase from *E. coli* are 0.028 mM and 30 mM respectively (Bamford *et al*, 2000a), indicating that OTR has a greater affinity for these substrates. However, the rates of these reactions with the *E. coli* enzyme occur more rapidly than with OTR, with rates of 770 $s^{-1}$ and 2380 $s^{-1}$.

The kinetic parameters obtained for the reductions of nitrite and hydroxylamine by OTR indicate that these reactions proceed more efficiently than the reduction of tetrathionate. In particular, the Michaelis constants for these reactions suggest that there is a preference for nitrite as a substrate over tetrathionate.

### 3.2.3 Solvent Kinetic Isotope Effects

The solvent kinetic isotope effect on the reduction of nitrite by OTR was studied by monitoring the rate of heme oxidation in both undeuterated and deuterated solvent (Table 3.4) in an attempt to determine whether proton delivery is a rate limiting step in this reaction.

The solvent isotope effect was calculated by the ratio $k_H$ / $k_D$ and found to be 2. The solvent isotope ratio is normally found to be between 1 and 8, where 1 implies that the rate of reaction is not limited by proton delivery and 8 implies complete dependence. Therefore, from this result is can be inferred that the rate of nitrite reduction by OTR is only mildly dependent on proton delivery.

**Table 3.4: The solvent isotope effect in the reduction of nitrite by OTR.**

*Parameters determined at pH 7.0, 25 °C, I = 0.1 M.*

| Solvent | $k_{obs}$ ($s^{-1}$) |
|---|---|
| **Non-deuterated** | 0.026 ± 0.001 |
| **Deuterated** | 0.013 ± 0.002 |

### 3.2.4 pH-Activity Dependence

The pH-activity dependence of the reduction of nitrite at a saturating concentration by OTR was studied over the pH range 5.0 – 10.0 (Figure 3.14). Nitrite reduction was found to be most

rapid at pH 5.5 and this rate decreased sharply as the pH was increased, leading to virtual inactivity at pH > 8. In addition to this, the rate of reduction decreased at pH values lower than 5.5. This decrease in rate is likely to be due to instability of the protein, leading to denaturation, at lower pH.

**Figure 3.14: pH-activity dependence of the reduction of nitrite by OTR.**

*Parameters determined at 25 °C. The blue curve is fitted to a single pH function and the red curve to a double pH function.*

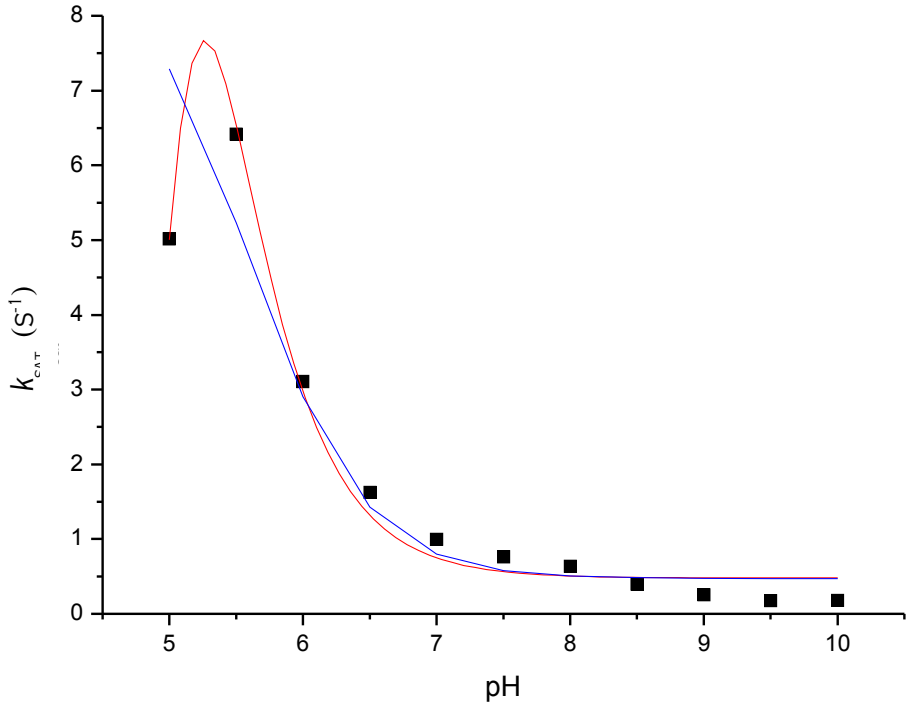


The data were fitted to two different pH functions in order to account for the decreased activity observed at pH 5.0. A single pH function was used with the assumption that this decrease was a result of the decreased activity of the enzyme at low pH, while a double pH function was used to fit this point as a non-specific protonation event.

The observed p$K_a$ for the single pH fit was found to be 5.60 ± 0.74, while that for the double pH function was 5.88 ± 0.60. These values may correspond to the protonation of a key active site residue, for example a histidine (p$K_a$ = 6.0), however as no crystal structures showing substrate bound in the active site of the enzyme are available any such assertions would be purely speculative.

This pH-activity relationship is different to that observed in the cytochrome *c* nitrite reductase from *Sulfurospirillum deleyianum*, in which activity is detectable in between pH 4.0 and 10.0, with the optimum rate of reaction occurring at pH 6.75 (Schumacher *et al*, 1991).

## 3.3 IDENTIFICATION OF REACTION PRODUCTS

Following the observation that OTR can reduce nitrite and hydroxylamine, experiments were undertaken to identify the products of these reactions. The product of the analogous reactions catalysed by the cytochrome *c* nitrite reductases, with which OTR shares its heme arrangement, is ammonia. Therefore, the possibility that the reaction product in this case might be ammonia was examined.

The detection of small quantities of ammonia in solution is non-trivial and a number of methods were tested including Nesslerisation, a commercially available ammonia assay kit and the indophenol method.

Nessler's reagent, a solution of potassium tetraiodomercurate (II) in potassium hydroxide, is a reagent used to detect the presence of ammonia in solution (Vogel, 1979). A positive test is observed as a yellow colouration of the solution, or a brown precipitate at high concentrations of ammonia. The assay solution resulting from the nitrite reduction assays (Section 3.2.2) was tested and a small amount of white precipitate was observed, resulting in an inconclusive test.

Following this, the reduction assay solution was tested using an ammonia assay kit (Sigma; AA0-100-1KT). The basis of this assay is that any ammonia present in the sample reacts with α-ketoglutaric acid and NADPH in the presence of L-glutamate dehydrogenase, yielding L-glutamate and $NADP^+$. The reaction is monitored spectrophotometrically and the oxidation of NADPH leads to a decrease in absorbance at 340 nm, which is proportional to the concentration of ammonia in the sample. While ammonia was detected in the OTR/nitrite assay mixture, the results of this assay kit were found to be unreliable and irreproducible.

In an attempt to confirm and quantify the production of ammonia in the reduction of nitrite by OTR, the indophenol method for ammonium detection (Scheiner, 1976) was used. In this method, ammonium reacts with hypohlorite ions and alkaline phenol in the presence of sodium nitroprusside to form the spectrophotometrically-detectable product indophenol blue (Figure 3.15). Nitrite was observed to interfere with this reaction leading to the possibility of false-positive results, however a modified version of this method which is unaffected by the presence of nitrite was identified (Section 2.8; HMSO, Department of the Environment, 1981) and tested.

**Figure 3.15: Indophenol**

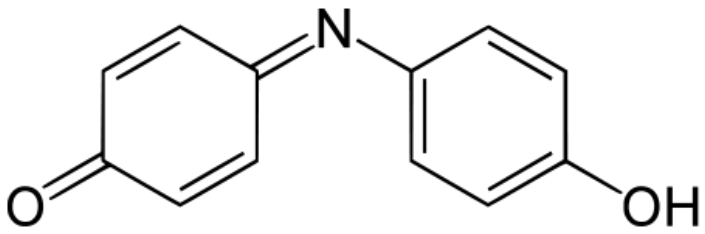


The modified indophenol method involves the *in situ* generation of hypochlorite ions from the alkaline hydrolysis of sodium dichloroisocyanurate, which then react with any ammonium ions present in the solution to from monochloramine. This monochloramine then reacts with salicylate ions in the presence of sodium nitroprusside to form a blue indophenol complex which can be detected colorimetrically at 660 nm.

The product of the reductions of nitrite and hydroxylamine by OTR was confirmed to be the ammonium ion using this modified version of the indophenol method (Section 2.8). Negative control samples (Table 3.5; samples 1-5) containing the assay components (including nitrite) were also analysed and found to contain no significant ammonium, indicating that all ammonium detected in the assay mixtures was a result of the enzymatic reaction. In addition to this, positive control samples (Table 3.5; samples 6 and 9) spiked with ammonium were analysed to provide a benchmark value for assay samples and confirm detection.

The assay mixture samples were prepared using 100 μM nitrite or hydroxylamine substrates and the reactions were allowed to proceed to completion. A theoretical conversion of 100 % substrate to ammonium would therefore yield a final assay concentration of 1.8 mg $NH_4^+$ $l^{-1}$.

As indicated in Figure 3.16, the quantity of ammonium detected in each of the negative control samples (1-5) was significantly lower than the assay samples and those spiked with ammonium. This demonstrates that the ammonium detected in the remaining samples is due to the presence of ammonium and is not an artefact resulting from non-reactive interactions of the assay components. In addition, the positive control samples (6 and 9) show that this method is successful in the detection of ammonium at these levels, although the absolute quantity of ammonium detected is significantly lower than that with which the samples are spiked, by a factor of 40 – 50 %.

Samples 7 and 8 (Figure 3.16) clearly show that the ammonium ion is present in the assay mixture, confirming that ammonium is the product of the reduction of nitrite and hydroxylamine by OTR. The levels of ammonium detected are comparable to those found in the spiked samples, indicating that a similar quantity of ammonium of present in each case. If

**Figure 3.16: Detection of ammonium as the product of the reduction of nitrite and hydroxylamine by OTR.** *The composition of each of the samples is indicated in Table 3.5.*

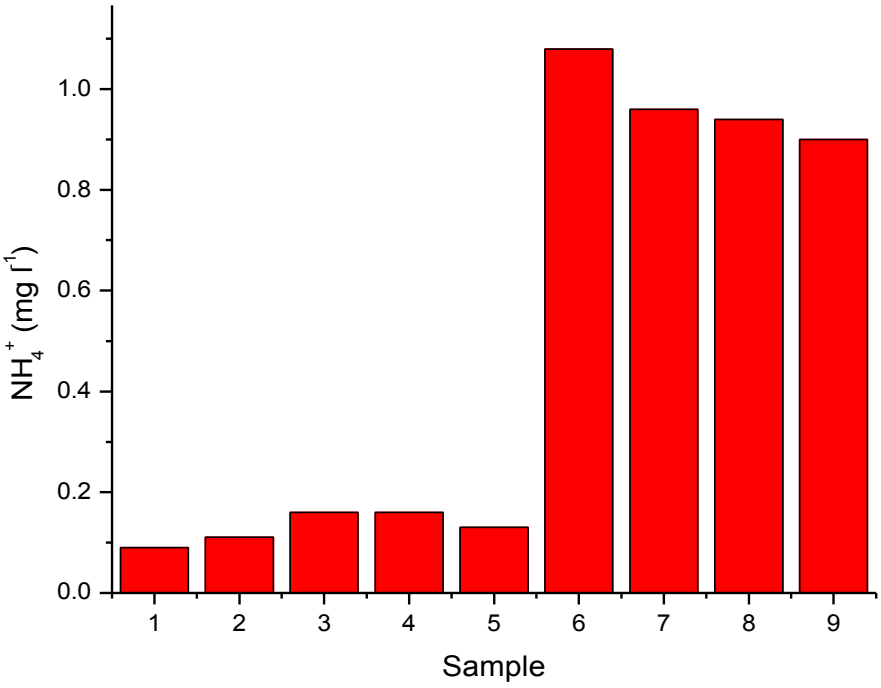


**Table 3.5: Composition of ammonium detection assay samples.**

| Sample | Composition |
|---|---|
| **1** | Buffer only |
| **2** | Buffer + MV |
| **3** | Buffer + OTR |
| **4** | Buffer + $NO_2^-$ |
| **5** | Buffer + $NH_2OH$ |
| **6** | Buffer + $NH_4^+$ |
| **7** | $NO_2^-$ assay mixture |
| **8** | $NH_2OH$ assay mixture |
| **9** | $NH_4^+$ assay mixture |

it is assumed that similar discrepancies in expected and detected ammonium levels are obtained with assay samples as with spiked samples, it may be hypothesised that the assay samples also contained in the region of 1.8 mg $l^{-1}$ ammonium, theoretically indicating a complete conversion of nitrite and hydroxylamine to ammonium by OTR. However, this speculation remains unconfirmed.

In order to confirm these findings, additional methods for the detection of ammonium could be explored. For example, the assay solution could be treated with an excess of alkyl halide (RX). Any ammonia present in the sample would then undergo a repeated $S_N2$ displacement reaction to form the quaternary salt $N(R)_4^+ X^-$ which could be measured.

Alternatively, a modification of the technique used in amino acid detection could be used, taking advantage of the reaction of ammonia with ninhydrin (Figure 3.17). The reaction of ninhydrin with amino groups produces a chromophore of deep purple colour, known as Ruhemann's Purple, which can be detected spectrophotometrically at 570 nm (Friedmann, 1974; Bottom, 1979). The assay solution could be passed through an ion exchange resin in order to separate any ammonia in the sample, and this ammonia could then be quantified by reaction with the organic molecule ninhydrin.

Significantly, the identification of ammonium as the product of the reduction of nitrite by OTR suggests that no intermediates are released during the reaction. This direct 6-electron transfer process is characteristic of the pentaheme cytochrome *c* nitrite reductases and suggests that the reduction of nitrite by OTR may proceed in a similar manner.

**Figure 3.17: Ninhydrin**

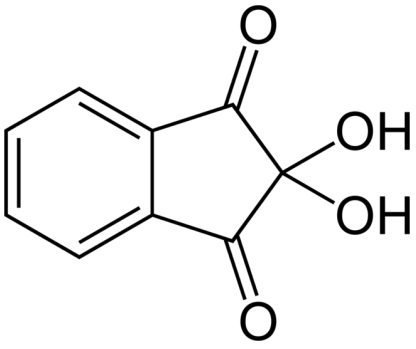

## 3.4 DISCUSSION

An improved protocol for the purification of OTR has been presented, leading to increased yields and purity of the enzyme. Progress has also been made in understanding the reactions of OTR and a number of new substrates have been identified for this interesting enzyme, raising important questions about its physiological role.

### 3.4.1 Peroxidase activity

OTR has been found to show peroxidase activity with both hydrogen peroxide and cumene hydroperoxide. The ability of OTR to function as a peroxidase is perhaps not surprising as this reaction is characteristic of many hemoproteins. Hydrogen peroxide is a common end product of oxidative metabolism. As a consequence of its strongly oxidising properties it may prove toxic if permitted to accumulate in the cell. The function of peroxidase enzymes, therefore, is to reduce peroxide to water, rendering it harmless and so unable to cause damaging reactions in the cell. Although OTR has been shown to be capable of carrying out this reaction, it has been found to be considerably less efficient than physiological peroxidases and it is unlikely that this is the true function of the enzyme in the cell.

### 3.4.2 Nitrite and hydroxylamine reduction

The potential for OTR to catalyse the reduction of nitrite and hydroxylamine has been proposed on the basis of significant similarities between the structure of the enzyme and the nitrogen cycle enzymes cytochrome *c* nitrite reductase and hydroxylamine oxidoreductase (Section 1.7.2.3).

This hypothesis has been confirmed and the ability of OTR to catalyse the reduction of a number of nitrogenous substrates has been conclusively demonstrated. The data presented in this thesis show that the catalytic efficiencies of the reduction of nitrite, hydroxylamine and tetrathionate by OTR are of the same order (Table 3.3). However, comparison of the $K_M$ values for these reactions suggests that nitrite is in fact the better substrate, while the rate of hydroxylamine reduction is notably large.

The product of the reductions of nitrite and hydroxylamine by OTR was directly detected in solution and shown to be the ammonium ion. This reductase activity is consistent with an enzyme that is involved in the biological nitrogen cycle, with the conversion of nitrite to ammonia representing a "short cut" in this cycle. In addition to this, the 6-electron reduction of nitrite to ammonium, without the release of any detectable intermediates, is characteristic of the cytochrome *c* nitrite reductases (Stach *et al*, 2000).

The ability of OTR to reduce both nitrite and hydroxylamine is further evidence of its similarity to cytochrome *c* nitrite reductase. The kinetic parameters obtained for these reactions by OTR are comparable to those seen in the cytochrome *c* nitrite reductase from *Sulfurospirillum deleyianum* (Stach *et al*, 2000). This nitrite reductase has also been shown to reduce the

nitrogen cycle intermediates nitric oxide and nitrous oxide, and these reactions have been observed for OTR, although not characterised.

### 3.4.3 Reclassification of octaheme tetrathionate reductase as a nitrogen cycle enzyme

In the light of the evidence reported in this Chapter, one could certainly propose a role for OTR as a nitrogen cycle enzyme. This then calls into question the suggestion that the physiological role of this enzyme lies in the reduction of tetrathionate. Data presented in this thesis show that the catalytic efficiencies of the reduction of nitrite, hydroxylamine and tetrathionate by OTR are of the same order. However, comparison of the $K_M$ values for these reactions suggests that nitrite is in fact the better substrate. The catalytic rates of these reductions are satisfactory, with the rate of hydroxylamine reduction being particularly notable, and the values of these parameters are comparable with the rates of these reactions with the cytochrome *c* nitrite reductases (Stach *et al*, 2000).

Additionally, it may be significant that prior to the identification of OTR, only one other tetrathionate reductase had been identified. This enzyme, the tetrathionate reductase from *Salmonella typhimurium*, is a membrane-bound multi-subunit molybdoenzyme and shares no similar characteristics to OTR. No other heme-containing tetrathionate reductases have been identified to date and so there is no precedent to the classification of OTR in this role.

The significant similarities between the structures of OTR and the nitrogen cycle enzymes cytochrome *c* nitrite reductase and hydroxylamine oxidoreductase has been previously discussed (Section 1.7.2.3), leading to the hypothesis that OTR may be involved in the reactions of the nitrogen cycle. This hypothesis is supported by the ability of OTR to perform analogous reactions to these enzymes, reducing nitrite and hydroxylamine. The ability of OTR to reduce both of these substrates is further evidence of its similarity to cytochrome *c* nitrite reductase, and additionally, the 6-electron reduction of nitrite to ammonium without the release of any detectable intermediates observed of OTR, further strengthens this suggestion.

The similarity in catalytic capability and highly conserved heme architecture between OTR, hydroxylamine oxidoreductase and cytochrome *c* nitrite reductase all provide significant evidence of a role for OTR as a nitrogen cycle enzyme. In the light of these findings, it is therefore proposed that the octaheme tetrathionate reductase from *Shewanella oneidensis* be reclassified as a nitrite reductase.

This reclassification of OTR as a nitrogen cycle enzyme rather than an electron transfer protein is very novel and its importance cannot be over stated. As a consequence of this discovery, research into this interesting enzyme must now be redirected to include the full characterisation of OTR in its new context. It would, of course, be of particular significance to determine the physiological role of OTR in the *Shewanella oneidensis* MR-1. This could be carried out using gene knockouts and conducting phenotype studies. The *S. oneidensis* MR-1 genome does contain a *nrfA* gene (locus tag SO3980; Heidelberg, 2002) and so it is of interest to examine whether OTR functions physiologically in addition to this cytochrome *c* nitrite reductase under certain conditions. Further investigation into the role of the unusually- and unexpectedly-

ligated active site heme of OTR is also necessary and a program of site directed mutagenesis and crystallography may be useful for that purpose.

# *CHAPTER 4*

# *CHARACTERISATION OF K56A OCTAHEME TETRATHIONATE REDUCTASE*

# 4 PURIFICATION AND CHARACTERISATION OF K56A OTR

The site-directed mutant of octaheme tetrathionate reductase, K56A, was constructed in order to probe the importance of the unusual heme-iron ligand, lysine 56, in the active site of OTR (Figure 4.1). This residue was substituted with alanine, a much smaller residue which does not project into the active site and so should not be able to coordinate to the heme iron.

**Figure 4.1: The structure of the active site of wild type OTR, showing the position of the lysine 56 heme ligand.**

*In the K56A mutant, the heme-ligating lysine residue 56 is replaced by an alanine residue which is expected to be unable to penetrate into the active site and ligate the heme iron.*

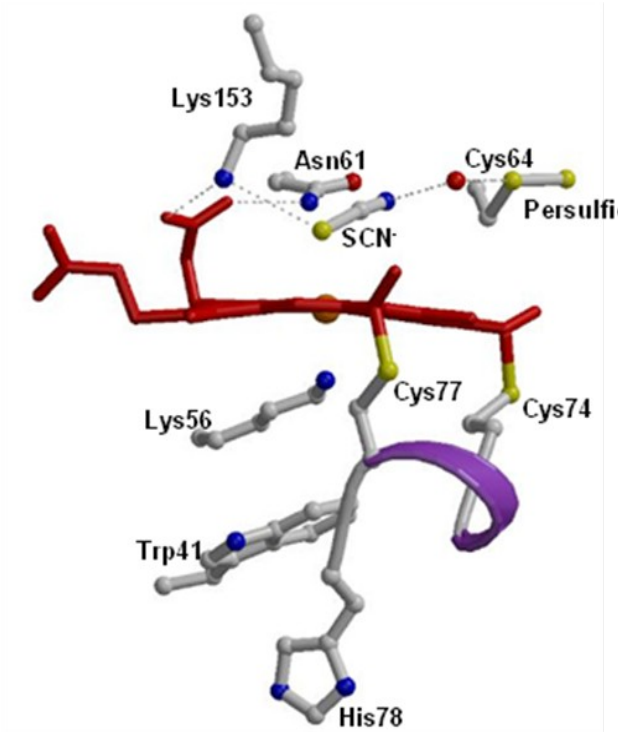

**Figure 4.2: The alteration of a lysine to an alanine residue, as observed in the K56A mutation.**

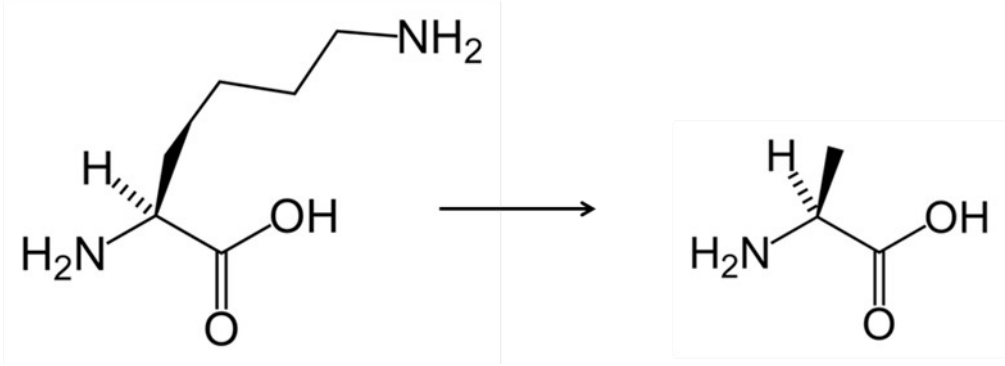


## 4.1 PURIFICATION OF OTR K56A

The K56A mutant was constructed by Dr. C.S. Miles (Section 2.1.2; Institute for Structural and Molecular Biology, University of Edinburgh). Screening for the K56A mutation was carried out by DNA sequencing and the OTR K56A coding sequence was checked to verify that no secondary mutations had been introduced. The resulting plasmid, pCM178, was used to transform the mobilising *E. coli* strain SM10 and was subsequently transferred into the *Shewanella oneidensis* MR-1 octaheme knockout strain (constructed by Dr. L. McIver, Department of Chemistry, University of Edinburgh) by conjugation.

The OTR K56A mutant was grown and purified in the same manner as the wild type enzyme (Figures 4.3 and 4.4; see Section 3.1 for WT procedure). A heme stained SDS-PAGE gel was used to confirm that heme is covalently bound in the protein (Figure 4.3).

**Figure 4.3: Heme-stained SDS-PAGE gel showing purified K56A OTR protein.**

*M = molecular weight marker, lanes 1 and 2 contain purified K56A OTR protein. This protein is estimated to be > 95 % pure.*

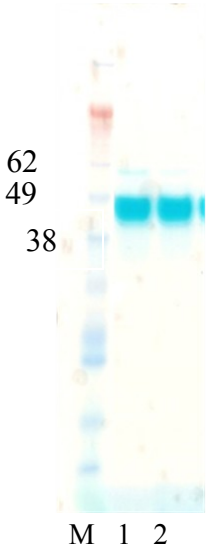


**Figure 4.4: UV/visible spectra of K56A OTR**

*The oxidised spectrum is shown in black and the reduced spectrum in red. In this sample, $A_{408}/A_{270}$ = 4, indicating that the enzyme is of sufficient purity for use in assays.*

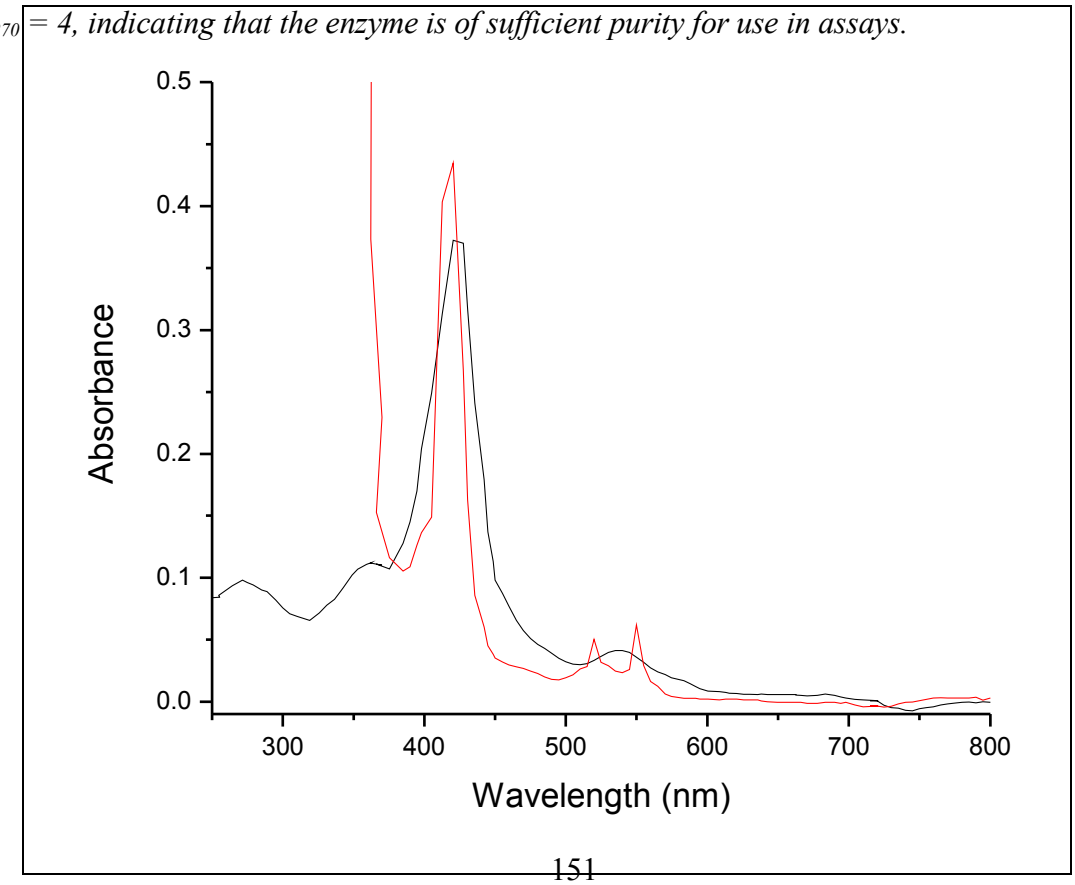

The UV/visible spectra of the oxidised and reduced K56A protein were determined as for the wild type enzyme (Figure 4.4; see Figure 3.5 for wild type spectra) and the absorbance ratio $A_{408}/A_{270} > 4$ was again used to indicate that the enzyme was of sufficient purity for use in assays.

The UV/visible spectra of the K56A mutant are very similar to those of the wild type enzyme, as would be expected. While the removal of a lysine ligand from the heme might be expected to have some effect on the spectrum, any changes which might result are expected to be masked by the spectra of the remaining seven bis-histidine ligated hemes in the protein. The increase in size of the shoulder on the Soret peak in the mutant spectrum (at approx 370 nm) is the only significant difference between the two spectra, and may be a result of the non-equivalence of the hemes, although it is not confirmed. The effect of the weaker field lysine ligand, as compared to the histidine residues ligating the remaining seven hemes, would be to red shift d-d transitions. However, any change in the spectrum as a result of the loss of the lysine ligand would not be expected to be obvious as these transitions will be Laporte forbidden, in addition to being masked by the absorptions of the other seven normally-ligated hemes.

It can been seen from these spectra that water does not appear to be bound as the sixth ligand to the active site iron atom, as this would be expected to cause a spectral change because of the exchange of a nitrogen ligand for the water. However, as before, any effect caused by a change in ligation at the active site is likely to be obscured by the transitions of the seven other hemes in the protein.

## 4.2 KINETIC ANALYSIS OF K56A OTR

### 4.2.1 Substrate-dependent reductase activity

The ability of K56A OTR to catalyse the reduction of nitrite and hydroxylamine, previously identified as substrates for the wild type enzyme, was assayed and activity was detected. The Michaelis curves for the reduction of nitrite and hydroxylamine by K56A OTR are shown in Figures 4.5 and 4.6 respectively and the kinetic parameters for these reactions are summarised in Table 4.1.

**Table 4.1: Kinetic parameters for the reduction of nitrite and hydroxylamine by K56A OTR.**

*Data for the wild type enzyme are included for comparison. Data recorded at pH 7.0, 25 °C, I = 0.1 M.*

| Enzyme | Substrate | $K_M$ (mM) | $k_{cat}$ ($s^{-1}$) | $k_{cat}$ / $K_M$ ($M^{-1}$ $s^{-1}$) |
|---|---|---|---|---|
| **K56A OTR** | $NO_2^-$ | 65.6 ± 41.1 | 0.51 ± 0.15 | 7.70 |
| | $NH_2OH$ | 10.8 ± 4.1 | 349.3 ± 46.6 | $3.5 \times 10^4$ |
| **WT OTR** | $NO_2^-$ | 0.0052 ± 0.0010 | 2.8 ± 0.4 | $5.3 \times 10^5$ |
| | $NH_2OH$ | 2.2 ± 0.4 | 849 ± 7 | $3.9 \times 10^5$ |

**Figure 4.5: Michaelis curve showing the steady state reduction of nitrite by OTR K56A.**

*Data recorded at pH 7.0, 25 °C, I = 0.1 M.*

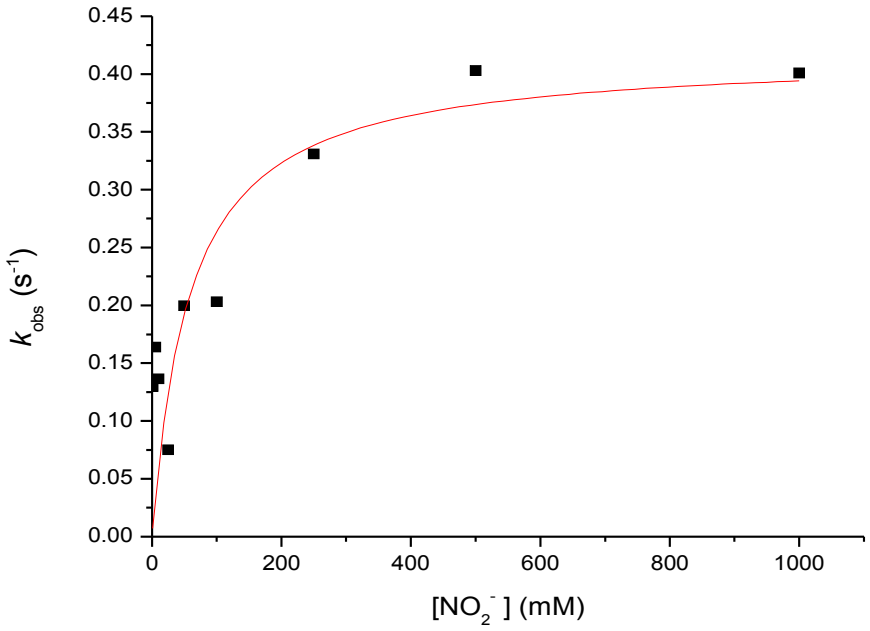


**Figure 4.6: Michaelis curve showing the steady state reduction of hydroxylamine by OTR K56A.** *Data recorded at pH 7.0, 25 °C, I = 0.1 M.*

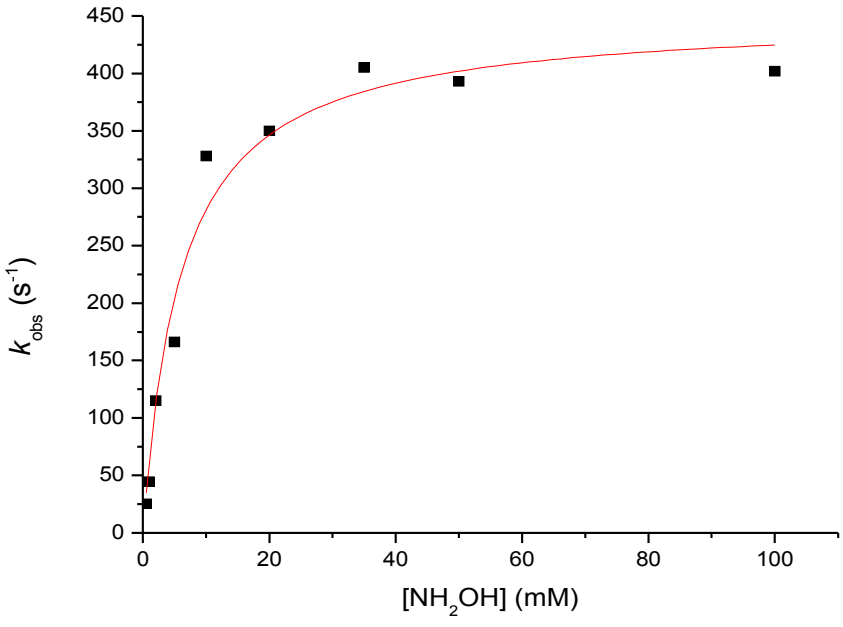


K56A OTR has been demonstrated to function effectively as both a nitrite and hydroxylamine reductase. This is perhaps surprising in view of the fact that the K56A mutation represents a

serious alteration to the active site of the enzyme, with the substitution of the heme-ligating residue by alanine. The kinetic parameters observed for these reductions show the mutant enzyme to be less efficient than the wild-type by a factor of ~ $10^5$, but this is not unexpected; the wild type enzyme is likely to represent the "optimal" structure and so any alterations are likely to result in a decreased catalytic efficiency. This is also the case for the reduction of hydroxylamine, although in this reaction the catalytic efficiency is decreased by a factor of only about ten fold. Interestingly, in the wild type enzyme the reduction of nitrite is more efficient than that of hydroxylamine, while in the K56A mutant this trend is reversed. The reason for this reversal of efficiency is unclear.

### 4.2.2 pH-Activity Dependence

The reduction of nitrite at a saturating concentration by K56A OTR was studied over the pH range 5.0 – 10.0 (Figure 4.7). The pH-activity profile observed was similar to that of the wild type enzyme (Section 3.2.4), with nitrite reduction found to be most rapid at pH 5.5 with a sharp decrease in rate at higher pH. The data was fitted to both a single and double pH curve.

The data were fitted to two different pH functions in order to account for the decreased activity observed at pH 5.0. A single pH function was used with the assumption that this decrease was a result of the decreased activity of the enzyme at low pH, while a double pH function was used to fit this point as a non-specific protonation event.

**Figure 4.7: pH-activity dependence of OTR K56A.**

*Data recorded at 25 °C. The blue curve is fitted to a single pH function and the red curve to a double pH function.*

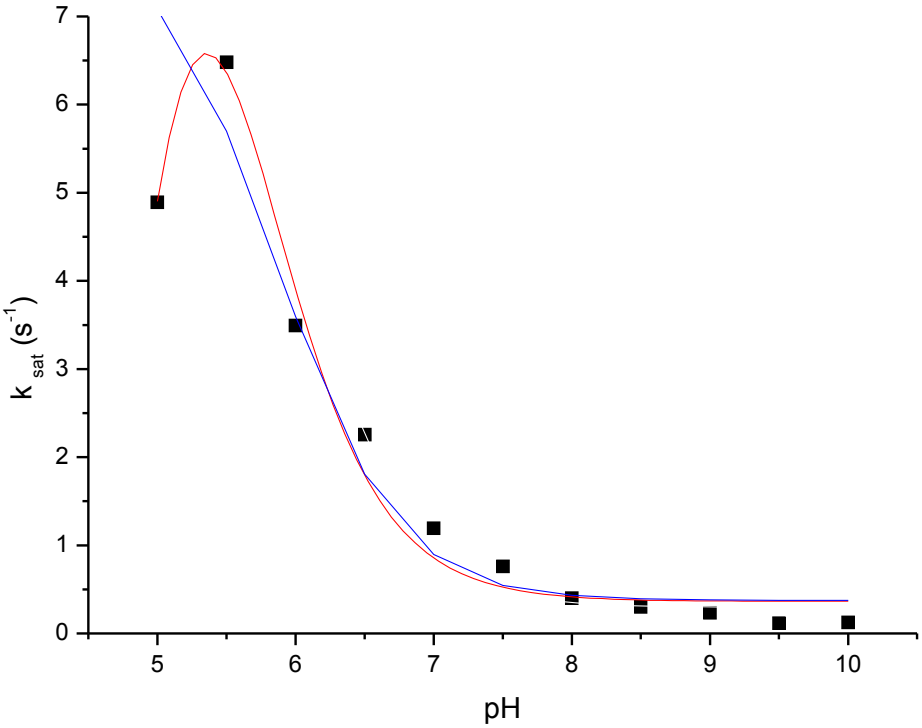


The observed $pK_a$ for the single pH fit was found to be 5.86 ± 0.13, while that for the double pH was 5.57 ± 0.68. These values are very similar to those observed for the wild type enzyme, and again may correspond to the protonation of a key active site residue such as a histidine ($pK_a$ = 6.0). It may be significant that this active site substitution does not result in a change in the pH-activity profile of the enzyme, suggesting that the protonation event being observed is not related to lysine 56.

## 4.3 IDENTIFICATION OF REACTION PRODUCTS

The product of the reduction of nitrite and hydroxylamine by K56A OTR was confirmed as the ammonium ion using a modified version of the indophenol method (Section 2.8). Negative and positive control samples (Table 4.2; Figure 4.8; samples 1-5) containing the assay components were also analysed in order to verify the results of the experiment. The assay mixture samples were prepared as for the wild type enzyme, using 100 μM nitrite or hydroxylamine and the reactions were allowed to proceed to completion. A theoretical conversion of 100 % substrate to ammonium would therefore yield a final assay concentration of 1.8 mg $NH_4^+$ $l^{-1}$ (Section 3.3).

As observed in the wild-type experiment, the quantity of ammonium detected in each of the negative control samples (1-5) was significantly lower than the assay samples and those spiked with ammonium, indicating that any ammonium detected in the remaining samples was not an artefact resulting from non-reactive interactions of the assay components. Additionally, the positive control samples (6 and 9) show that this method is successful in the detection of ammonium at these levels, although the absolute quantity of ammonium detected is lower than that expected by a factor of 40 – 50 %.

Samples 7 and 8 (Figure 4.8) clearly show that the ammonium ion is present in the assay mixture, confirming that ammonium is the product of the reduction of nitrite and hydroxylamine by OTR K56A. The levels of ammonium detected are similar to those found in the spiked samples, indicating that a similar quantity of ammonium is present in each case.

**Figure 4.8: Detection of ammonium as the product of the reduction of nitrite and hydroxylamine by K56A OTR.** *The composition of each of the samples is indicated in Table 4.2.*

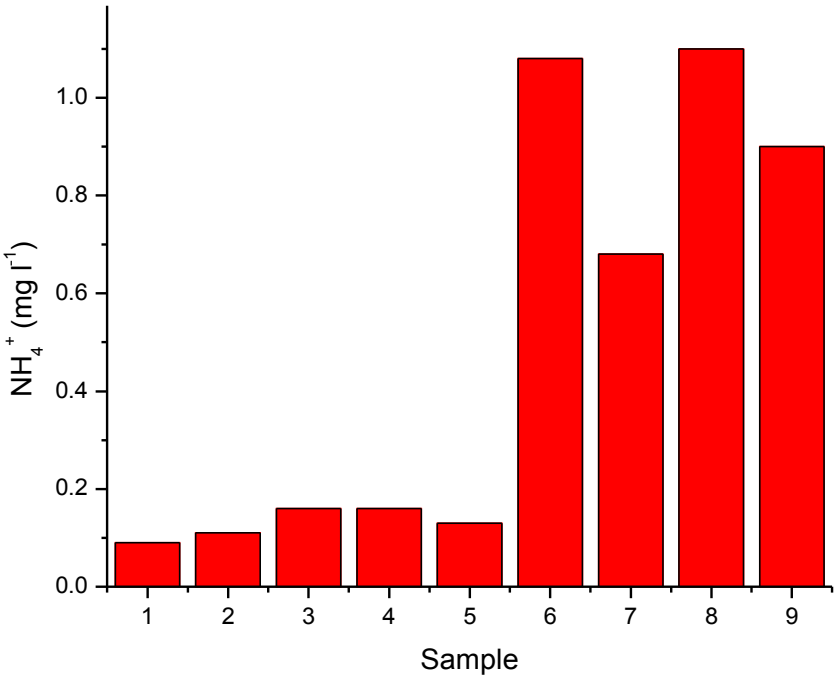


**Table 4.2: Composition of ammonium detection assay samples.**

| Sample | Composition |
|---|---|
| **1** | Buffer only |
| **2** | Buffer + MV |
| **3** | Buffer + OTR |
| **4** | Buffer + $NO_2^-$ |
| **5** | Buffer + $NH_2OH$ |
| **6** | Buffer + NH4+ |
| **7** | NO2- assay mixture |
| **8** | NH2OH assay mixture |
| **9** | NH4+ assay mixture |

As with the wild-type enzyme, the identification of ammonium as the product of the reduction of nitrite by OTR K56A suggests that no intermediates are released during the reaction, as is observed in the cytochrome *c* nitrite reductases (1.7.2.3).

## 4.4 CRYSTALLOGRAPHY OF K56A OTR

Crystal trays have been prepared by Vivek Jassal and Dr. Chris Mowat in an attempt to obtain crystals of K56A OTR. Similar conditions to those successfully used in the crystallography of the wild type enzyme were employed (hanging drop method; 200 mM ammonium acetate, pH 5.7) and the first crystal of this mutant has been obtained (Figure 4.9). No other crystallography conditions were tested. It is expected that the optimisation of crystal growth conditions will lead to crystals suitable for the determination of the structure of this mutant enzyme.

**Figure 4.9: Crystals of K56A OTR.**

*Image courtesy of Dr. Chris Mowat.*

## 4.5 DISCUSSION

The purpose of constructing K56A OTR was to determine the effect of the unusual heme-ligating lysine residue found in the active site of the enzyme. The substitution of this residue by alanine would be expected to have a significant effect on the active site because of the removal of the ligand to the heme iron (Figure 4.1). Therefore, the discovery of nitrite and hydroxylamine reductase activity in this mutant enzyme was unexpected.

The kinetic parameters for these reactions suggest that K56A OTR can function reasonably well in the roles of nitrite and hydroxylamine reduction. This enzyme was found to be less efficient that the wild type enzyme by a factor of approximately $10^5$ for nitrite reduction and 10 for hydroxylamine reduction, but as already discussed this is not surprising; any mutation is a deviation from the presumably "optimal" structure of the wild type enzyme.

The similarity in the pH-activity profiles of the K56A mutant and wild type enzymes provides a further interesting insight into the active site, suggesting that an important protonation event is conserved in the mutant enzyme. The $pK_a$ of this pH-dependence observed suggests that the residue required to be protonated may be a histidine.

The confirmation of ammonium as the product of the reduction of nitrite and hydroxylamine by OTR, with similar conversion efficiency to the wild type enzyme, suggests that the K56A substitution does not have a significant effect on the ability of the enzyme to catalyse the full 6-

electron reduction of nitrite to ammonium. This behaviour again suggests that the radical changes to the active site as a result of the substitution are not particularly deleterious.

The substitution of lysine by alanine, which is unable to coordinate the heme iron, theoretically results in the loss of a ligand to the active site heme. It is therefore suggested that another residue may act as the active site heme ligand. The most likely candidate for this ligation of the heme iron is histidine 78, which is found below the active site in the wild type crystal structure (Figure 4.10). This residue is thought to "flip" upwards to take the place of the mutated lysine, in the process re-creating a standard CXXCH heme-ligating motif.

**Figure 4.10: The structure of the active site of wild type OTR.**

*In the K56A mutant, the heme-ligating lysine residue 56 is replaced by an alanine residue which is unable to penetrate into the active site and ligate the heme iron. It is suggested that the vacant heme co-ordination site may be filled by histidine 78, which flips upward to re-create a standard heme co-ordination sphere.*

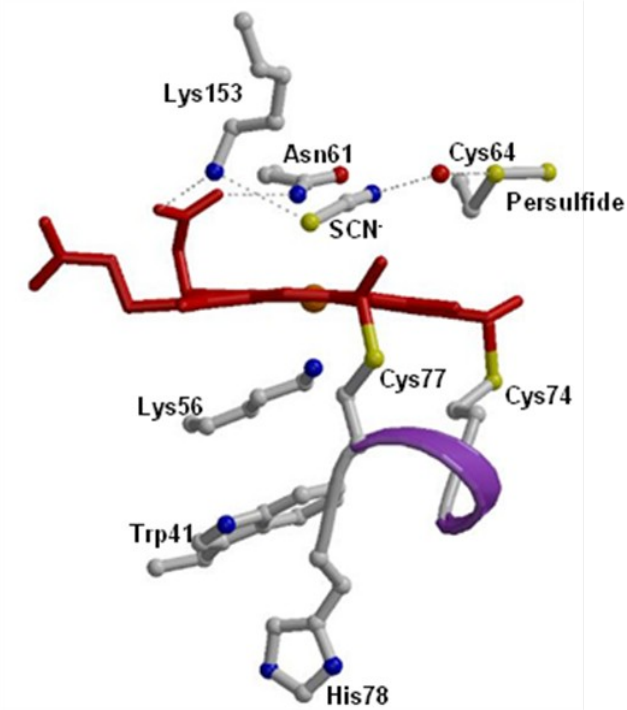

This speculation remains unconfirmed in the absence of a crystal structure of the K56A enzyme. However, it is hoped that the successful growth of K56A OTR crystals reported here will provide the opportunity for crystallographic studies to elucidate the structure and aid the characterisation of the reactions of this unusual and intriguing enzyme.

# *CHAPTER 5*

# *A BRIEF ANALYSIS OF GSU0357*

# 5. A BRIEF ANALYSIS OF GSU0357

Following the discovery of the nitrite reductase activity of OTR, it was proposed that other genes in this family might have similar activity. It was therefore hypothesised that the related gene product, GSU0357 from *Geobacter sulfurreducens*, may catalyse similar reactions. The sequences of both OTR and GSU0357 contain the unusual CXXCK heme-attachment motif, which has been found to be the active site in OTR. It was therefore determined that a preparation of GSU0357 should be obtained in order to analyse its enzymatic activity with nitrite. Given time constraints, and problems with purification, only partially pure samples of GSU0357 were produced. Nitrite reductase activity of the crude extracts has been observed.

## 5.1 OVEREXPRESSION OF GSU0357

*Shewanella frigidimarina* EG301 and *Escherichia coli* JM109(DE3) cells expressing recombinant GSU0357 were prepared by Dr. C.S. Miles, ISMB, University of Edinburgh, as described in Section 2.1.3. In both cases the intrinsic signal sequences of the targets were used.

### 5.1.1 Expression of GSU0357 in *Shewanella frigidimarina* EG301

*Shewanella frigidimarina* strain EG301 and the plasmid pMMB503EH were selected for the overexpression of GSU0357 as they had previously been used successfully in the overexpression of octaheme tetrathionate reductase (OTR). *Shewanella* strains are recognised for their ability to produce large numbers of *c* type cytochromes, and strain EG301 had previously been shown to be able to successfully mature the unusual lysine-ligated heme found at the active of OTR. A similarly ligated heme is predicted by the GSU0357 amino acid sequence.

Expression trials and the determination of growth conditions were carried out by Dr. E. Rothery, Department of Chemistry, University of Edinburgh.

### 5.1.2 Expression of GSU0357 in *Escherichia coli* JM019(DE3)

The pETBlue-1 vector, the pEC86 plasmid (which expresses the *E. coli* cytochrome *c* maturation genes) and the expression host *E. coli* JM109(DE3) were selected for the expression of GSU0357 following their successful use in the expression of a *Shewanella* decaheme (Pitts *et al*, 2003). The intrinsic signal sequence of the target was used. Expression trials and the determination of growth conditions were carried out by Dr. E. Rothery as above.

## 5.2 PROTEIN PURIFICATION STRATEGY

The purification of GSU0357 from both *S. frigidimarina* and *E. coli* was found to be challenging for various reasons:

During the purification of GSU0357 from *S. frigidimarina,* problems were encountered in separating the protein from the large number of cytochromes naturally expressed by this bacterium. It was hoped that purification of GSU0357 from *E. coli*, which expresses fewer cytochromes, would be more straightforward, but purification from *E. coli* was hampered by the discovery that the majority of the GSU0357 protein was not soluble, but located in the membrane fraction. Attempts were made to extract this protein using sodium cholate detergent prior to purification, however little protein appeared to be solubilised using this method. The possibility of misfolding of the protein, leading to inclusion-type bodies, was investigated and there was some success in purification using a refolding method.

The most successful purification protocol developed for each case is outlined below.

### 5.2.1 PURIFICATION FROM *SHEWANELLA FRIGIDIMARINA*

The most successful purification of GSU0357 from *S. frigidimarina* was obtained using a combination of anion exchange chromatography, ammonium sulfate precipitation and gel filtration, as described in Section 2.2.2.1.

The cell free extract was applied to a DE-52 anion exchange column, eluted in 0.25 M KCl and dialysed. The protein solution was then applied to a Q-Sepharose column and eluted in 0.3 M KCl (Figure 5.1). Protein-containing fractions were combined, dialysed and subjected to a 60 % $(NH_4)_2\ SO_4$ precipitation.

**Figure 5.1: Heme-stained SDS-PAGE gel of Q-Sepharose fractions obtained in the purification of GSU0357 overexpressed in *S. frigidimarina.***

*Lane M = molecular weight marker (corresponding mass in kDa is shown to the left), 1 = DE load, 2 = Q-Sepharose load, 3-8 = sequentially eluted fractions. GSU0357 is indicated in the circle*

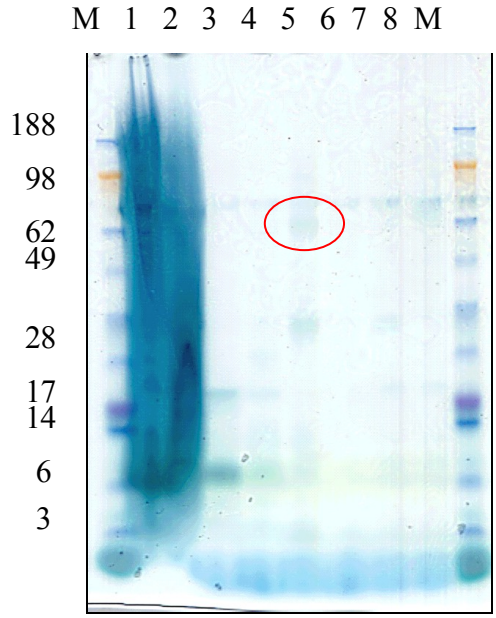


The GSU0357-containing protein solution was then applied to a Superdex 200 gel filtration column, but protein separation using this column was limited (Figure 5.2). An attempt at further purification using a Superdex 75 gel filtration column was also ineffective.

**Figure 5.2: Heme-stained SDS-PAGE gel of S200 fractions obtained in the purification of GSU0357 overexpressed in *S. frigidimarina*.**

*Lane M = molecular weight marker, L = load, 1-11 = sequentially eluted fractions. GSU0357 is indicated by the arrow.*

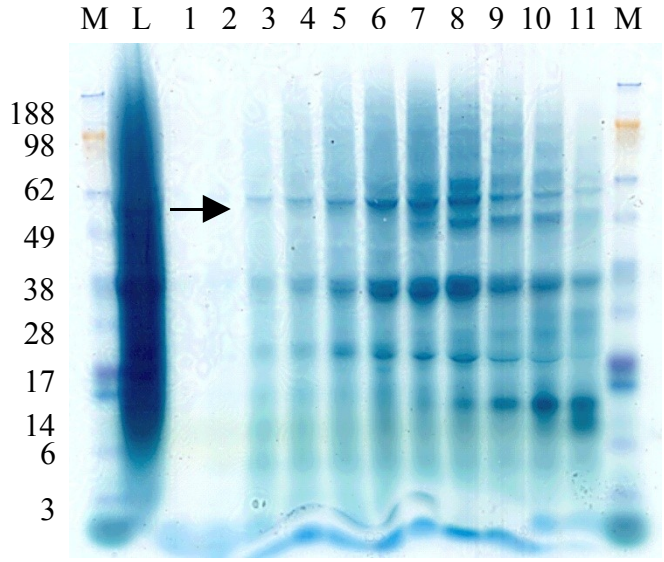


All attempts to purify GSU0357 overexpressed in *S. frigidimarina* have been limited by the inability to effect any further clean up of the sample following gel filtration. This is partly due to the large number of endogenous cytochromes expressed by *S. frigidimarina*, from which the protein of interest has been difficult to separate.

### 5.2.2 PURIFICATION FROM *ESCHERICHIA COLI*

On initial sonication and centrifugation of GSU0357-containing *E. coli* cells it was observed that the cell pellets were red in colour, indicating the presence of a large

number of cytochromes in the membrane fraction and SDS-PAGE of the supernatant indicated that very little protein was solubilised.

In order to recover protein from the membrane fraction, the membrane was disrupted by incubation with the detergent sodium cholate (5 mg $ml^{-1}$) (Liu *et al*, 1981), a non-denaturing agent, for 1 hour and then centrifuged. This slightly increased the amount of the cytochrome present in the supernatant, although the majority was still located in the membrane fraction (indicated by the red colouration of the cell pellet). Repeated treatment with cholate led to the solubilization of a little more protein, but was unable to completely remove it from the membrane. Cholate was removed from the protein solution by dialysis. A 30 - 60 % $(NH_4)_2$ $SO_4$ precipitation was performed on the treated cell free extract and the pellet resuspended, dialysed and assessed using SDS-PAGE. (Figure 5.3).

Very little GSU0357 was solubilised and it was therefore concluded that extraction of GSU0357 from the membrane using sodium cholate was not effective an effective approach. The alternative detergent Triton-X was similarly tested (Figure 5.4) and proved slightly more successful, although this detergent also solubilised a large amount of non-heme proteins and the majority of the GSU0357 protein remained membrane-associated.

This membrane association of GSU0357 following overexpression in *E. coli* JM091(DE3) was unexpected, as it was anticipated from presence of a periplasmic leader sequence that the protein would be soluble and exported to the periplasm. A possible explanation for this defective export may be that the unusual CXXCK amino acid motif predicted by the GSU0357 amino acid sequence caused the protein to fail

**Figure 5.3: Heme-stained SDS-PAGE gel showing the results of cholate and ammonium sulfate treatment of GSU0357 overexpressed in *E. coli*.**

*Lane M = molecular weight marker, 1 = cell free extract, 2 = cholate-treated supernatant, 3 = 30% $(NH_4)_2$ $SO_4$ supernatant, 4 = 30% $(NH_4)_2$ $SO_4$ pellet, 5 = 60% $(NH_4)_2$ $SO_4$ supernatant, 6 = 60% $(NH_4)_2$ $SO_4$ pellet.*

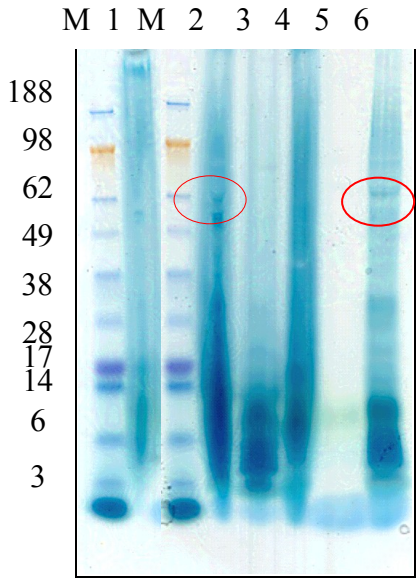


**Figure 5.4: Comparison of the detergents sodium cholate and Triton-X in the solublization of GSU0357 overexpressed in *E. coli*.**

*Lane M = MW marker, lanes 1 & 2 show the membrane fraction, lane 3 = cell supernatant, lanes 4 & 5 show the supernatant obtained after cholate treatment of the membrane fraction, lanes 6 & 7 show the supernatant after Triton-X treatment of the membrane fraction. GSU0357 is indicated by the arrow.*

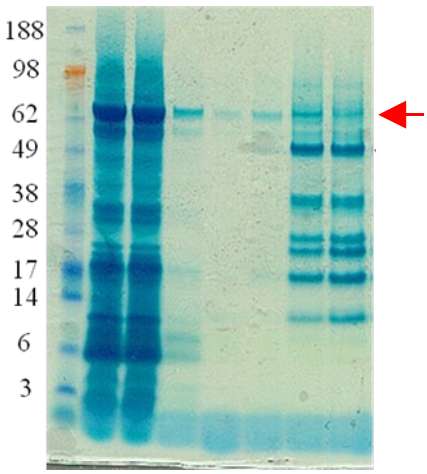

to be properly matured (Section 1.4.2). An inability of the cytochrome *c* maturation system to cope with this protein may also have resulted in misfolding leading to the formation of insoluble and possibly membrane-attached aggregates, and so an inclusion body type extraction was attempted.

Inclusion bodies may form when recombinant proteins do not reach their correctly folded tertiary structure, leading to the formation of insoluble aggregates. This may occur under high inducer concentrations (for example, where the rate of protein production exceeds that of correct folding) or it may result from the inability of the bacterium to support all of the post-translational modifications needed for the protein to fold (Baneyx *et al*, 2004). Although *E. coli* itself expresses a cytochrome *c* nitrite reductase with a single lysine-ligated heme (Bamford *et al*, 2002a) it is likely that the system responsible for maturing this unusual type of heme would be overwhelmed by the overexpression of GSU0357. Additionally, studies concerning the maturation of unusual *c*-type cytochrome heme-binding motifs in *E. coli* (Allen *et al*, 2003a & 2005b) suggest that the CXXCK motif fails to correctly mature. Cytochrome $b_{562}$ variants expressed in *E. coli* and containing the CXXCK motif were found to be improperly matured and located in the periplasmic membrane. Although the apocytochrome was shown to be present in large amounts the holocytochrome was present only minimally and, despite attempts to purify the holocytochrome using anion exchange chromatography, no pure protein could be obtained.

The formation of inclusion body protein can have several advantages which may be exploited; purification may be simplified as the inclusion bodies can be rapidly isolated

and large quantities of protein can be obtained in this form. The purification and recovery of active protein from inclusion bodies involves their initial isolation and purification from the cell pellet using a series of wash steps including treatment with detergent (in this case, Triton-X). The inclusion bodies are then solubilized using either chaotropic agents (such as guanidine salts or urea) or detergents to produce denatured protein. Dialysis of the solution to gradually remove the denaturants allows the protein to refold.

Figure 5.5 shows the progress of the inclusion body purification (Section 2.2.2.2), followed using SDS-PAGE. The wash steps (Lanes 1 and 2) remove other cell

**Figure 5.5: Coomassie-stained SDS-PAGE gel showing the stages of the inclusion body purification.**

*Lane M = molecular weight marker, 1 = 1st centrifugation supernatant, 2 = 2nd centrifugation supernatant, 3 = 1st centrifugation pellet, 4 = 2nd centrifugation pellet, 5 = purified inclusion body-type protein. GSU0357 is indicated in the red circle.*

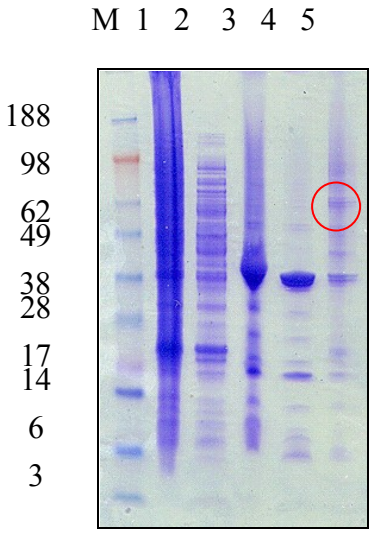


proteins from the solution and the solution is then centrifuged at two points during dialysis to remove any unfolded proteins (Lanes 3 and 4), leaving a final pellet

containing the purified inclusion bodies (Lane 5). Following the isolation of the inclusion body protein, the sample was subjected to weak anion exchange, followed by hydroxyapatite chromatography and gel filtration.

The refolded inclusion body-type protein was applied to the DE-52 column, eluted using 0.3 M NaCl (Figure 5.6) and dialysed. This anion exchange step did not significantly purify the sample, but was primarily used to filter the protein in order to facilitate the running of the hydroxyapatite column. The protein solution was then applied to the hydroxyapatite column and eluted using 0.1 M $K_2HPO_4$ (Figure 5.7).

**Figure 5.6: Coomassie-stained SDS-PAGE gel showing the elution of the GSU0357-containing inclusion body sample from a DE-52 anion exchange column.** *Lane M = molecular weight marker, 1 = crude inclusion body-type protein sample, 2 = flow through, 3 = 0.1 M NaCl fraction, 4 = 0.2 M NaCl fraction, 5 = 0.3 M NaCl fraction. GSU0357 is indicated in the red circle.*

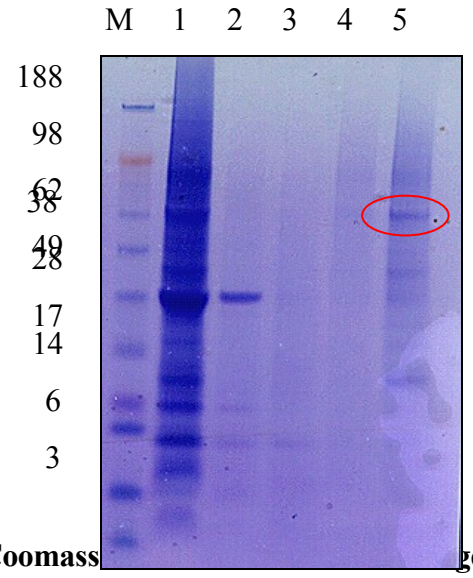


**Figure 5.7: Coomass gel showing hydroxyapatite chromatography of the GSU0357-containing inclusion body protein.**

*M = molecular weight marker, 1 = load (diluted sample), 2 = load, 3 = flow through (diluted sample), 4 = flow through, 5 = 0.1 M $K_2HPO_4$ fraction (diluted sample), 6 =*

*0.1 M $K_2HPO_4$ fraction. Specified fractions were diluted by a factor of 3, (-) indicates no sample. GSU0357 is indicated in the red circle.*

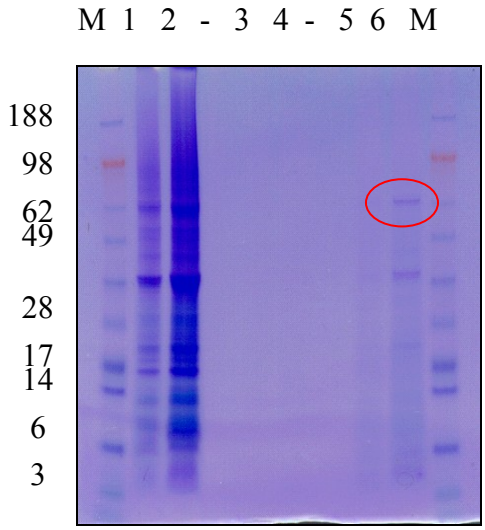


The protein sample was then applied to a Superdex 200 gel filtration column. Some separation was achieved on this column (Figure 5.8), but several protein bands still remained on the SDS-PAGE gel of the sample.

Although there has been some success in the purification of GSU0357 from inclusion bodies, it has proved difficult to effect any further clean up of the sample following gel filtration. As a result of this, and with potentially problematic expression of the protein by the cytochrome *c* maturation apparatus of *E. coli*, it is not known whether any protein produced did in fact contain the full complement of correctly incorporated hemes. Additionally, refolding experiments were not carried out and so it is unknown whether the protein had refolded to its native conformation.

**Figure 5.8: Coomassie-stained SDS-PAGE of S200 fractions**

*M: molecular weight marker, lanes 1-13 refer to sequentially-eluted S200 fractions. GSU0357 is indicated in the red circle.*

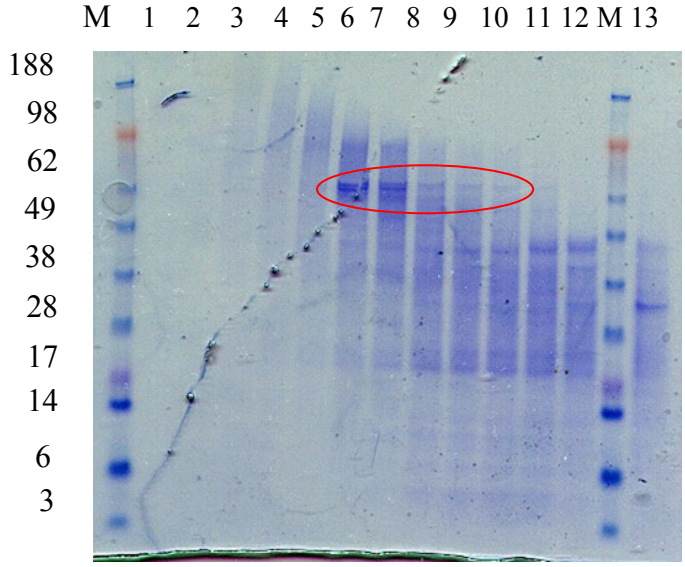


## 5.2 STEADY STATE KINETIC ANALYSIS OF GSU0357

The ability of the crude GSU0357 extracts isolated from *S. frigidimarina* and *E. coli* to catalyse the reduction of nitrite was determined at pH 7.0, 25 °C, $I$ = 0.1 M, using the method described in Section 2.5.2. Although no pure GSU0357 had been isolated, approximate concentrations of the protein in the partially pure extracts were estimated using the extinction coefficient for OTR ($\varepsilon_{420}$ = 1226.6 $mM^{-1}$ $cm^{-1}$; Rothery, 2003). It is acknowledged that the presence of additional cytochromes in the samples means that these concentrations will be a measure of the amount of cytochromes in the sample, and not specifically the GSU0357 protein. The approximate cytochrome concentrations of the partially pure extracts from *S. frigidimarina* and *E. coli* were 13 μM and 11 μM respectively. The Michaelis curves for the reduction of nitrite by GSU0357 from *S. frigidimarina* and *E. coli* are shown in Figures 5.9 and 5.10 and the steady-state kinetic

data is summarised in Table 5.1. From these data it can be seen that both extracts are similarly active and that their components can function as a nitrite reductase. As previously stated, these are purely tentative results due to the use of impure enzyme samples and it cannot be assumed that GSU0357 is responsible for the activity observed. Table 5.2 summarises the results and shows literature values for nitrite reductases from other systems for comparison.

**Table 5.1: Steady state kinetic data for the reduction of nitrite by crude protein extracts containing GSU0357.**

*Data recorded at pH 7.0, 25 °C, I = 0.1 M.*

| **Preparation** | $k_{obs}$ **($s^{-1}$)** | $V_{max}$ **(μM)** |
|---|---|---|
| ***S. frigidimarina*** | 0.12 ± 0.01 | 32.5 ± 7 |
| ***E. coli*** | 0.24 ± 0.02 | 45.9 ± 13 |

**Figure 5.9: Michaelis curve showing the steady-state turnover of nitrite by the crude extract of the *S. frigidimarina* preparation containing GSU0357.**

*Data recorded at pH 7.0, 25 °C, I = 0.1 M.*

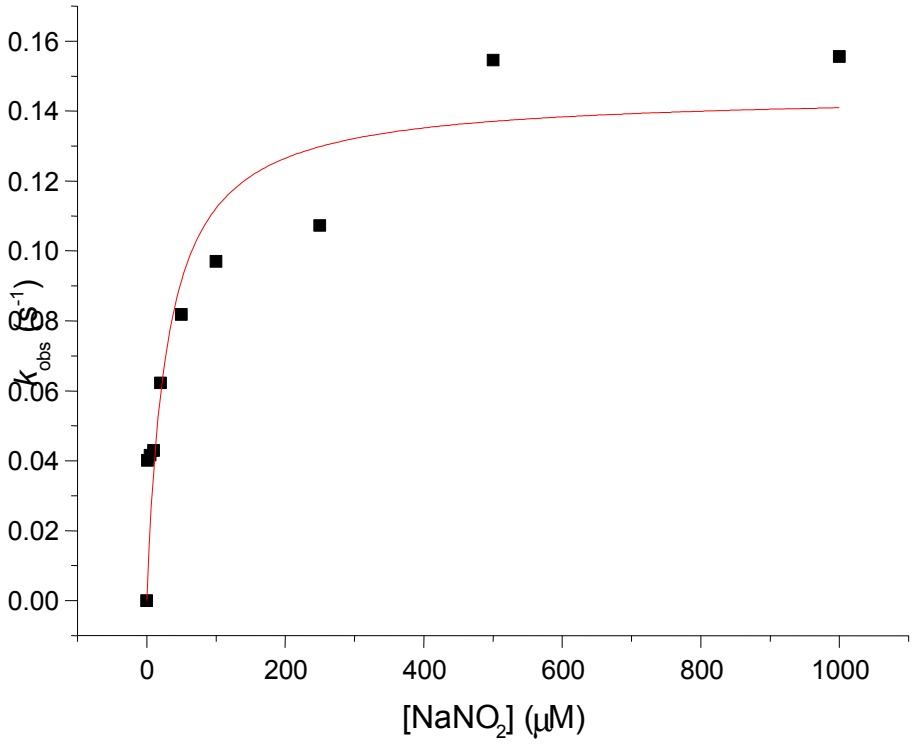


**Figure 5.10: Michaelis curve showing the steady-state turnover of nitrite by the crude extract of the *E. coli* preparation containing GSU0357.**

*Data recorded at pH 7.0, 25 °C, I = 0.1 M.*

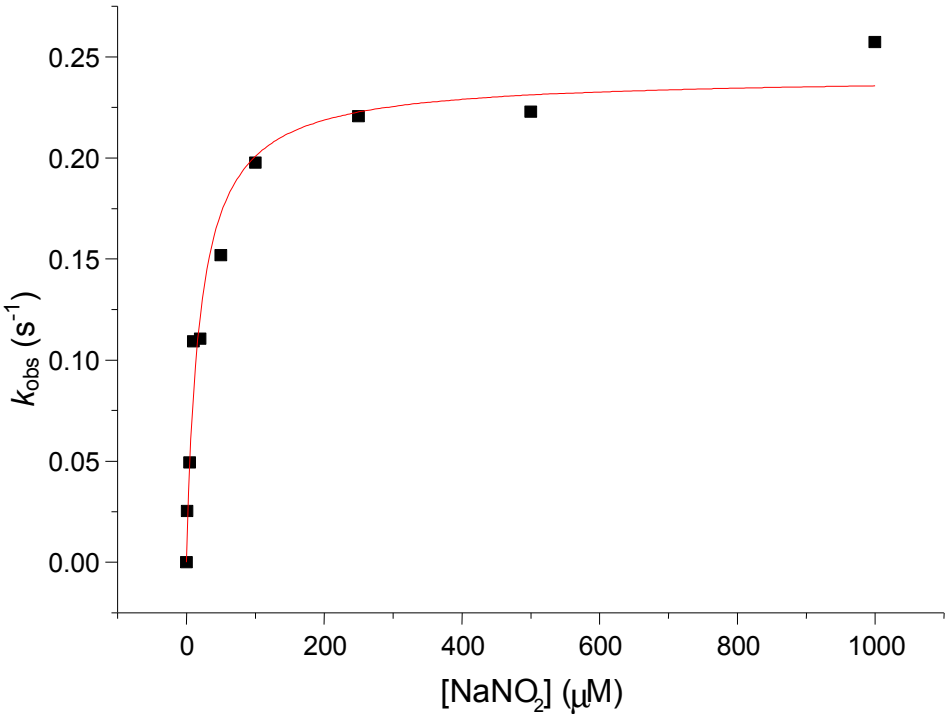


**Table 5.2: Summary of nitrite reductase activity of crude extracts containing GSU0357 and other cytochrome *c* nitrite reductases.**

*Literature values obtained from Murillo et al, 1999.*

| **System** | $V_{max}$ ($s^{-1}$) | $K_M$ (μM) |
|---|---|---|
| GSU0357 from *G. sulfurreducens* (*S. frigidimarina*) | 0.15 | 29.4 |
| GSU0357 from *G. sulfurreducens* (*E. coli*) | 0.24 | 19.7 |
| *Geobacter metallireducens* | - | 10 |
| *Escherichia coli* | - | 110 |
| *Desulfovibrio desulfuricans* | - | 1100 |
| OTR from *Shewanella oneidensis* | 2.8 | 5.2 |

From these data it can be seen that the crude extracts containing both enzymes are active in the reduction of nitrite, to a similar degree. However, the potential for the comparison of these two results is limited with literature data is limited by the fact that it is not known whether or not it is the GSU0357 protein which is responsible fo the observed activity. In addition to this, the impurity of the enzyme samples means that the precise concentration of GSU0357 in each was not known and so parameters such as the catalytic rates and Michaelis constants cannot be determined.

## 5.4 DISCUSSION

The purification of the putative nitrite reductase, GSU0357, from *Geobacter sulfurreducens* has proved to be significantly more complex that initially anticipated,

despite overexpression in two different systems that had previously been successful in the overexpression of other multiheme cytochromes *c*.

The isolation of the pure enzyme from *S. frigidimarina* was complicated by the presence of a large number of endogenous cytochromes, while purifications from *E. coli* were hampered by membrane association and possible misfolding of the protein, probably due to improper heme maturation by the cytochrome *c* maturation apparatus. As discussed in Section1.4.2, a series of specific maturation proteins are necessary for the functional incorporation of hemes, and for this reason it has previously been found difficult to overexpress holocytochromes *c*, particularly those containing multiple hemes (Shi *et al*, 2005). The heterologous expression of cytochromes *c* in *E. coli* tends to fail on account of the low efficiency of the required post-translational covalent attachment of heme (Pollock *et al*, 1989; Grisshammer *et al*, 1991) and, in addition to this, a high rate of protein synthesis may result in saturation of the maturation system, leading to a high percentage of immature species (containing only one or two hemes per molecule). The addition of an unusual CXXCK amino acid motif in the protein sequence may also have resulted in the failure of the protein to be properly matured. However, some purification of crude preparations from each system was achieved.

Steady-state kinetic assays have confirmed that the crude extracts containing GS0357 isolated following overexpression in *S. frigidimarina* and *E. coli* are able to reduce nitrite. However, the scope for comparison of the data obtained and with that for any nitrite reductase enzyme is limited as the GSU0357-containing preparations used in the assays were impure. At best, it can only be determined that the crude preparations

contain an enzyme with nitrite reductase activity, but it cannot be assumed that that enzyme is GSU0357.

Further work may help to develop and optimise a reliable and reproducible purification of the GSU0357 enzyme. Preliminary investigations have involved His-tagging of the protein in an attempt to facilitate purification, although it appears that inclusion of the tag has further compromised protein expression (His-tagging has previously been suggested to be detrimental to the correct maturation of *c*-type cytochromes (Londer *et al*, 2004)).

Once the enzyme has been reproducibly purified a full characterisation may be undertaken, including mass spectrometry, isoelectric focussing, potentiometry and the determination of the pyridine hemochrome for this enzyme. Substrate screening may reveal enzymatic substrates and it would be of interest to assess the activity of GSU0357 with the range of substrates OTR has been found capable of turning over. Further to this, crystallography may yield the structure of the enzyme and its active site in detail, allowing for characterisation of the unusually-ligated heme.

# *CHAPTER 6*

# *CONCLUSIONS AND FURTHER WORK*

# 6 CONCLUSIONS AND FURTHER WORK

## 6.1 OCTAHEME TETRATHIONATE REDUCTASE

Significant advances in our knowledge of the octaheme tetrathionate reductase from *Shewanella oneidensis* have been presented in this thesis. An improved protocol for the purification of the enzyme has been presented, resulting in increased yield and purity of the enzyme. A number of new substrates for OTR have been identified, including hydrogen peroxide, cumene hydroperoxide, nitrite and hydroxylamine.

The ability of OTR to function as a peroxidase has been characterised and the steady state kinetic parameters for this reaction determined (hydrogen peroxide: $K_M$ = 15.8 mM, $k_{cat}$ = 17.5 $s^{-1}$; cumene hydroperoxide: $K_M$ = 9.2 mM, $k_{cat}$ = 2.2 $s^{-1}$). These parameters show OTR to be significantly less efficient than physiological peroxidase enzymes and it is unlikely that OTR has this role in the cell.

The potential for OTR to catalyse the reduction of nitrite and hydroxylamine was initially proposed on the basis of significant similarities between the structure of the enzyme and the nitrogen cycle enzymes cytochrome *c* nitrite reductase and hydroxylamine oxidoreductase. This has been found to be the case, and OTR found to function efficiently as both nitrite and hydroxylamine reductase with kinetic parameters comparable to those for the cytochrome *c*

nitrite reductases (nitrite: $K_M$ = 5.2 μM, $k_{cat}$ = 2.8 $s^{-1}$; hydroxylamine: $K_M$ = 2.2 mM, $k_{cat}$ = 849 $s^{-1}$). The catalytic efficiencies of these reductions are of the same order as that of tetrathionate reduction; however, comparison of the $K_M$ values for these reactions suggests that nitrite is in fact the best substrate. Therefore it is proposed that OTR may have a role as a nitrogen cycle enzyme.

The product of the reductions of nitrite and hydroxylamine by OTR was directly detected in solution and shown to be the ammonium ion. This conversion of nitrite to ammonium without the release of any detectable intermediates is characteristic of the cytochrome *c* nitrite reductases, again suggesting that OTR may in fact function as a physiological nitrite reductase. In addition to this, the solvent kinetic isotope effect for the reduction of nitrite by OTR was determined and it was found that the rate of this reaction is only mildly dependent on proton delivery. The reaction was also found to be dependent upon pH, with a p$K_a$ value of 5.8, which may correspond to the protonation of a key active site residue, such as a histidine.

Site-directed mutagenesis of the unusual heme-ligating lysine 56 in the active site of OTR has allowed the investigation of its role. The replacement of the lysine with an alanine residue might have been expected to eradicate enzyme activity due to the removal of the ligand to the active site heme. However, the K56A OTR mutant was found to be active as both a nitrite and hydroxylamine reductase (nitrite: $K_M$ = 65.6 mM, $k_{cat}$ = 0.51 $s^{-1}$; hydroxylamine: $K_M$ = 10.8 mM, $k_{cat}$ = 349.3 $s^{-1}$). In addition to this, very little difference was observed in the pH-activity dependence of the mutant as compared to the wild type enzyme, suggesting that an important protonation event is conserved in the mutant. The confirmation of ammonium as the product of the reductions of nitrite and hydroxylamine by K56A OTR, with a similar conversion

efficiency to the wild type enzyme, again suggests that the K56A mutation does not have a significant effect on the ability of the enzyme to catalyse the full 6 electron reduction of nitrite to ammonium, suggesting that the changes to the active site as a result of the mutation are not particularly deleterious.

It has therefore been suggested that another residue may act as the active site heme ligand in the mutant enzyme. The most likely candidate for this ligation of the heme iron is histidine 78, which is found below the active site in the wild type crystal structure. This residue might possibly "flip" upwards to take the place of the lysine, in the process re-creating a conventional CXXCH heme-ligating motif.

The importance of the assertion that OTR be reclassified as a nitrogen cycle enzyme cannot be underestimated and it is hoped that future research into this interesting enzyme be redirected to fully investigate its role in this new context.

## 6.2 GSU0357

The purification of the putative nitrite reductase, GSU0357, from *Geobacter sulfurreducens* has proved to be significantly more complex than initially anticipated. However, partially pure preparations of the protein were isolated following over-expression in *Shewanella frigidimarina* and *Escherichia coli*. Steady-state kinetic assays have confirmed that crude preparations containing GSU0357 can do have nitrite reductase activity and kinetic parameters

were obtained (*S. frigidimarina* preparation: $V_{max}$ = 0.12 $s^{-1}$; *E. coli* preparation: $V_{max}$ = 0.24 $s^{-1}$). These data were found to be within the range of literature values for the cytochrome *c* nitrite reductases, raising the possibility that this may be a physiological role for GSU0357.

## 6.3 FURTHER WORK

Despite the availability of the crystal structure for this OTR, some uncertainty still exists as to the structure of the active site because of the presence of exogenous thiocyanate as the sixth ligand to the heme and the disorder of some active site residues (Gly147-Val152). It would therefore be of great interest to clarify the active site structure. A number of new substrates have been identified for the enzyme and many more may be screened for activity. The desirability of obtaining a crystal structure of the enzyme with substrate bound cannot of course be ignored and may be invaluable in elucidating its mechanism of action, which at present can merely be speculated upon. In addition to this, the successful growth of K56A OTR crystals reported in this thesis may provide the opportunity to confirm the hypothesis that histidine 78 is able to ligate the active site heme of the mutant enzyme.

It would be of great interest to determine whether OTR has a physiological role as a nitrite reductase. Therefore, the creation of a knockout mutant may be important and there is great potential to investigate the possible upregulation of mRNA under a range of growth conditions for *Shewanella oneidensis* MR-1. Little is known as yet about the respiratory pathway of this interesting and multifunctional enzyme and what its redox partners may be. For example, the operon encoding OTR also contains a monoheme *c*-type cytochrome which may be involved in

electron transfer, or it is possible that OTR may be reduced by another protein such as CymA. These possibilities have not yet been probed, but may be of great interest in understanding the role of OTR in the complex cellular reactions of *Shewanella oneidensis*.

In the case of GSU0357 from *Geobacter* sulfurreducens, further work may aid in the development and optimisation of a reproducible purification protocol. Preliminary investigations have involved His-tagging of the protein in an attempt to facilitate purification, although it appears that inclusion of the tag has further compromised protein expression.

Once the enzyme has been reproducibly purified a full characterisation may be undertaken, including mass spectrometry, isoelectric focussing, potentiometry and the determination of the pyridine hemochrome for this enzyme. Substrate screening may reveal addition substrates and it would be of interest to assess the activity of GSU0357 with the range of substrates OTR has been found capable of turning over. Further to this, crystallography may yield the structure of the enzyme and its active site in detail, allowing for characterisation of the unusually-ligated heme.

# *REFERENCES*

**Adrain, C., Martin, S.J. (2001)** "The mitochondrial apoptosome: a killer unleashed by the cytochrome seas" *Trends Biochem. Sci.*, **26**, 390-397.

**Allen, J.W.A., Tomlinson, E.J., Hong, L., Ferguson, S.J. (2002)** "The *Escherichia coli* cytochrome *c* maturation (Ccm) system does not detectably attach heme to single cysteine variants of an apocytochrome *c*" *J. Biol. Chem.*, **277**, 33559-33563.

**Allen, J.W.A., Barker, P.D., Ferguson, S.J. (2003a)** "A cytochrome $b_{562}$ variant with a *c*-type cytochrome CXXCH heme-binding motif as a probe of the *Escherichia coli* cytochrome *c* maturation (Ccm) system" *J. Biol. Chem.*, **278**, 52075-52083.

**Allen, J.W.A., Daltrop, O., Stevens, J.M., Ferguson, S.J. (2003b)** "*c*-type cytochromes: diverse structures and biogenesis systems pose evolutionary problems" *Philos. Trans. R. Soc. London, Ser. B*, **358**, 255-266.

**Allen, J.W.A., Ginger, M.L., Ferguson, S.J. (2004)** "Maturation of the unusual single-cysteine (XXXCH) mitochondrial *c*-type cytochromes found in trypanosomatids must occur through a novel biogenesis pathway" *Biochem. J.*, **383**, 537-542.

**Allen, J.W.A., Ginger, M.L., Ferguson, S.J. (2005)** "Complexity and diversity in *c*-type cytochrome biogenesis systems" *Biochem. Soc. Trans.*, **33**, 145-146.

**Allen, J.W.A., Leach, N., Ferguson, S.J. (2005)** "The histidine of the *c*-type cytochrome CXXCH binding motif is essential for haem attachment by the *Escherichia coli* cytochrome *c* maturation (Ccm) apparatus" *Biochem. J.*, **389**, 587-592.

**Andersson, K.K., Kent, T.A., Lipscomb, J.D., Hooper, A.B., Munck, E. (1984)** "Mossbauer, EPR and optical studies of the P-460 centre of hydroxylamine oxidoreductase from *Nitrosomonas*. A ferrous heme with an unusually large quadrupole splitting" *J. Biol. Chem.*, **259**, 6833-6840.

**Andersson, K.K., Lipscomb, J.D., Valentine, M., Munck, E., Hooper, A.B. (1986)** "Tetraheme cytochrome $c_{554}$ from *Nitrosomonas europaea*: heme-heme interactions and ligand binding" *J. Biol. Chem.*, **261**, 1126-1138.

**Arciero, D.M., Balny, C., Hooper, A.B. (1991)** "Spectroscopic and rapid kinetic studies of the reduction of cytochrome $c_{554}$ by hydroxylamine oxidoreductase from *Nitrosomonas europaea*" *Biochemistry*, **30**, 11466-11472.

**Arciero, D.M., Golombek, A., Hendrich, M.P., Hooper, A.B. (1998)** "Correlation of optical and EPR signals with the P460 heme of hydroxylamine oxidoreductase from *Nitrosomonas europaea*" *Biochemistry*, **37**, 523-529.

**Arnoux, P., Sabaty, M., Alric, J., Frangioni, B., Guigliarelli, B., Adriano, J.M., Pignol, D. (2003)** "Structural and redox plasticity in the heterodimeric periplasmic nitrate reductase" *Nat. Struct. Biol.*, **10**, 928-934.

**Arslan, E., Schulz, H., Zufferey, R., Künzler, P., Thöny-Meyer, L. (1998)** "Overproduction of the *Bradyrhizobium japonicum c*-type cytochrome subunits of the $cbb_3$ oxidase in *Escherichia coli*" *Biochem. Biophys. Res. Com.*, **251**, 744-747.

**Assfalg, M., Bertini, I., Bruschi, M., Michel, C., Turano, P. (2002)** "The metal reductase activity of some multiheme cytochromes *c*: NMR structural characterization of the reduction of chromium (VI) to chromium (III) by cytochrome $c_7$" *Proc. Natl. Acad. Sci. USA*, **99**, 9750-9754.

**Atkinson, S.J., Mowat, C.G., Reid, G.A., Chapman, S.K. (2007)** "An octaheme *c*-type cytochrome from *Shewanella oneidensis* can reduce nitrite and hydroxylamine" *FEBS Lett.*, **581**, 3805-3808.

**Bamford, V.A., Angove, H.C., Seward, H.E., Thomson, A.J., Cole, J.A., Butt, J.N., Hemmings, A.M., Richardson, D.J. (2002a)** "Structure and spectroscopy of the periplasmic cytochrome *c* nitrite reductase from *Escherichia coli*" *Biochemistry*, **41**, 2921-2931.

**Bamford, V.A., Bruno, S., Rasmussen, T., Appia-Ayme, C., Cheeseman, M.R., Berks, B.C., Hemmings, A.M. (2002b)** "Structural basis for the oxidation of thiosulfate by a sulfur cycle enzyme" *EMBO J.*, **21**, 5599-5610.

**Baneyx, F., Mujacic, M. (2004)** "Recombinant protein folding and misfolding in *Escherichia coli*" *Nature Biotechnol.*, **22**, 1399-1408.

**Barbosa-Jefferson, V.L., Zhao, F.J., McGrath, .P., Magan, N. (1998)** "Thiosulfate and tetrathionate oxidation in arable soils" *Soil Biol. Biochem.*, **30**, 553-559.

**Barker, P.D., Ferguson, S.J. (1999)** "Still a puzzle: why is heme covalently attached in *c*-type cytochromes?" *Struct. Fold Des.*, **1999**, R281-R290.

**Barrett, E.L., Clark, M.A. (1987)** "Tetrathionate reduction and production of hydrogen sulphide from thiosulfate" *Microbiol. Rev.*, **51**, 192-205.

**Baumann, L., Baumann, P., Mandell, M., Alen, R.D. (1972)** "Taxonomy of aerobic marine bacteria" *J. Bacteriol.*, **110**, 402-409.

**Beliaev, A.S., Saffarini, D.A. (1998)** "*Shewanella putrefaciens* mtrB encodes an outer membrane protein required for Fe(III) and Mu(IV) reduction" *J.Bacteriol.*, **180**, 6292-6297.

**Berks, B.C., Ferguson, S.J., Moir, J.W.B., Richardson, D.J. (1995)** "Enzymes and associated electron transport systems that catalyse the respiratory reduction of nitrogen oxides and oxyanions" *Biochim. Biophys. Acta*, **1232**, 97-173.

**Beratan, D.N., Onuchic, J.N., Winkler, J.R., Gray, H.B. (1992)** "Electron-tunnelling pathways in proteins" *Science*, **258**, 1740-1741.

**Berman, H.M., Westbrook, J., Feng, Z., Gilliland, G., Bhat, T.N., Weissig, H., Shindyalov, I.N., Bourne, P.E. (2000)** "The Protein Data Bank" *Nucleic Acids Res.*, **28**, 235-242.

**Bernard, D.G., Gabilly, S.T., Dujardin, G., Merchant, S., Hamel, P.P. (2004)** "Overlapping specificities of the mitochondrial cytochrome *c* and $c_1$ lyases" *J. Biol. Chem.*, **278**, 49732-49742.

**Bertero, M.G., Rothery, R.A., Palak, M., Hou, C., Lim, D., Blasco, F., Weiner, J.H., Strynadka, N.C. (2003)** "Insights into the respiratory electron transfer pathway from the structure of nitrate reductase A" *Nat. Struct. Biol.*, **10**, 681-687.

**Biel, S.W., Biel, A.J. (1990)** "Isolation of a *Rhodobacter capsulatus* mutant that lacks *c*-type cytochromes and excretes porphyrins" *J. Bacteriol.*, **172**, 1321-1326.

**Birch-Andersen, A., Maaløe, O., Sjostrand, F.S. (1953)** "High resolution micrographs of sections of *E. coli*" *Biochim. Biophs. Acta*, **12**, 395-400.

**Blümle, S., Zumft, W.G. (1991)** "Respiratory nitrate reductase from denitrifying *Pseudomonas stutzeri*, purification, properties and target of proteolysis" *Biochim. Biophys. Acta*, **1057**, 102-108.

**Bond, D.R., Lovley, D.R., (2003)** "Electricity production by *Geobacter sulfurreducens* attached to electrodes" *Appl. Env. Microbiol.*, **69**, 1548-1555.

**Bordo, D., Deriu, D., Colnaghi, R., Carpen, A., Pagani, S., Bolognesi, M. (2000)** "The crystal structure of a sulfur transferase from *Azobacter vinlandii* highlights the evolutionary relationship between the rhodanese and phosphatise enzyme families" *J. Molec. Biol.*, **298**, 691-704.

**Bottom, C.B., Hanna, S.S., Siehr, D.D. (1979)** "Mechanism of the ninhydrin reaction" *Biochem. Educ.*, **6**, 4-5.

**Bowman, J.P., McCammon, S.A., Nichols, D.S., Skerratt, J.H., Rea, S.M., Nichols, P.D., McMeekin, T.A. (1997)** "*Shewanella gelidimarina* sp. nov. and *Shewanella frigidimarina* sp. nov., novel Antarctic species with the ability to produce eicosapentoic acid (20:5ω3) and grow anaerobically by dissimilatory $Fe^{III}$ reduction" *Int. J. Syst. Bacteriol.*, **47**, 1040-1047.

**Brown, K., Tegoni, M., Prudencio, M., Pereira, A.S., Besson, S., Moura, J.J., Moura, I., Cambillau, C. (2000a)** "A novel type of catalytic copper cluster in nitrous oxide reductase" *Nat. Struct. Biol.*, **7**, 191-195.

**Brown, K., Djinovic-Carugo, K., Haltia, T., Cabrito, I., Saraste, M., Moura, J.J., Moura, I., Tegoni, M., Cambillau, C. (2000b)** "Revisiting the catalytic CuZ cluster

of nitrous oxide ($N_2O$) reductase. Evidence of a bridging inorganic sulfur" *J. Biol. Chem.*, **275**, 41133-41136.

**Butler, C.S., Charnock, J.M., Bennett, B., Sears, H.J., Reilly, A.J., Ferguson, S.J., Garner, C.D., Lowe, D.J., Thomson, A.J., Berks, B.c., Richardson, D.J. (1999)** "Molybdenum coordination during the catalytic cycle of periplasmic nitrate reductase from *Paracoccus denitrificans* derived from EPR and EXAFS spectroscopy" *Biochemistry*, **38**, 9000-9012.

**Caccavo, F., Lonergan, D.J., Lovley, D.R., Davis, M., Stolz, J.F., McInerney, M.J. (1994)** "*Geobacter sulfurreducens* sp. Nov., a hydrogen- and acetate-oxidising dissimilatory metal-reducing microorganism" *Appl. Env. Microbiol*., **60**, 3752-3759.

**Chen, Y-S., Liu, Y.C., Yen, M-Y., Wang, J-H., Wann, S-R., Cheng, D-L. (1997)** "Skin and soft tissue manifestations of *Shewanella putrefaciens* infection" *Clin. Infect. Dis.*, **25**, 225-229.

**Clairborne, A., Yeh, J.I., Mallett, T.C., Luba, J., Crane, E.J., Charrier, V., Parsonage, D. (1999)** "Protein sulfenic acids: diverse roles for an unlikely player in enzyme catalysis and redox regulation" *Biochemistry*, **25**, 1675-1681.

**Clarke, T.A., Dennison, V., Seward, H.E., Burlatt, B., Cole, J.A., Hemmings, A.M., Richardson, D.J. (2004)** "Purification and spectropotentiometric characterization of *Escherichia coli* NrfA, a decaheme homodimer that transfers electrons to the decaheme periplasmic nitrite reductase complex" *J. Biol. Chem.*, **279**, 41333-41339.

**Costa, C., Moura, J.J.G., Moura, I., Liu, M-Y., Peck, H.D., Le Gall, J., Wang, Y., Huynh, B.H. (1990)** "Hexaheme nitrite reductase from *Desulfovibrio desulfuricans*" *J. Biol. Chem.*, **265**, 14382-14387.

**Crow, A., Acheson, R.M., Le Brun, N.E., Oubrie, A. (2004)** "Basis of redox-coupled protein substrate selection by the cytochrome *c* biosynthesis protein ResA" *J. Biol. Chem.*, **279**, 23654-23660.

**Cunha, C.A., Macieira, S., Dias, J.M., Almeida, G., Gonçalves, L.L., Costa, C., Lampreia, J., Huber, R., Moura, J.J.G., Moura, I., Romão, M.J. (2003)** "Cytochrome *c* nitrite reductase from *Desulfovibrio desulfuricans* ATCC 27774: The relevance of the two calcium sites in the structure of the catalytic subunit (NrfA)" *J. Biol. Chem.*, **278**, 17455-17465.

**Czjzek, M., Arnoux, P., Haser, R., Shepard, W., (2001)** "Structure of cytochrome $c_7$ from *Desulfuromonas acetoxidans* at 1.9 Å resolution" *Acta Crystallogr., Sect. D*, **57**, 670-678.

**Daltrop, O., Stevens, J.M., Higham, C.W., Ferguson, S.J. (2002)** "The CcmE protein of the *c*-type cytochrome biogenesis system: unusual in vitro heme incorporation into apo-CcmE and transfer from holo-CcmE to apocytochrome" *Proc. Natl. Acad. Sci. U.S.A.*, **99**, 9703-9708.

**De Jong, G.A.U., Hazeu, W., Bos, P., Kuenen, J.G. (1997a)** "Isolation of tetrathionate hydrolase from *Thiobacilus acidophilus*" *Eur. J., Biochem.*, **243**, 678-683.

**De Jong, G.A.U., Hazeu, W., Bos, P., Kuenen, J.G., (1997b)** "Polythionate degradation by tetrathionate hydrolase of *Thiobacilus ferrooxidans*" *Microbiol.*, **143**, 499-504.

**Derby, H.A., Hammer, B.W. (1931)** "Bacteriology of butter. IV. Bacteriological studies on the surface taint butter" *Iowa Agric. Exp. Stn. Res. Bull.*, **145**, 389-416.

**Dhawan, B., Chaudry, B.M., Mishra, B.M., Agarwal, R. (1998)** "Isolation of *Shewanella putrefaciens* from a rheumatic heart disease patient with infective endocadatis" *J. Clin. Microbiol.*, **36**, 2394.

**Dias, J.M., Than, M.E., Humm, A., Huber, R., Bourenkov, G.P., Bartunik, H.D., Bursakov, S., Calvete, J., Calderira, J., Carneiro, C., Moura, J.J., Moura, I, Romão (1999)** "Crystal structure of the first dissimilatory nitrate reductase at 1.9 Å solved by MAD methods" *Structure*, **7**, 65-79.

**Dodd, F.E., Van Beeumen, J., Eady, R.R., Hasnain, S.S. (1998)** "X-ray structure of a blue-copper nitrite reductase in two crystal forms. The nature of the copper sites, mode of substrate binding and recognition by redox partner" *J. Mol. Biol.*, **282**, 369-382.

**Eaves, D.J., Staudenmann, W., James, P., Poole, R.K., White, S.A., Griffiths, L, Cole, J.A. (1998)** "Involvement of products of the nrfEFG genes in the covalent attachment of haem *c* to a novel cysteine-lysine motif in the cytochrome $c_{552}$ nitrite reductase from *Escherichia coli*" *Mol. Microbiol.*, **28**, 205-216.

**Edeling, M.A., Guddat, L.W., Fabianek, R.A., Thöny-Meyer, L., Martin, J.L. (2002)** "Structure of CcmG/DsbE at 1.14 Å resolution: high fidelity reducing activity in an indiscriminately oxidizing environment" *Structure (Cambridge)*, **10**, 973-979.

**Einsle, O., Messerschmidt, A., Stach, P., Bourenkov, G.P., Bartunik, H.D., Huber, R., Kroneck, P.M. (1999)** "Structure of cytochrome *c* nitrite reductase" *Nature*, **400**, 476-480.

**Einsle, O., Stach, P., Messershmidt, A., Simon, J., Kroger, A., Huber, R., Kroneck, P.M. (2000)** "Cytochrome *c* nitrite reductase from *Wolinella succinogenes*. Structure at 1.6 Å resolution, inhibitor binding and heme-packing motifs" *J. Biol. Chem*., **275**, 39608-39616.

**Einsle, O., Tezcan, F.A., Andrade, S.L.A., Schmid, B., Yoshida, M., Howard, J.B., Rees, D.C. (2002)** "Nitrogenase MoFe-protein at 1.16 Å resolution: a central ligand in the FeMo-cofactor" *Science*, **297**, 1696-1700.

**Einsle, O., Messerschmidt, A., Huber, R., Kroneck, P.M.H., Neese, F. (2002)** "Mechanism of the six-electron reduction of nitrite to ammonia by cytochrome *c* nitrite reductase" *J. Am. Chem. Soc.*, **124**, 11737-11745.

**Ensign, S.A., Hyman, M.R., Arp, D.J. (1993)** "Invitro activation of ammonia monooxygenase from *Nitrosomonas europaea* by copper" *J. Bacteriol.*, **175**, 1971-1980.

**Ferguson, S.J. (1998)** "Nitrogen cycle enzymology" *Curr. Op. Chem. Biol.*, **2**, 182-193.

**Field, S.J., Dobbin, P.S., Cheeseman, M.R., Watmough, N.J., Thomson, A.J., Richardson, D.J. (2000)** "Purification and magneto-optical characterization of cytoplasmic membrane and outer membrane multiheme *c*-type cytochromes from *Shewanella frigidimarina* NCIMB400" *J. Chem. Biol.*, **275**, 8515-8522.

**Frangioni, B., Arnoux, P., Sabaty, M., Pignol, D., Bertrand, P., Guigliarelli, B., Léger, C. (2004)** "In *Rhodobacter sphaeroides* respiratory nitrate reductase, the kinetics of substrate binding favours intramolecular electron transfer" *J. Am. Chem. Soc.*, **126**, 1328-1329.

**Freidmann, M., Williams, L.D. (1974)** "Stoichiometry of formation of Ruhemann's purple in the ninhydrin reaction" *Bioorg. Chem.*, **3**, 267-280.

**Fulop, V., Moir, J.W., Ferguson, S.J., Hajdu, J. (1995)** "The anatomy of a bifunctional enzyme: structural basis for reduction of oxygen to water and synthesis of nitric oxide by cytochrome $cd_1$" *Cell*, **81**, 369-377.

**Gaballa, A., Koedam, N., Cornelis, P. (1996)** "A cytochrome *c* biogenesis gene involved in pyoverdine production in *Pseudomonas fluorescens* ATCC 17400" *Mol. Microbiol.*, **21**, 777-785.

**Gillardi, G., Fantuzzi, A. (2001)** "Manipulating redox systems: application to nanotechnology" *Trends Biotechnol.*, **19**, 468-476.

**Gilmour , R., Goodhew, C.F., Pettigrew, G.W., Prazeres, S., Moura, J.J.G., Moura, I. (1994)** "The kinetics of the oxidation of cytochrome *c* by *Paracoccus* cytochrome *c* peroxidase" *Biochem. J.*, **300**, 907-914.

**Glascoe, P.K., Long, F.A. (1960)** "Use of glass electrodes to measure acidities in deuterium oxide" *J. Phys. Chem.*, **64**, 118-191.

**Godden, J.W., Turley, S., Teller, D.C., Adman, E.T., Liu, M.Y., Payne, W.J., LeGall, J. (1991)** "The 2.3 Å X-ray structure of nitrite reductase from *Achromobacter cycloclastes*" *Science*, **253**, 438-442.

**González, P.J., Correia, C., Moura, I., Brondino, C.D., Moura, J.J.G. (2006)** "Bacterial nitrate reductases: molecular and biological aspects of nitrate reduction" *J. Inorg. Biochem.*, **100**, 1015-1023.

**Goodhew, C.F., Brown, K.R., Pettigrew, G.W. (1986)** "Haem staining in gels, a useful tool in the study of bacterial cytochromes" *Biochim. Biophys. Acta.*, **852**, 288-294.

**Gordon, E.H.J., Pike, A.E., Cuthbertson, P.M., Chapman, S.K., Reid, G.A., (2000)** "Identification and characterisation of a novel cytochrome $c_3$ from *Shewanella frigidimarina* that is involved in Fe (III) respiration" *Biochem. J.*, **349**, 153-158.

**Grisshammer, R., Oeckl, C., Michel, H. (1991)** "Expression in *Escherichia coli* of *c*-type cytochromes from *Rhodopseudomonas viridis*" *Biochim. Biophys. Acta*, **1088**, 183-190.

**Haltia, T., Brown, K., Tegoni, M., Cambillau, C., Saraste, M., Mattila, K, Djinovic-Carugo, K. (2003)** "Crystal structure of nitrous oxide reductase from *Paracoccus denitrificans* at 1.6 Å resolution" *Biochem. J.*, **369**, 77-88.

**Heidelberg, J.F., Paulsen, I.T., Nelson, K.E., Gaidos, E.J., Nelson, W.C., Read, T.D., Eisen, J.A., Seshadri, R., Ward, N., Methé, B., Clayton, R.A., Mayer, T., Tsapin, A., Scott, J., Beanan, M., Brinkac, L., Daugherty, S., DeBoy, R.T., Dodson, R.J., Durkin, A.S., Haft, D.H., Kolonay, J.F., Madupu, R., Peterson, J.D., Umayan, L.A., White, O., Wolf, A.M., Vamathevan, J., Weidman, J., Impraim, M., Lee, K., Berry, K., Lee, C., Mueller, J., Khouri, H., Gill, J., Utterback, T.R., McDonald, L.A., Feldblyum, T.V., Smith, H.O., Venter, J.C., Nealson, K.H., Fraser, C.M. (2002)** "Genome sequence of the dissimilatory metal ion-reducing bacterium *Shewanella oneidensis*" *Nat. Biothechnol.*, **20**, 1118-1123.

**Hendrich, M.P., Petasis, D., Arciero, D.M., Hooper, A.B. (2001)** "Correlations of structure and electronic properties from EPR spectroscopy of hydroxylamine oxidoreductase" *J. Am. Chem. Soc.*, **123**, 2997-3005.

**Hendriks, J., Warne, A., Gohlke, U., Haltia, T., Ludovici, C., Lubben, M., Saraste, M. (1998)** "The active site of the bacterial nitric oxide reductase is a dinuclear iron centre" *Biochemistry*, **37**, 13102-13109.

**Hensel, M., Hinsley, A.P., Nikolaus, T., Sawers, G., Berks, B.C. (1999)** "The genetic basis of tetrathionate respiration in *Salmonella typhimurium*" *Mol. Microbiol.*, **32**, 275-287.

**HMSO, Department of the Environment (1981)** "Ammonia in waters; Method for the examination of waters and associated materials".

**Hooper, A.B., Debey, P., Anderson, K.K., Balny, C. (1983)** "Heme P460 of hydroxylamine oxidoreductase of *Nitrosomonas*. Reaction with CO and $H_2O_2$" *Eur. J. Biochem.*, **134**, 83-87.

**Ibers, J.A., Holm, R.H. (1980)** "Modelling coordination sites in metallobiomolecules" *Science*, **209**, 223-235.

**Igarashi, N., Moriyama, H., Fujiwara, T., Fukumori, Y., Tanaka, N. (1997)** "The 2.8 Å structure of hydroxylamine oxidoreductase from a nitrifying bacterium, *Nitrosomonas europaea*" *Nat. Struct. Biol.*, **4**, 276-284.

**Iverson, T.M., Arciero, D.M., Hsu, B.T., Logan, M.S.P., Hooper, A.B., Rees, D.C. (1998)** "Heme packing motifs revealed by the crystal structure of the tetra-heme cytochrome $c_{554}$ from *Nitrosomonas europaea*" *Nat. Struct. Biol.*, **5**, 1005-1012.

**Iverson, T.M., Luna-Chavez, C., Cecchini, G., Rees, D.C. (1999)** "Structure of the *Escherichia coli* fumarate reductase respiratory complex" *Science*, **284**, 1961-1966.

**Jensen, M.J., Tebo, B.M., Baumann, P., Mandel, M., Nealson, K.H. (1980)** "Characterisation of *Alteromonas hanedai* (sp. nov.), a non-fermentative luminous species of marine origin" *Curr. Microbiol.*, **3**, 311-315.

**Jormakka, M., Tornroth, S., Byrne, B., Iwata, S. (2002)** "Molecular basis of proton motive force generation: structure of formate dehydrogenase-N" *Science*, **295**, 1863-1868.

**Jormakka, M., Richardson, D., Byrne, B., Iwata, S. (2004)** "Structure of NarGH reveals a structural classification of Mo-*bis*MGD enzymes" *Structure*, **12**, 95-104.

**Karpishin, T.B., Grinstaff, M.W., Komarpanicucci, S., McLendon, G., Gray, H.B. (1994)** "Electron transfer in cytochrome *c* depends upon the structure of the intervening medium" *Structure*, **2**, 415-422.

**Katzen, F., Beckwith, J. (2000)** "Transmembrane electron transfer by the membrane protein DsbD occurs via a disulfide bond cascade" *Cell*, **103**, 769-779.

**Khashe, S., Janda, J.M. (1998)** "Biochemical and biophysical properties of *Shewanella alga* and *Shewanella putrefaciens*" *J. Clin. Microbiol.*, **36**, 783-787.

**Kluck, R.M., Bossy-Wertzel, E., Green, D.R., Newmeyer, D.D. (1997)** "The release of cytochrome *c* from mitochondria: a primary site for Bcl-2 regulation of apoptosis" *Science*, **275**, 1132-1136.

**Kranz, R., Lill, R., Goldman, B., Bonnard, G., Merchant, S. (1998)** "Molecular mechanisms of cytochrome *c* biogenesis: three distinct systems" *Molec. Microbiol.*, **29**, 383-396.

**Kukimoto, M., Nishiyama, M., Ohnuki, T., Turley, S., Adman, E.T., Horinouchi, S., Beppu, T. (1995)** "Identification of interaction site of pseudoazurin with its redox partner, copper-containing nitrite reductase from *Alcaligenes faecalis* S-6" *Protein. Eng.*, **8**, 153-158.

**Leslie, A.G., Walker, J.E. (2000)** "Structural model of $F_1$-ATPase and the implications for rotary catalysis" *Philos. Trans. R. Soc. Lond., B, Biol. Sci.* **355**, 465-471.

**Liu, M-C., Peck, H.D. (1981)** "The isolation and characterisation of a hexaheme cytochrome from *Desulfovibrio desulfuricans* and its identification as a new type of nitrite reductase" *J. Biol. Chem.*, **256**, 13159-13164.

**Liu, M-C., Liu, M-Y., Payne, W.J., Peck, H.D., Le Gall, J. (1983)** "*Wolinella succinogenes* nitrite reductase: purification and properties" *FEMS Microbiol. Lett.*, **19**, 201-206.

**Lloyd, J.R., Leang, C., Hodges Meyerson, A.L., Coppi, M.V., Cuifo, S., Methé, B., Sandler, S.J., Lovley, D.R. (2003)** "Biochemical and genetic characterization of PpcA, a periplasmic *c*-type cytochrome in *Geobacter sulfurreducens*" *Biochem. J.*, **369**, 153-161.

**Londer, Y.Y., Pokkuluri, P.R., Schiffer, M. (2004)** "Functional expression of multiheme cytochromes *c* in *E. coli*" *PharmaGenomics*, **4**, 24-30.

**Long, H.F., Hammer, B.W. (1941a)** "Classification of organisms important in dairy products. III. *Pseudomonas putrefaciens*" *Iowa Agric. Exp. Stn. Res. Bull.*, **285**, 176-195.

**Long, H.F., Hammer, B.W., (1941b)** "Distribution of *Pseudomonas putrefaciens*" *J. Bacteriol.*, **41**, 100-101.

**Lovley, D.R. (2003)** "Cleaning up with genomics: applying microbiology to bioremediation" *Nat. Rev. Microbiol.*, **1**, 35-44.

**Lovley, D.R., Giovannoni, S.J., White, D.C., Champine, J.E., Phillips, E.J.P., Gorby, Y.A., Goodwin, S. (1993)** "*Geobacter metallireducens* gen. nov. sp. Nov., a microorganism capable of coupling the complete oxidation of organic compounds to the reduction of iron and other metals" *Arch. Microbiol.*, **159**, 336-344.

**MacDonell, M.T., Colwell, R.R. (1985)** "Phylogeny of the Vibrionacaea, and recommendation for two new genera, *Listonella* and *Shewanella*" *Syst. Appl. Microbiol.*, **6**, 171-182.

**Marcus, R.A. (1956)** "On the theory of oxidation-reduction reaction involving electron transfer. I" *J. Chem. Phys.*, **24**, 966-978.

**Marcus, R.A., Sutia, N. (1985)** "Electron transfers in chemistry and biology" *Biochim. Biophys. Acta.*, **811**, 265-322.

**Masataka, S., Hiroshi, I., Yutaka, Y. (2003)** "*Shewanella marinintestina* sp. nov., *Shewanella schlegeliana* sp. nov. and *Shewanella sairae* sp. nov., novel eicosapentoic acid-producing marine bacteria isolated from sea-animal intestines" *Int. J. Syst. Bacteriol.*, **53**, 491-499.

**Methé, B.A., Nelson, K.E., Eisen, J.A., Paulsen, I.T., Nelson, W., Heidelberg, J.F., Wu, D., Wu, M., Ward, N., Beanan, M.J., Dodson, R.J., Madupu, R., Brinkac, L.M., Daugherty. S.C., DeBoy, R.T., Durkin, A.S., Gwinn, M., Kolonay, J.F., Sullivan, S.A., Haft, D.H., Selengut, J., Davidsen, T.M., Zafar, N., While, O., Tran, B., Romero, C., Forberger. H.A., Weidman, J., Khouri, H., Feldblyum, T.V., Utterback, T.R., Van Aken. S.E., Lovley, D.R., Fraser, C.M. (2003)** "Genome of *Geobacter sulfurreducens*: metal reduction in subsurface environments" *Science*, **302**, 1967-1969.

**Meyer, T.E., Tsapin, A.I., Vandenberghe, I., De Smet, L., Frishman, D., Nealson, K.H., Cusanovich, M.A., Van Beeumen, J.J. (2004)** "The identification of 42 possible cytochrome *c* genes in the *Shewanella oneidensis* genome and characterization of six soluble cytochromes" *Omics*, **8**, 57-77.

**Moser, C.C., Keske, J.M., Warncke, K., Farid, R.S., Dutton, P.L. (1992)** "Nature of biological electron transfer" *Nature*, **355**, 796-802.

**Moser, C.C., Page, C.C., Farid, R., Dutton, P.L. (1995)** "Biological electron transfer" *J. Bioenergetics Biomembranes*, **27**, 263-274.

**Moser, D.P., Nealson, K.H. (1996)** "Growth of the facultative anaerobe *Shewanella putrefaciens* by elemental sulfur reduction" *Appl. Env. Microbiol.*, **62**, 2100-2105.

**Mowat, C.G., Chapman, S.K. (2005)** "Multi-heme cytochromes – new structures, new chemistry" *Dalton Trans.*, 3381-3389.

**Mowat, C.G., Rothery, E., Miles, C.S., McIver, L., Doherty, M.K., Drewette, K., Taylor, P., Walkinshaw, M.D., Chapman, S.K., Reid, G.A. (2004)** "Octaheme

tetrathionate reductase is a respiratory enzyme with novel heme ligation" *Nat. Struct. Molec. Biol.*, **11**, 1023-1024.

**Murillo, F.M., Gugliuzza, T., Senko, J., Basu, P., Stolz, J.F. (1999)** "A Heme-*c* containing enzyme complex that exhibits nitrate and nitrite reductase activity from the dissimilatory iron-reducing bacterium *Geobacter metallireducens*" *Arch. Microbiol.*, **172**, 313-320.

**Murphy, M.E.P., Turley, S., Adman, E.T. (1997)** "Structure of nitrite bound to copper-containing nitrite reductase from *Alcaligenes faecalis*" *J. Biol. Chem.*, **272**, 28455-28460.

**Myers, C.R., Myers, J.M. (1997)** "Cloning and sequence of *cymA*, a gene encoding a tetraheme cytochrome *c* required for the reduction of iron(III), fumarate and nitrate by *Shewanella putrefaciens* MR-1" *J. Bacteriol.*, **179**, 1143-1152.

**Myers, C.R., Nealson, K.H., (1988)** "Bacterial manganese reduction and growth with manganese oxide as a sole electron acceptor" *Science*, **240**, 1319-1321.

**Nicholson, D.W., Hergersberg, C., Neupert, W. (1988)** "Role of cytochrome *c* lyase in the import of cytochrome *c* into mitochondria" *J. Biol. Chem.*, **263**, 19034-19042.

**Nicholson, D.W., Köhler, H., Neupert, W. (1987)** "Import of cytochrome *c* into mitochondria: cytochrome *c* lyase" *Eur. J. Biochem.*, **164**, 147-157.

**Nurizzo, D. Silvestrini, M.C., Mathieu, M., Cutruzzola, F., Bourgeois, D., Fulop, V., Hajdu, J., Brunori, M., Tegoni, M., Cambillau, C. (1997)** "N-terminal arm exchange is observed in the 2.15 Å crystal structure of oxidized nitrite reductase from *Pseudomonas aeruginosa*" *Structure*, **5**, 1157-1171.

**Overbye Michel, L., Sandkvist, M., Bagdasarian, M. (1995)** "Specificity of the protein secretory apparatus: secretion of the heat-labile enterotoxin B subunit pentamers by different species of Gram - bacteria" *Gene*, **152**, 41-45.

**Page, C.C., Moser, C.C., Chen, X., Dutton, P.L. (1999)** "Natural engineering principles of electron tunnelling in biological oxidation-reduction" *Nature*, **402**, 47-52.

**Page, C.C., Moser, C.C., Dutton, P.L. (2003)** "Mechanism for electron transfer within and between proteins" *Curr. Op. Chem. Biol.*, **7**, 551-556.

**Page, M.D., Sambongi, Y., Ferguson, S.J. (1998)** "Contrasting routes of *c*-type cytochrome assembly in mitochondria, chloroplasts and bacteria" *Trends Biochem. Sci.*, **23**, 103-108.

**Park, S-Y., Shimizu, H., Adachi, S., Nagagawa, A., Tanaka, I., Nakahara, K., Shoun, H., Obayashi, E., Nakamura, H., Iizuka, T., Shiro, Y. (1997)** "Crystal structure of nitric oxide reductase from denitrifying fungus *Fusarium oxysporum*" *Nat. Struct. Biol.*, **4**, 827-832.

**Pfennig, N., Biebl, H. (1976)** "*Desulfuromonas acetoxidans* gen. nov. and sp. nov., a new anaerobic, sulfur-reducing, acetate-oxidizing bacterium" *Arch. Microbiol.*, **110**, 3-12.

**Pickard, C., Foght J.M., Pickard, M.A., Westlake, D.W.S. (1993)** "Oil field and freshwater isolates of *Shewanella putrefaciens* have lipopolysaccharide polyacrylamide gel profiles characteristic of marine bacteria" *Can. J. Microbiol.*, **39**, 715-717.

**Pitts, K.E., Dobbin, P.S., Reyes-Ramirez, F., Thomson, A.J., Richardson, D.J., Seward, H.E. (2003)** "Characterisation of the *Shewanella oneidensis* MR-1 decaheme

cytochrome MtrA: expression in *Escherichia coli* confers the ability to reduce soluble Fe(III) chelates" *J. Biol. Chem.*, **278**, 27758-27765.

**Pokkuluri, P.R., Londer, Y.Y., Duke, N.E.C, Erickson, J., Pessanha, M., Salguiero, C., Schiffer, M. (2004a)** "Structure of a novel $c_7$-type three-heme cytochrome domain from a multidomain cytochrome *c* polymer" *Protein Sci.*, **13**, 1684-1692.

**Pokkuluri, P.R., Londer, Y.Y., Duke, N.E.C., Long, W.C., Schiffer, M. (2004b)** "Family of cytochrome $c_7$-type proteins from *Geobacter sulfurreducens*: structure of one cytochrome $c_7$ at 1.45 Å resolution" *Biochemistry*, **43**, 849-859.

**Pollock, W.B., Chemerika, P.J., Forrest, M.E., Beatty, J.T., Voordouw, G. (1989)** "Expression of the gene encoding cytochrome $c_3$ from *Desulfovibrio vulgaris* (Hildenborough) in *Escherichia coli*: export and processing of the apoprotein" *J. Gen. Microbiol.*, **135**, 2319-2328.

**Polyakov, K.M., Boiko, K.M., Tikhonova, T.V., Stekhanova, T.N., Antipov, A.N., Bourenkov, G.P., Popov, A.N., Lamzin, V.S., Popov, V.O. (2003)** EMBL Annual Report.

**Reid, G.A., Gordon, E.H.J. (1999)** "Phylogeny of marine and freshwater *Shewanella*: reclassification of *Shewanella putrefaciens* NCIMB400 as *Shewanella frigidimarina*" *Int. J. Syst. Bacteriol.*, **49**, 189-191.

**Ren, Q., Thöny-Meyer, L (2002)** "Physical interaction of CcmC with heme and the heme chaperone CcmE during cytochrome *c* maturation" *J. Biol. Chem.*, **276**, 32591-32596.

**Rees, D.C., Howard, J.B. (2000)** "Nitrogenase: standing at the crossroads" *Curr. Op. Chem. Biol.*, **4**, 59-566.

**Ribbe, M., Gadkari, D., Meyer, O. (1997)** "$N_2$ fixation by *Streptomyces thermoautotrophicus* involves a molybdenum-dinitrogenase and a manganese-superoxide oxidoreductase that couple $N_2$ reduction to the oxidation of superoxide produced from $O_2$ by a molybdenum-Co dehydrogenase" *J. Biol. Chem.*, **272**, 26627-26633.

**Richardson, D.J., Wehrfritz, J.M., Keech, A., Crossman, L.C., Roldan, M.D., Sears, H.J., Butler, C.S., Reilly, A., Moir, J.W., Berks, B.C. *et al* (1998)** "The diversity of redox proteins involved in bacterial heterotrophic nitrification and aerobic denitrification" *Biochem. Soc. Trans.*, **26**, 401-408.

**Rothery, E.L. (2003)** "Mechanistic studies on multiheme cytochromes from *Shewanella*" Ph.D. Thesis, University of Edinburgh.

**Rubinstein J.L., Walker J.E., Henderson R. (2003)** "Structure of the mitochondrial ATP synthase by electron cryomicroscopy" *EMBO J.*, **22**, 6182–6192.

**Schalk, J., Outstad, H., Kuenen, J.G., Jetten, M.S. (1998)** "The anaerobic oxidation of hydrazine: a novel reaction in microbial nitrogen metabolism" *FEMS Microbiol. Lett.*, **158**, 61-67.

**Scheiner, D., (1976)** "Determination of ammonia and Kjeldahl nitrogen by indophenol method" *Water Res.*, **10**, 31-36.

**Schulz, H., Fabianek, R.A., Pelliciolo, E.C., Hennecke, H., Thöny-Meyer, L. (1999)** "Heme transfer to the heme chaperone CcmE during cytochrome *c* maturation requires the CcmC protein, which may function independently of the ABC-transporter CcmAB" *Proc. Natl. Acad. Sci. U.S.A.*, **96**, 6462-6467.

**Schulz, H., Hennecke, H., Thöny-Meyer, L. (1998)** "Prototype of a heme chaperone essential for cytochrome *c* maturation" *Science*, **281**, 1197-1200.

**Schumacher, W., Hole, U., Kroneck, P.M.H. (1994)** "Ammonia-forming cytochrome *c* nitrite reductase from *Sulfurospirillum deleyianum* is a tetraheme protein: new aspects of the molecular composition and spectroscopic properties" *Biochem. Biophys. Res. Commun.*, **205**, 911-916.

**Schumacher, W., Kroneck, P.M.H. (1991)** "Dissimilatory hexaheme *c* nitrite reductase of "Spirillum" strain 5175: purification and properties" *Arch. Microbiol.*, **156**, 70-74.

**Schwalb, C., Chapman, S.K., Reid, G.A. (2003)** "The tetraheme cytochrome CymA is required for anaerobic respiration with dimethyl sulfoxide and nitrite in *Shewanella oneidensis*" *Biochemistry*, **42**, 9491-9497.

**Shi, L., Lin, J-T., Markillie, L.M., Squier, T.C., Hooker, B.S. (2005) "**Overexpression of multi-heme C-type cytochromes" *BioTechniques*, **38**, 297-299.

**Simon. J., Gross, R., Einsle, O., Kroneck, P.M.H., Kröger, A., Klimmeck, O. (2000)** "A NapC/NirT-type cytochrome *c* (NrfH) is the mediator between the quinone pool and the cytochrome *c* nitrite reductase of *Wolinella succinogenes*" *Mol. Microbiol.*, **35**, 686-696.

**Smalley, J.F., Feldberg, S.W., Chidsey, C.E.D., Lindford, M.R., Newton, M.D., Liu, Y-P. (1995)** "The kinetics of electron transfer through ferrocene terminated alkanethiol monolayers on gold" *J. Phys. Chem.*, **99**, 13141-13149.

**Stach, P., Einsle, O., Schumacher, W., Kurun, E., Kroneck, P.M.H. (2000)** "Bacterial cytochrome *c* nitrite reductase: new structural and functional aspects" *J. Inorg. Biochem.*, **79**, 381-385.

**Stevens, J.M., Daltrop, O., Allen. J.W.A., Ferguson, S.J. (2004)** "*C*-type cytochrome formation: chemical and biological enigmas" *Acc. Chem. Res.*, **37**, 999-1007.

**Suigo, T., Kanao, T., Furukawa, H., Nagasawa, T., Blake, R.C. (1996)** "Isolation and identification of an iron-oxidising bacterium which can grow in tetrathionate medium and the properties of a tetrathionate-decomposing enzyme isolated from the bacterium" *J. Ferment. Bioeng.*, **82**, 233-238.

**Tano, T., Kitaguhi, H., Harada, K., Nagasawa, T., Suigo, T. (1996)** "Purification and some properties of tetrathionate decomposing enzyme from *Thiobacilus thiooxidans*" *Biosci. Biotech. Biochem.*, **60**, 224-227.

**Taylor, P., Pealing, S.L., Reid, G.A., Chapman, S.K., Walkinshaw, M.D. (1999)** "Structural and mechanistic mapping of a unique fumarate reductase" *Nat. Struct. Biol.*, **6**, 1108-1112.

**Thöny-Meyer (1997)** "Biogenesis of respiratory cytochromes in bacteria" *Microbiol. Molec. Biol. Rev.*, **61**, 337-376.

**Thöny-Meyer, L. (2000)** "Haem-polypeptide interactions during cytochrome *c* maturation" *Biochim. Biophys. Acta*, **1459**, 316-324.

**Thöny-Meyer, L. (2002)** "Cytochrome *c* maturation: a complex pathway for a simple task?" *Biochem. Soc. Trans.*, **30**, 633-638.

**Thöny-Meyer, L. (2003)** "A heme chaperone for cytochrome *c* biosynthesis" *Biochemistry*, **42**, 13099-13015.

**Thöny-Meyer, L., Kunzler, P. (1997)** "Translocation to the periplasm and signal sequence cleavage of preapocytochrome *c* depend on *sec* and *lep*, but not on the *ccm* gene products" *Eur. J. Biochem.*, **246**, 794-799.

**Tomlinson, E.J., Ferguson, S.J. (2000a)** "Conversion of a *c*-type cytochrome to a *b*-type that spontaneously forms in vitro from apo protein and heme: implications for *c*-type cytochrome biogenesis and folding" *Proc. Natl. Acad. Sci. U.S.A.*, **97**, 5156-5160.

**Tomlinson, E.J., Ferguson, S.J. (2000b)** "Loss of either of the two heme-binding cysteines from a class I *c*-type cytochrome has a surprisingly small effect on physiocochemical propeties" *J. Biol. Chem.*, **275**, 32530-32534.

**Turner, K.L., Doherty, M.K., Heering, H.A., Armstrong, F.A., Reid, G.A., Chapman, S.K. (1999)** "Redox properties of flavocytochrome $c_3$ from *Shewanella frigidimarina* NCIMB400" *Biochemistry*, **38**, 3302-3309.

**Van der Graf, A., de Bruijn, P., Robertson, L.A., Jetten, M.S.M., Kuenen, J.G. (1998)** "Metabolic pathway of anaerobic ammonium oxidation on the basis of $^{15}N$ studies in a fluidized bed reactor" *Microbiol*., **143**, 2415-2421.

**Venkataswaran, K., Dollhopf, M.E., Aller, R., Stackebrandt, E., Nealson, K.H. (1998)** "*Shewanella amazonensis* sp. nov., a novel metal-reducing facultative anaerobe from Amazonin shelf muds" *Int. J. Syst. Bacteriol.*, **48**, 965-972.

**Vogel, A.I., Svehla, G. (1971)** "Vogel's Textbook of Macro and Semimicro Qualitative Inorganic Analysis" (5th Edition), Longman, London.

**Wain, R. Redfield, C., Ferguson, S.J., Smith, L.J. (2004)** "NMR analysis shows that a *b*-type variant of *Hydrogenobacter thermophilus* cytochrome $c_{552}$ retains its native structure" *J. Biol. Chem.*, **279**, 15177-15182.

**Weiner, R.M., Coyne, V.E., Brayton, P., West, P., Raiken, S.F. (1998)** "*Alteromonas colwelliana* sp. nov. an isolate from oyster habitats" *Int. J. Syst. Bacteriol.*, **38**, 240-244.

**Worthington, C.C. (1998) "**Enzyme Manual: Enzymes and related biochemicals" Freehold, New Jersey.

**Yamada, T., Goto, M., Vasu, P., Zaborina, O., Kimbara, K., Das Gupta, T.K., Chakrabarty, A.M. (2002)** "Bacterial redox protein azurin induces apoptosis in J774 marcophages through complex formation and stabilization of the tumor suppressor protein p53" *Infect. Immun.*, **70**, 7054-7062.

**Yang, C-H., Azad, H.R., Cooksey, D.A. (1996)** "A chromosomal locus required for copper resistance, competitive fitness and cytochrome *c* biogenesis in *Pseudomonas fluorescens*" *Proc. Natl. Acad. Sci. USA*, **93**, 7315-7320.

**Yankovskaya, V., Horsfield, R., Tornroth, S., Luna-Chavez, C., Hideto, M., Leger, C., Byrne, B., Cecchini, G., Iwata, S. (2003)** "Architecture of succinate dehydrogenase and reactive oxygen species generation" *Science*, **299**, 700-704.

**Yeoman, K.H., Delgado, M.J., Wexler, M., Downie, J.A., Johnston, A.W.B. (1997)** "High affinity iron acquisition in *Rhizobium leguminosarum* reuires the *cycHJKL* operon and the *feuPQ* gene products, which belong to the family of two-component transcriptional regulators" *Microbiol.*, **143**, 127-134.

# *APPENDICES*

# APPENDIX I DERIVATION OF EQUATIONS

## I-i The Michaelis-Menten Equation

The Michaelis-Menten Equation can be applied to enzyme-catalysed reactions in which complex formation is rapid and reversible and the rate-determining step is product formation, according to the reaction:

$$\mathbf{E + S} \underset{k_{-1}}{\overset{k_1}{\rightleftharpoons}} \mathbf{ES} \xrightarrow{k_2} \mathbf{E + P} \qquad \textbf{Equation A.1}$$

where E, S, ES and P are enzyme, substrate, enzyme-substrate complex and product respectively. The rate of change of concentration of the intermediate species, the enzyme-substrate complex, is given by Equation A.2:

$$\boxed{\frac{\mathrm{d[ES]}}{\mathrm{dt}} = k_1[\mathrm{E}][\mathrm{S}] - k_{-1}[\mathrm{ES}] - k_2[\mathrm{ES}]} \qquad \textbf{Equation A.2}$$

Under steady-state conditions, the concentration of the intermediate, ES, is assumed to remain constant as the concentration of substrate is depleted, and therefore the rate of formation of the ES complex is equal to the rate of decay into free enzyme and product. Hence, Equation A.2 is equal to zero.

During the course of the reaction, the concentration of free enzyme is not directly measurable at any given instant, and so is expressed in terms of the initial, measurable concentration at time t = 0. This concentration is defined as $[E]_0$ and is related to the concentration of free enzyme and the concentration of the enzyme-substrate complex by Equation A.3:

$$[E] = [E]_0 - [ES]$$ **Equation A.3**

The expression for the concentration of free enzyme, E, is then substituted in Equation A.2 to give Equation A.4:

$$0 = ([E]_0 - [ES])k_1[S] - k_{-1}[ES] - k_2[ES]$$ **Equation A.4**

which is rearranged to give an expression for [ES]:

$$[ES] = \frac{[E]_0[S]}{\left(\frac{k_{-1} + k_2}{k_1}\right) + [S]}$$ **Equation A.5**

The rate of the reaction, V, is given by Equation A.6:

$$V = \frac{d[P]}{dt} = k_2[ES]$$ **Equation A.6**

Finally, the familiar form of the Michaelis-Menten equation is obtained by combining Equations A.5 and A.6:

$$V = \frac{k_2[E]_0[S]}{\left(\frac{k_{-1} + k_2}{k_1}\right) + [S]}$$

**Equation A.7**

From this expression, the rate of the reaction, $k_{cat}$, is given as $k_2$, and the Michaelis constant, $K_m$ is defined according to Equation A.8:

$$K_m = \frac{k_{-1} + k_2}{k_1}$$

**Equation A.8**

## I-ii Solvent Isotope Effects

Solvent isotope effects are a result of the differences in the free energies of the ground and transition states of a deuterated compound compared to a protonated compound.

The difference in mass between a hydrogen and a deuterium atom leads to different specific bond vibrational energy levels in the compounds, resulting from the lowering of the zero-point energy of the deuterated bond compared to the protonated bond. Primary isotope effects arise from the breaking of a hydrogen or deuterium bond during the rate-determining step of the reaction.

At equilibrium in a mixed isotopic solution, any exchangeable hydrogenic sites will contain a mixture of hydrogen and deuterium. The ratio of hydrogenic sites, i, is expressed as the isotopic fractionation factor, $\phi_i$:

$$\phi_i = \frac{[D]_i}{[H]_i} \cdot \frac{(1-n)}{n} \qquad \textbf{Equation A.9}$$

where n is the fraction of deuteration in the mixed isotope solvent.

Under these constraints:

$\phi_i = 1$, if the strength of binding is the same as an average site in the bulk solvent.

$\phi_i < 1$, if binding is weaker than an average solvent site (for example, protium will accumulate at these sites

$\phi_i > 1$, if binding is stronger than an average solvent site; deuterium will accumulate at these sites.

The kinetic solvent isotope effect is determined by the fractionation factors of the reactant and transition states of a reaction. These factors change upon the activation of the compound. A range of fractionation factors have been experimentally determined and these are generalised by the functional group rule, which states that the values of $\phi_i$ depend upon the functional group in which the $i^{th}$ site is located, and not on a more remote feature of the molecular environment.

Hydrogenic sites may be classified according to their contributions to the free energy of transfer as follows:

*Internal $\phi$ sites*: These are exchangeable hydrogenic sites within the structural framework of the solute. They have substantially different binding potential from the average bulk water site and so the contribution to the free energy of transfer is substantial.

*External $\phi$ sites*: These are sites within the solvent (water molecules) that are strongly interacting with the solute, so that the binding potential is substantially altered. This results in a considerable contribution to the free energy.

*Z-sites*: These are hydrogenic sites either in weakly interacting water molecules or within the structural framework of the solute, where the binding potential is so similar to the bulk water as to produce only a very small isotope effect. Such sites are only important if their aggregate effect becomes significant.

All ϕ-sites must be accounted for when considering hydrogenic sites. However, the Z-sites have individual isotope effects that are so small they can be dealt with in the aggregate state, and hence as an average.

The use of fractionation factors has allowed the determination of a large number of these parameters to be determined experimentally. They have a systematic relationship to molecular structure, and are, to a fair approximation, transferable at the functional-group level.

The solvent isotope effect observed can be expressed in terms of the fractionation factors for the single reactant and transition sites according to the scheme:

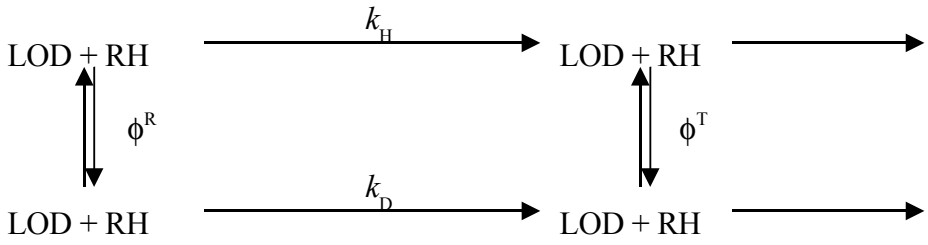


Therefore, as the cycle is thermodynamically closed:

$$\frac{k_D}{k_H} = \frac{\phi^T}{\phi^R}$$ **Equation A.10**

where:

$k_H$ is the rate of formation of TH

$k_D$ is the rate of formation of TD

$\phi^R$ is the equilibrium constant of exchange in the reactant state

$\phi^T$ is the equilibrium constant of exchange in the transition state

## I-iii pH-Dependence of Kinetic Turnover Rate

The ionisation constant for acids and bases can be described using the following equations:

For an acid: $$K_a = \frac{[A^-][H^+]}{[AH]}$$ **Equation A.11**

For a base: $$K_a = \frac{[B][H^+]}{[BH^+]}$$ **Equation A.12**

The p$K_a$ of such systems is defined by Equation A.13:

$$pK_a = -\log K_a$$ **Equation A.13**

Rearrangement of the above equations allows derivation of the Henderson-Hasselbach equation:

$$pH = pK_a + \log\left(\frac{[B]}{[BH^+]}\right)$$ **Equation A.14**

It follows that the p$K_a$ of a species can be described as the pH at which the concentrations of protonated and deprotonated forms are equal, or that at which the species is half-neutralised.

In enzymology, three species are commonly in equilibrium:

$$E + 2H^+ \overset{K_{A1}}{\rightleftharpoons} EH^+ + H^+ \overset{K_{A2}}{\rightleftharpoons} EH_2^{2+}$$ **Equation A.15**

Equations for $K_{A1}$ and $K_{A2}$ can then be derived:

$$K_{A1} = \frac{[EH]}{[E][H^+]}$$ **Equation A.16**

$$K_{A2} = \frac{[EH_2^{2+}]}{[EH^+][H^+]}$$ **Equation A.17**

and the log of each of these equations yields:

$$pH = \log\left(\frac{[EH]}{[E]}\right) + pK_{A1}$$ **Equation A.18**

$$pH = \log\left(\frac{[EH_2]}{[EH]}\right) + pK_{A2}$$ **Equation A.19**

From these equations, expressions for each enzyme species in Equations A.16 and A.17 as follows:

$$[E] = \frac{10^{(pK_{A1}-pH)}}{1+10^{(pK_{A1}-pH)}+10^{(pH-pK_{A2})}}$$ **Equation A.20**

$$[EH^+] = \frac{1}{1+10^{(pK_{A1}-pH)}+10^{(pH-pK_{A2})}}$$ **Equation A.21**

$$[EH_2^{2+}] = \frac{10^{(pH-pK_{A2})}}{1+10^{(pK_{A1}-pH)}+10^{(pH-pK_{A2})}}$$ **Equation A.22**

The total activity measured at any pH value is equal to the sum of the contributions from each of the three species:

$$\text{Activity} = k_0[\text{E}] + k_1[\text{EH+}] + k_2[\text{EH}_2^{2+}] \qquad \textbf{Equation A.23}$$

Finally, substituting for values of [E], [$EH^+$] and [$EH_2^{2+}$] yields the Equation A.24:

$$\text{Activity} = \frac{k_0 10^{(pK_{A1}-pH)} + k_1 + k_2 10^{(pH-pK_{A2})}}{1+10^{(pK_{A1}-pH)}+10^{(pH-pK_{A2})}} \qquad \textbf{Equation A.24}$$

Fitting the experimental data to this equation allows two p$K_A$ values to be resolved. However, if only two enzyme species (E and $EH^+$) are relevant, then a single p$K_A$ value may be resolved:

$$\text{Activity} = \frac{k_0 10^{(pK_{A1}-pH)} + k_1}{1+10^{(pK_{A1}-pH)}} \qquad \textbf{Equation A.25}$$

**APPENDIX II**

**AMINO ACID SEQUENCE OF OCTAHEME TETRATHIONATE REDUCTASE**

The eight CXXCH heme binding motifs are shown in red. In each instance, the sixth heme ligand is shown in blue (this ligand is histidine for each of hemes I and III-IV and lysine for the unusually-coordinated active site heme II). The cysteine residue at the active site is shown in green.

Shown in purple are the residues for which there is no definable electron density. These residues are proposed to form a mobile capping loop.

```
         10          20          30          40          50
          |          |          |          |          |
ANPHKDVLKG PFTTGSEVTT QCLTCHEEQA TDMMKTSHWT WELEQKLPDR
   I                                        IV

         60          70          80          90         100
          |          |          |          |          |
TVVRGKKNSI NNFCVAISSN EPRCTSCHAG YGWKDNTFDF KDKTKVDCLI
     II

        110         120         130         140         150
          |          |          |          |          |
CHDTTGTYVK DPAGAGEPMA KLDLAKIAQN VGAPVRDNCG SCHFYGGGGD

        160         170         180         190         200
          |          |          |          |          |
AVKHGDLDSS MAYPDKATDV HMDSDGNNFQ CQNCHTTEKH QISGNAMGVS
                      VI                    III
```

```
        210         220         230         240         250
| PGGIDHIGCE NCHDSAPHSN KKLNTHTATV ACQTCHIPFF AKNEPTKMQW
                    VII         VIII

        260         270         280         290         300
          |         |         |         |         |
DWSTAGDDKP ETVDQYGKHT YQKKKGNFVW EKMVKPQYAW YNGTANAYMA

        310         320         330         340         350
          |         |         |         |         |
GDKMDSNVVT KLTYPMGDIN DAKAKIYPFK VHTGKQIYDK KLNIFITPKT

        360         370         380         390         400
          |         |         |         |         |
YGKGGYWSEF DWNLAAKLGM EANPTMLEKG IKYSGEYDFA ATEMWWRINH
                                                     V

        410         420         430         440         450
          |         |         |         |         |
MVSPKEQALN CNDCHNKGTR LDWQALGYQG DPMKNKQGPK HKQ
```

## APPENDIX III AMINO ACID SEQUENCE ALIGNMENT OF GSU0357 WITH NrfA FROM *DESULFOVIBRIO DESULFURICANS* ATCC 27774

```
CLUSTAL 2.0.10 multiple sequence alignment


GSU0357     MWKKRLAVLAVAAGAAVALSIPALSTAAKGKPAATGAKGDGRETCYGCHEEVKALKEGSK 60
NrfA_Dds    -MNKRIVTTALALATLLGVALLSGCQDVSTELKAP------------------KYKTGIA 41
              :**:.. *:* .: :.::: : .  .. :  *.                   * *

GSU0357     HARLACDSCHDKLKEHLANYETKPGTNLDPAKCGSCHKNEYSSFFTVNYDAQPRKEKGIP 120
NrfA_Dds    ETETKMSAFKGQFPQQYASYMKNNEDRIMTDYKGSVPYHKND-----NVNPLPKG----F 92
            .:.   .: :.:: :: *.* .:   .: .   **   :: .     * :. *:

GSU0357     TGRSPMQDKLLAGHGFTFEHNEPRGHAFMVVDQFIVDRFQGGRFQYKKGAWGMDATGKAW 180
NrfA_Dds    KHAQPYLKNLWLGYPFMYEYNETRGHTYAIDDFLNIDRIN-------------------- 132
            .  .*  .:*  *: * :*:**.***:: : * : :**::

GSU0357     DILTDTGKKLPETAMAGNPTCIQCKTSDHILKWKFMGDKDPKATWDRSSDIVAVAKDTQN 240
NrfA_Dds    RFAADGKGNLPAT-------CWNCKTPKMMEWVSQYGDKFWSMDVN-EFRAKDKINAHDE 184
             : :*   :** *       * :***.. :   .  ***  .   : .       :  ::

GSU0357     PVGCIHCHDPHGTQPRVVRDGLIQAIEKDPTANIFAKNGKTDLKVISFRDGFRKIGVMEK 300
NrfA_Dds    TIGCANCHDPATMELRLY---------SEPLKDWLKRSGK----------DWQKMSRNEK 225
            .:** :****   : *:          .:*  : : :.**          .::*:.  **

GSU0357     TDSRLMCAQCHVEYNCNAGSQWSDGQKVGYDDQRTNHFPLKNAKDLLAHYKKLDFYDFKH 360
NrfA_Dds    --RTLVCAQCHVEYYFT-------------------------------------------- 240
                *:********  .

GSU0357     AITGARLVKLQHPEAETYAGSVHDRAGVGCADCHMPRMKGKDGKMFKSHGVIRPAHHVKE 420
NrfA_Dds    ------------------------------------------------------------


GSU0357     ACLGCHPKSTVEQKSYQIEGTRNYIRGKMRKAEYWLGQLIDTYAAAKRMGIGEDVLAKAR 480
NrfA_Dds    ------------------------------------------------------------


GSU0357     EKHEEAHVLWEYWTAENSDGFHNPELARDSLTSSIAASKAGVKLLNDAMEPKK 533
NrfA_Dds    ---------------------------------------------------
```

## APPENDIX IV CONFERENCES AND COURSES ATTENDED

**9th, 10th and 11th Redox Enzymes Meeting (incorporating 1st, 2nd and 3rd EaStChem Biological Chemistry Meetings), Firbush Point Field Centre, Perthshire, UK**

8th - 10th June 2005 (Delegate)

7th - 9th June 2006 (Delegate)

6th - 8th June 2007 (Speaker)

**Dalton Discussion Meeting No 8 (Metals: centres of biological activity), University of Nottingham, UK**

7th - 9th Spetember 2005 (Abstract and poster presented)

**13th International Conference of (ICBIC XIII), Vienna, Austria**

15th-20th July, 2007 (Poster presented)

**Inorganic Chemistry Section Meetings, Firbush Point Field Centre, Perthshire, UK**

**Chemical Biology and Biophysics Section Seminars**

**School of Chemistry Colloquia**

## APPENDIX V PUBLICATIONS

**Atkinson, S.J., Mowat, C.G., Reid, G.A., Chapman, S.K. (2007)** "An octaheme *c*-type cytochrome from *Shewanella oneidensis* can reduce nitrite and hydroxylamine" *FEBS Lett.*, **581**, 3805-3808.

**Mowat, C.G., Atkinson, S.J., Reid, G.A. (2007)** "Octaheme tetrathionate reductase" Handbook of Metalloproteins, Ed. Albrecht Messerschmidt, Wiley Blackwell.